UNIVERSIDAD TÉCNICA FEDERICO SANTA MARÍA
DEPARTAMENTO DE INDUSTRIAS
SANTIAGO - CHILE

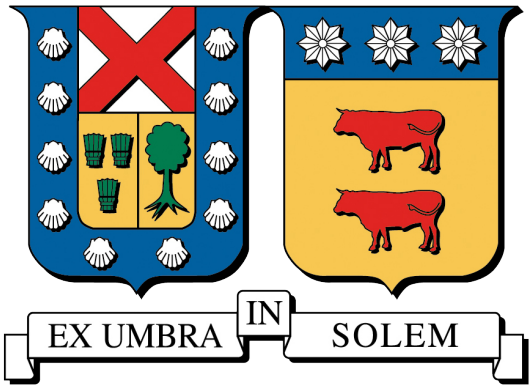

CALORIMETRIC STUDY OF RENEWABLE FUELS WITH THE SENSIBLE HEAT CALORIMETRY APPARATUS

CHRISTOPHER HANNIE VOLKWEIN BARREDA

TESIS PARA OPTAR AL TÍTULO DE
INGENIERO CIVIL INDUSTRIAL
Y AL GRADO DE
MAGÍSTER EN CIENCIAS DE LA INGENIERÍA INDUSTRIAL

PROFESOR GUÍA	:	Dr. PEDRO RESZKA C.
PROFESOR CORREFERENTE	:	Dr. ANDRÉS FUENTES C.
PROFESOR CORREFERENTE	:	Dr. JUAN CARLOS ELICER C.

AGOSTO 2016

Acknowledgments

The process that for a long time seemed that would never end, finally is being ended and with satisfactory results. This work demanded me several hours, long trips to Valparaíso and to solve countless difficulties that arose in the process. In this long and difficult process I would like to thank Anita María Cristi for all her support during this process. Thanks for the good talks and for listening to me when I needed. Thanks to Julio Cattan for his companionship and his disposition to help when it was needed. Also thanks to Giuli for his friendship specially in the first stage of the project. This project would have been much more difficult without the work done by Gonzalo Olivares. Thank you very much for the countless times you helped me to solve difficulties in the laboratory. Special thanks to Professor Pedro Reszka for inciting me to continue studying and to enter to the MSc and also for all the opportunities he gave me since we met and started to work together. Thanks for the trust you deposited on me. Another important person in this project was Professor Andrés Fuentes. Thank you for all the confidence you put on me for years, for believing in my capacities and for the advises and ideas you give me. Thanks to Alejandro Vidal for all his advises in the electricity field and for his great disposition to help. Thanks to Leonardo Lobos for all the help provided in the first stage of the project. Thanks to Gonzalo Severino for giving opinions and advises when were needed and also for tolerating all the disorders in the laboratory caused by the failed inventions that Julio, Giuli and I did. Thanks to Maël Pau and Adrien Cotton, the students that helped me with the tedious experiments in the last stage of the thesis.

Thanks to all my friends of the MSc, specially to Javier Vera. Thanks for the talks and for the encouragement words. I had a great experience during all these years in the UTFSM. I would like to thank to all the friends I made in the university, specially to Luis, Thomy, Sepu, Max, Cobo, Gamal, Coke, Mauro, Merchak, Cami, Feña, Marcos, Krebs, Hernán,

Chelo, Javi and Fer.

Special thanks to my family, for letting me to work in a calm ambient and for all the affection and sacrifices done. Thanks also to Anita Cristi family for all the support and kindness during this work. Also thanks to my friends and family from Concepción. Thanks to the Departamento de Industrias and the DGIP for the financial scholarships provided and to the UTFSM for the good experiences and the great opportunities that gave me.

Abstract

Biomass is commonly used in Chile as feedstock for boilers to produce energy. Some companies linked to forest resources production and management, uses their wood wastes and other biomass supplies for energy production. These power plants are commonly located in the south of Chile, where the climate benefits the trees growth but also increases the biomass moisture content. Companies use different biomass mixes with high and variable moisture content to supply their boilers. This study is aimed to characterize the biomass used by Celulosa Arauco S.A. for energy production. Celulosa Arauco S.A. is a company that produce and manage renewable forest resources and also is involved in the electric energy generation industry. Biomass in commonly characterized by the heat of combustion, particle size distributions, proximate composition, ultimate elemental and ash elemental analysis (Demirbas, 2004). In this study a calorimetric study on the biomass mix used by Celulosa Arauco S.A. in the power plant Arauco is carried out. The analysis includes different scenarios where eight mixes with different biomass compositions at three different moisture contents are tested. The calorimetric analysis includes the determination of the following parameters: peak heat release rates, ignition delay times, flaming time and the effective heat of combustion of each mix at each moisture content. The study is also aimed to predict the combustion efficiency of each type of biomass in the boiler. Average efficiencies between 30 % and 50 % were found for the sawdust, pine bark and wood chips at the original moisture content. Average efficiencies between 45 % and 68 % were found in the samples with less moisture content. And average efficiencies between 62 % and 73 % were found in the samples with the lowest moisture contents. Wood chips registered the highest average peak heat release rate at the original moisture content, followed by pine bark. Decreasing the moisture content to the following level improves significantly the performance of pine bark, reporting high improvements in the average peak heat release rate of the samples composed mostly of this type of biomass. By drying all biomass mixes during one day at ambient temperature, the average peak heat release rate of all mixes increase in 60 % and the ignition delay time decrease in 50 %. In order to perform all the experiments described above, a calorimeter has been designed, constructed and

validated. The calorimeter is called the Sensible Heat Calorimetry Apparatus (SCALA). The calorimeter is principally composed of the following components: a combustion chamber, where the specimens are placed, a fan that provides the apparatus with a constant adjustable air flow, radiant heaters that supplies the specimen with a constant adjustable incident heat flux, a precision balance that measures the mass loss of the sample, a Tunable Diode Laser Spectroscopy (TDLAS) instrument that measures the oxygen concentrations of the outlet gases at the exhaust duct, and thermocouples that measure the temperature at different points. This calorimeter uses three different methods to determine the heat release rate (HRR) of a burning specimen; the sensible enthalpy rise (SER) method, the oxygen consumption (OC) method and the mass loss rate (MLR) method. The main difference between this calorimeter and other standard calorimeters is that the SCALA uses the TDLAS technique to measure the oxygen concentrations of the outlet gases. This technique avoids the use of filters to perform the oxygen concentrations measurements and thus reduces the apparatus response time. The principle of operation, the methods to determine the heat release rates and the calibrations procedures are established and described in this study. The calorimeter is experimentally validated using PMMA. The results obtained with the three methods are compared between them. Agreement between the three techniques is achieved. The results are compared with other results obtained with the standard calorimeter Fire Propagation Apparatus (FPA). There was agreement between the results obtained with the SCALA and the FPA. The SCALA enthalpy rise method showed to achieve better results than the sensible enthalpy rise method performed by the FPA. The OC method achieved good agreement but reported the highest magnitudes. The uncertainty of the OC and the SER results are calculated in function of the HRR. The total relative uncertainty of the oxygen consumption HRR calculations vary between 10 % and 85 %, where 10% correspond to 16 kW and 85 % correspond to 0.5 kW. The total relative uncertainty of the sensible enthalpy rise HRR calculations vary between 4 % and 23 %, where 4% correspond to 16 kW and 23 % correspond to 0.5 kW.

Keywords. Calorimeter, calorimetry, biomass, heat release rate, effective heat of combustion

Contents

List of Tables

List of Figures

Nomenclature

C	Calibration constant of the Cone Calorimeter $\mathrm{m}^{\frac{1}{2}}\mathrm{kg}^{\frac{1}{2}}\mathrm{K}^{\frac{1}{2}}$
$C_{O_2}^A$	Oxygen concentration in the combustion products (%)
$C_{O_2}^0$	Oxygen concentration in the incoming air (%)
C_{base}	Oxygen concentration at the baseline ethylene flow (%)
C_{high}	Oxygen concentration at the high ethylene flow (%)
c_p	Specific heat of air ($\mathrm{kJ{\cdot}kg^{-1}{\cdot}K^{-1}}$)
$c_{p,w}$	Specific heat of the OSU walls ($\mathrm{kJ{\cdot}kg^{-1}{\cdot}K^{-1}}$)
E	Energy constant ($\mathrm{kJ{\cdot}g^{-1}}$)
E_{CH_4}	Energy constant for methane ($\mathrm{kJ{\cdot}kg^{-1}}$)
E'	Energy constant assuming carbon goes to carbon dioxide ($\mathrm{MJ{\cdot}m^{-3}}$)
E''	Energy constant in the burning of carbon monoxide ($\mathrm{MJ{\cdot}m^{-3}}$)
EHC	Effective heat of combustion ($\mathrm{kJ{\cdot}g^{-1}}$)
$EHC(t)$	Effective heat of combustion at time t ($\mathrm{kJ{\cdot}g^{-1}}$)
F	Corrected upper flow rate of the calibration gas ($\mathrm{L{\cdot}min^{-1}}$)
F_0	Corrected baseline flow rate of the calibration gas ($\mathrm{L{\cdot}min^{-1}}$)
$\dot{H}_R$	Heat released by the OSU burning sample (kW)
$\dot{H}_e$	Heat carried by the air in the OSU (kW)
$\dot{H}_i$	Heat produced by the OSU radiant panels (kW)
$\dot{H}_l$	Heat losses to the surroundings (kW)
$\dot{H}_w$	Heat absorbed by the OSU walls (kW)
I_{supply}	Total current consumed by the heaters (kW)
$I_\lambda(L)$	Intensity of radiation after it travels along path L (W)

$I_\lambda(0)$	Initial intensity of radiation (W)
K	Calibration constant ($kW \cdot K^{-1}$)
K_{SER}	Calibration constant for the SER method of the SCALA ($kW \cdot K^{-1}$)
$K_{SER,D}$	Daily calibration constant for the SER method ($kW \cdot K^{-1}$)
$K_{SER,W}$	Weekly calibration constant for SER method ($kW \cdot K^{-1}$)
$K_{SER,i}$	Calibration constant at ethylene flow i ($kW \cdot K^{-1}$)
K_{OC}	Calibration constant of the oxygen equation ($kW \cdot \%_{O_2}^{-1}$)
$K_{OC,D}$	Daily calibration constant for the OC method ($kW \cdot \%_{O_2}^{-1}$)
$K_{OC,W}$	Weekly calibration constant for the OC method ($kW \cdot \%_{O_2}^{-1}$)
$K_{OC,i}$	Calibration constant at ethylene flow i ($kW \cdot \%_{O_2}^{-1}$)
$K_{l,OSU}$	Heat transfer coefficient ($kW \cdot K^{-1}$)
k_h	Calibration constant of the OSU Calorimeter ($kW\ mV \cdot m^{-2}$)
L	Optical path length of the laser beam (m)
L_{max}	Calculated flame height limit (m)
L_{ref}	Reference flame height (m)
M_{AIR}	Molecular weight of air ($g \cdot mol^{-1}$)
M_{O_2}	Molecular weight of oxygen ($g \cdot mol^{-1}$)
$MC\%_{GB}$	Moisture content at green basis (%)
$MC\%_{OB}$	Moisture content at ovendry basis (%)
m	Mass (g)
m_{OSU}	Mass of the OSU (kg)
$\dot{m}$	Mass loss rate of air ($kg \cdot s^{-1}$)
$\dot{m}_a$	mass flow of the air entering the combustion zone ($kg \cdot s^{-1}$)
$\dot{m}_e$	mass flow of the combustion products leaving the control volume ($kg \cdot s^{-1}$)
$\dot{m}_v$	mass flow of volatiles ($kg \cdot s^{-1}$)
$\dot{m}(t)$	Mass loss rate at time t ($g \cdot s^{-1}$
$\dot{m}_i$	High ethylene flow at step i ($kg \cdot s^{-1}$)
$\dot{m}_{base}$	Baseline ethylene flow ($kg \cdot s^{-1}$)
$\dot{m}_{high}$	High ethylene flow ($kg \cdot s^{-1}$)
$n^\circ_{CO_2}$	Molar flow rate of carbon dioxide in the incoming air ($mol \cdot s^{-1}$)

$n^{\circ}_{H_2O}$	Molar flow rate of water vapor in the incoming air (mol·s^{-1})
$n^{\circ}_{N_2}$	Molar flow rate of nitrogen in the incoming air (mol·s^{-1})
$n^{\circ}_{O_2}$	Molar flow rate of oxygen in the incoming air (mol·s^{-1})
n^{s}_{CO}	Molar flow rate of carbon monoxide in the exhaust duct (mol·s^{-1})
$n^{s}_{CO_2}$	Molar flow rate of carbon dioxide in the exhaust duct (mol·s^{-1})
$n^{s}_{H_2O}$	Molar flow rate of water vapor in the exhaust duct (mol·s^{-1})
$n^{s}_{O_2}$	Molar flow rate of oxygen in the exhaust duct (mol·s^{-1})
n^{s}_{soot}	Molar flow rate of soot in the exhaust duct (mol·s^{-1})
P	Ambient atmospheric pressure (mm Hg)
P_y	Water vapor pressure of wet test meter (mm Hg)
P_{supply}	Power supply of the radiant heaterrs (kW)
$\dot{Q}$	Heat release rate (kW)
$\dot{Q}_{SER}$	Heat release rate determined with the SCALA (kW)
$\dot{Q}_{SER}(t)$	Heat release rate with SER method at time t (kW)
$\dot{Q}_{OC}$	Heat release rate determined with the oxygen consumption method (kW)
$\dot{Q}_{OC,K}$	Heat release rate determined with OC method with a constant calibration (kW)
$\dot{Q}_{MLR}$	Heat release rate determined with the mass loss rate method (kW)
$\dot{Q}_{loss}$	heat release rate lost to the surroundings (kW)
$\dot{Q}_{conv}$	Convective heat release rate (kW)
$\dot{Q}_{cone}(t)$	Heat release rate determined with the Cone Calorimeter in time t (kW)
$\dot{Q}_{OSU}$	Heat release rate determined with the OSU Calorimeter (kW)
$\dot{Q}_{R,OSU}$	Corrected heat release rate determined by the OSU (kW)
$\dot{Q}_{e,OSU}$	Heat carried by the air with the steady state as reference (kW)
$\dot{Q}_{l,OSU}$	Heat losses to the surroundings with the steady state as reference (kW)
$\dot{Q}_{max}$	Maximum heat release rate limit (kW)
$\dot{Q}_{ref}$	Reference flame heat release rate (kW)
$\dot{q}''_i$	Incident heat flux measured in position i (kW·m^{-2})
$\dot{q}''_{inc}$	Incident heat flux on the specimen (kW·m^{-2})
$\dot{q}''_{ref}$	Incident heat flux measured at the center (kW·m^{-2})
RSD	Relative standard deviation (%)

S_i	Variation of heat flux measured in position i (%)
T_a	Temperature of the air entering the combustion zone (K)
T_e	Temperature of combustion products leaving the control volume (K)
T_o	Reference temperature (K)
T_v	Temperature of volatiles entering the combustion zone (K)
T_{om}	Absolute temperature of gas at the orifice meter (K)
T_{ss}	Temperature of the outlet gases at steady state (K)
T_w	Temperature of the walls (K)
T_{wss}	Wall temperature at the steady state (K)
T_{wssi}	Initial wall temperature at the steady state (K)
T_{high}^{ss}	High temperature at steady state (K)
T_{base}^{ss}	Baseline temperature at steady state(K)
T_i	High temperature at ethylene flow i (K)
t	Time (s)
t_d	Delay time (s)
u_T	Standard uncertainty of the test results (kW)
u_1	Standard uncertainty of the heat release measurement (kW)
u_2	Standard uncertainty due to specimen variation (kW)
u_3	Standard uncertainty due test conditions (kW)
V	Voltage of the thermopile (mV)
V_0	Thermopile voltage at baseline flow rate (mV)
V_1	Thermopile voltage at upper flow rate (mV)
$\dot{V}_T$	Total volumetric flow rate of air into the system ($m^3 \cdot s^{-1}$)
X_{CO}^A	Carbon monoxide concentration in the analyzer (-)
$X_{CO_2}^\circ$	Carbon dioxide concentration in the incoming air (-)
$X_{N_2}^\circ$	Nitrogen concentration in the incoming air (-)
$X_{H_2O}^\circ$	Water vapor concentration in the incoming air (-)
$X_{O_2}^0$	Oxygen analyzer reading in the incoming air (-)
$X_{O_2}^1$	Oxygen concentration before delay time correction (-)
$X_{O_2}(t)$	Corrected oxygen analyzer reading at time t (-)

$X_{O_2}^{A}$	Oxygen analyzer reading in the combustion products, mole fraction (-)
$X_{O_2}^{A^0}$	Oxygen concentration in the analyzer before test, water vapor is trapped (-)
X_{PPMM}^{0}	Oxygen concentration in the incoming air (parts per million-meter)
X_{PPMM}^{A}	Oxygen concentration in the combustion products (parts per million-meter)

Greek Symbols

$\kappa(\lambda)$	Absorption coefficient of the medium (-)
$\Delta\dot{m}_{O_2}$	Rate of oxygen consumed in the combustion $g{\cdot}s^{-1}$
ΔP	Orifice meter pressure differential (Pa)
Δh_c	Heat of combustion ($kJ{\cdot}kg^{-1}$)
η	Combustion efficiency with the gross heat of combustion as reference (-)
λ	Wavelength of the light source (nm)
ρ_0	Density of air ($kg{\cdot}m^{-3}$)
ϕ	Oxygen depletion factor (-)
χ_r	Fraction of the heat lost to surroundings (-)
χ	Combustion efficiency (-)

Superscripts

A	After test ignition
A^0	Incoming air, before test ignition, water is trapped
$\circ$	Incoming air, before test ignition
s	Exhaust duct

Subscripts

a	Entering air
e	Exhaust gases
o	Reference
v	Volatiles
w	Wall
$base$	At the baseline ethylene flow
$high$	At high ethylene flow
OSU	OSU calorimeter
$cone$	Cone Calorimeter
OC	Oxygen consumption method
SER	Sensible enthalpy rise method
MLR	Mass loss rate method
D	Daily
W	Weekly
GB	Green basis
OB	Ovendry basis

1 Introduction

In the history of Chile it has been common the use of conventional and nonrenewable fuels to produce energy without caring about the environmental impact. The energy matrix had in the past and has now low variety of energy sources and it has been predominated by hydro, coal, natural gas and diesel (Comisión Nacional de Energía, 2015). Nowadays, the laws are getting stricter about the volatile pollution and the society is increasingly caring about the toxic emissions that are produced to generate electricity. But Chile is growing and the energy consumption is increasing with time. The energy demand has been duplicated every ten years (Ministerio de Energía de Chile, 2015a). Therefore, the country is increasing the energy supply and encouraging projects of renewable energy power plants. One renewable energy source with high potential for development is biomass. Biomass is organic matter that can proceed from animals (zoomass) and plants (phytomass). Biomass has been used by mankind to produce energy for thousands of years. Nowadays there are power plants that use biomass to produce energy. In this study the term biomass will be applied to refer to phytomass, specifically to the organic fuels used as feedstock for boilers to produce energy in Chile. These fuels are generally wood wastes and sub products that come from cellulose production processes and from sawmills. Plants convert the sun energy into chemical energy through photosynthesis and store it. Biomass is composed of varying amounts of cellulose, hemicellulose, lignin, small amounts of other organics and inorganics (Abbasi and Abbasi, 2010). The sustainable use of biomass for energy production does not increase the carbon dioxide present in the atmosphere. The US Environmental Protection Agency stated that the carbon dioxide emitted from biomass-based fuels does not increase the atmospheric carbon dioxide concentrations, assuming the carbon dioxide emitted is offset by the uptake of carbon dioxide resulting from the growth of new biomass (Agency,

2009). According to the International Energy Agency (2015), in 2013 10.2 % of the world total primary energy supply correspond to biofuels and waste. In Chile 23.7 % of the total energy primary supply corresponds to energy produced from firewood and biomass, and biomass represents the 4 % of the electricity generation matrix (Ministerio de Energía de Chile, 2015b).

Biomass is becoming an interesting energy source, because of its renewable nature. The climate in Chile promotes trees and plants growth. Through a sustainable use, these resources can become an important source for power generation. There is a potential feasible power from biomass wastes in the range of 310 MW and 470 MW that can be installed in Chile (Bertran and Morales, 2008). A problem in the power generation based on biomass combustion in large scale is the quality of the biomass feedstock. The biomass usually comes with high and variable moisture content. There are commonly various biomass types mixed in different proportions, giving varied behaviors in the boilers. Each biomass type has particular properties. The size of the biomass particles are different for each type. These variables have an influence in the efficiency of the combustion in the boiler. Currently there is no study of the influence of the mix composition with variable moisture content in the biomass used as feedstock for boilers in Chile. This work is about making a characterization of the biomass used for energy production. The characterization will give parameters that can be considered in decision making. Decisions based on knowing the biomass quality and combustion efficiency. The study will be applied on a specific power plant located in the south of Chile; Arauco unit of the holding Celulosa Arauco S.A. This company develops forest products, and produce energy by using their own wood residues and by buying biomass to other suppliers. Currently the studies that Celulosa Arauco commonly makes on their own biomass feedstock consist in moisture content measurements to samples of each biomass type, particle size measurements and gradually some heat of combustion measurement of each biomass type. The heat of combustion is defined as the amount of heat released when unit quantity is oxidized completely to yield stable end products (Drysdale, 2016). It is measured with an oxygen bomb calorimeter. It is a good parameter to know the energy contribution of each biomass type, but it has

some pros and cons. One advantage is that the heat of combustion is a material property. This means that its magnitude has no dependence on the experimental conditions. One disadvantage is that the mass is limited usually to 1 g. No mixes can be tested with that capacity. The heat of combustion is usually calculated with dried samples. But this is far from reality, where the samples have high moisture contents. An other disadvantage of the oxygen bomb calorimeter is that it takes several hours to obtain the results. The measurements in the oxygen bomb calorimeter are performed under complete combustion. This can be also not the reality, incomplete combustion is a possible scenario while burning biomass in the boiler. The goal of this work is to obtain other parameters to predict the behavior of the biomass mixes in the boiler, optimize the fuel mixes and classify the fuels according to their performance. These parameters are: the heat release rate of the burning sample (kW), the peak heat release rate of the sample (kW), ignition delay time (s), flaming time (s) and the effective heat of combustion ($kJ \cdot g^{-1}$). These parameters will be explained in the following chapters. To obtain these parameters it is necessary the use of a heat release rate calorimeter. A calorimeter is defined as an apparatus used for measuring the heat release rate, and the measurement of heat release rate is called calorimetry (Janssens, 2016). Calorimeters apply different techniques to measure the heat release rate of a burning sample. Depending on the calorimeter type, other parameters can also be measured (e.g. mass loss rates, species concentrations in the product gases, visible smoke development of materials (ASTM E1354-11b, 2011)). With calorimeters the behavior of fuels can be studied in different experimental conditions (e.g. different air flow rates, incident heat fluxes, atmospheres). The sample size can be significantly greater than the sample size of an oxygen bomb calorimeter. This means that the samples will be tested under more realistic conditions. With a heat release rate calorimeter several tests can be performed in less time.

A new calorimeter was designed and built in order to characterize fuels used as feedstock for boilers. The calorimeter is called the Sensible Heat CALorimetry Apparatus (SCALA). The main reason for using a calorimeter instead of another instrument, is that the calorimeter allows more realistic test conditions. Test conditions are an important factor when dealing

with fuels with high and variable moisture content, variable composition, particle size and properties. The first part of this study consists in the design, construction and validation of a calorimeter and the second part is about the characterization of the biomass used as feedstock for boilers by Celulosa Arauco using the calorimeter.

1.1 Characterization of biomass

Biomass is a complex fuel, with varied properties. It is necessary to characterize biomass in order to improve its combustion efficiency. Demirbas (2004) listed the methods commonly used to characterize biomass :

- Heat of combustion
- Particle size distribution
- Proximate composition
  - Moisture
  - Ash
  - Volatile matter
  - Fixed carbon
- Ultimate elemental
  - Carbon
  - Hydrogen
  - Sulfur
  - Chlorine
  - Oxygen
- Ash elemental

These parameters give important information about the biomass combustion behavior. For example, the nitrogen and sulfur content are related with the combustion emissions (NO_x and SO_x emissions). The presence of chlorine can lead to corrosion in the boiler, low ash melting points leads to fouling problems, high moisture and ash content can cause ignition and combustion problems (Demirbas, 2004).

The goal of this work is to complement the conventional biomass analysis with a calorimetric analysis and introduce the concept of calorimetry in order to characterize biomass fuels used as feedstock for boilers. The aim of this project is to assess the fuels just as they are fed into the boiler. Evaluate the performance of biomass fuels under different moisture content, mix composition and incident heat fluxes. The combustion efficiency of the each biomass type will be determined at different moisture contents. Furthermore, with the calorimeter several studies can be performed in the future in order to analyze the influence of other variables in the tested fuels, e.g. the particle size, porosity, emissions, etc. This will be discussed in the future work in section 5.1.

1.1.1 Combustion efficiency: The performance of biomass in boilers

The combustion efficiency is defined as the ratio of the effective heat of combustion to the net heat of combustion (Janssens, 2016). The effective heat of combustion is the heat released per unit mass of a gasified material measured by a calorimeter (Tewarson, 1995; Janssens, 2016). The net heat of combustion is determined from the gross heat of combustion. As described above, the gross heat of combustion is measured with an oxygen bomb calorimeter and considers that the reactants and products are in their standard states. In contrast, in the net heat of combustion the products are in the state in which they are formed (Drysdale, 2016). So, the net heat of combustion is also determined under complete combustion, and it also assumes that all the fuel mass has been consumed (See Section 3.5.3 for more details of the heat of combustion). Considering that the net heat of combustion is a fixed value and does not depend on the experimental conditions, the combustion efficiency depends on the effective heat of combustion. The effective heat of combustion depends on the combustion reaction (complete or incomplete) and the amount of mass consumed

during combustion (Janssens, 2016). It is also dependent on the moisture content of the specimen (Babrauskas, 2006). Incomplete combustion (low efficiency) is responsible of CO, soot and unburnt hydrocarbons production. The product gases named before, the heat released and the extent of oxidation depends on the flame temperature, amount of oxygen available for the reaction, entrainment of the air by the flame and the generations rates of pyrolysis products (Tewarson, 1994).

In wood fired boilers it has been demonstrated that combustion process cannot be maintained if the wood moisture content exceeds 60 % (Green basis) (Koppejan and Van Loo, 2012). The moisture content of some biomass types used by Celulosa Arauco are near the 60 % limit, and in some cases the moisture content reaches 60 % (See Table 3.1). This can be a good reason to decrease the moisture content of the biomass before using it in the boilers. The amount of moisture that has to be removed from the biomass in order to have a determined combustion efficiency can be performed with a calorimeter. This is part of the study, where biomass mixes with different moisture contents are tested in the SCALA. Knowing the heat released by biomass mixes at different moisture content is a good parameter to study the feasibility of a project aimed to decrease the moisture content of the biomass. So, the combustion efficiency of all biomass types at different moisture contents will be determined.

Demirbas (2005) establishes that the biomass particle size has an influence on the combustion reaction, and that the particle size should be as much as 0.6 cm. The particle size of the biomass used in Celulosa Arauco varies from less than a millimeter to various centimeters. So, this is an other aspect that can be improved in order to have more efficiency in the reaction. But for this study, the influence of particle size in the combustion efficiency will not be considered.

1.2 Fire calorimetry

There is extensive information in the literature about many heat release rate calorimeters developed through time (Babrauskas, 1992). These calorimeters use different techniques

to determine the heat release rate of materials. Each technique have advantages and disadvantages in reference to each other. Some techniques are more suitable for some kind of materials and not so accurate for others. This is a good reason to use different methods to calculate the hear release rate. This will be discussed later in the following sections. Calorimeters are used to determine fire behaviors and different parameters related to the combustion of materials and also are commonly used to evaluate the flammability of materials (ASTM E2058-03, 2003). Typical parameters determined with fire calorimeters are (ASTM E1354-11b, 2011; ASTM E2058-03, 2003; ASTM E906 / E906M-10, 2010):

- Heat release rate
- Ignitability (time to ignition, also called ignition delay time)
- Flaming time
- Mass loss rates before ignition and during flaming combustion
- Peak heat release rate
- Mean heat release rate
- Total energy release
- Effective heat of combustion
- Visible smoke development of materials and products
- Estimation of material properties

The calculation of these parameters depends on the features of the calorimeter. In the following section the methods used to determine the heat release rate will be described.

1.2.1 Methods to measure the heat release rate

As described above, there are different methods to measure the heat release rate of burning materials. The most common methods available in the literature based on the selection made by Babrauskas (1986) and Janssens (1995) are the following:

- **Sensible enthalpy rise method**

  This method is based on measuring the temperature of a constant air flow that pass through a combustion chamber. The enthalpy rise determines the heat release rate of the burning sample (Babrauskas, 1986; Janssens, 1995).

  - **Compensation method**

    It consists on maintaining a constant temperature in the gases produced by the combustion of the material. To achieve the constant temperature it is necessary to supply heat with a burner to the sample. The heat required to maintain the temperature constant, is the negative of the specimen heat release rate (Babrauskas, 1986; Janssens, 1995)

  - **Substitution method**

    The heat release rate is determined from the flow supplied to a gas burner during a second run, duplicating the temperature time curve of the products of combustion measured for a test specimen during the first run (Janssens, 1995)

- **Oxygen consumption method**

  There is a relationship between the oxygen consumed in a combustion reaction and the heat release rate of the burning fuel. It is necessary to determine the amount of oxygen removed of the combustion stream (Babrauskas, 1986; Janssens, 1995).

- **Carbon dioxide and carbon monoxide evolution method**

  It is similar to the oxygen consumption method. In this case the production of carbon dioxide and carbon monoxide is monitored. There is a relationship between carbon dioxide and carbon monoxide production and the heat release rate of the fuel (Babrauskas, 1986).

- **Flame heights of freely-burning fires method**

  This method estimates the heat release rate and other properties of the specimen on the basis of flame heights. It is used in free burning fires (Babrauskas, 1986).

- **Mass loss rate method**

  The heat release rate is determined by knowing the heat of combustion of the material and by measuring the mass loss of the sample. The multiplication of the heat of combustion and the mass loss rate gives the heat release rate of the burning sample.

The calorimeter built for this study uses three of the methods described above. These methods are:

- Sensible enthalpy rise method (SER)
- Oxygen consumption method (OC)
- Mass loss rate method (MLR)

In the following section, these three methods will be explained in detail.

1.2.1.1 Sensible enthalpy rise method

This method is based on the temperature rise of a continuous air stream that flows through a combustion chamber. The enthalpy rise and the air mass flow rate determine the heat release rate of the burning fuel. Assume a control volume as described in figure 1.1.

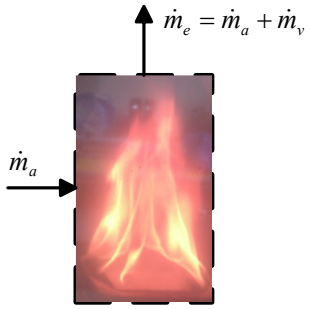

Figure 1.1: Mass flow balance

The mass flow $\dot{m}_a$ enters into the system. Part of the mass flow is involved in the combustion reaction. The fuel vaporizes at a rate $\dot{m}_v$. Thus, the outlet gases $\dot{m}_e$ are the sum of the inlet air flow $\dot{m}_a$ and the vapors generated $\dot{m}_v$. Janssens (1995) defines the heat release rate of a combustion reaction in a control volume with the following equation:

$$\dot{Q} - \dot{Q}_{loss} = c_p \dot{m}_e (T_e - T_o) - c_p \dot{m}_a (T_a - T_o) - c_p \dot{m}_v (T_v - T_o) \tag{1.1}$$

Where the term $\dot{Q}$ is the heat release rate (kW) of the combustion reaction, $\dot{Q}_{loss}$ is the heat lost to the surroundings (kW), c_p is the specific heat ($kJ \cdot kg^{-1} \cdot K^{-1}$), T_e is the temperature of combustion products leaving the control volume (K), T_a is the temperature of the air entering the combustion zone (K), T_v is the temperature of volatiles entering the combustion zone (K), T_o is the reference temperature (K). The heat loss to the surroundings $\dot{Q}_{loss}$ is the radiative component of the total heat released by the flame.

If $\dot{m}_a$ is much greater than $\dot{m}_v$, then $\dot{m}_v$ is negligible, and $\dot{m}_a \approx \dot{m}_e$. This leads to equation 1.2:

$$\dot{Q} - \dot{Q}_{loss} = c_p \dot{m}_a (T_e - T_a) \tag{1.2}$$

Assuming that the heat losses are fuel-independent, and that they are a constant fraction of the total rate of heat released (Janssens, 1995):

$$\chi_r \equiv \frac{\dot{Q}_{loss}}{\dot{Q}} \tag{1.3}$$

The term χ_r is the proportion of the heat losses (or radiative fraction) of the total flame heat release rate. Replacing Equation 1.3 in Equation 1.2 yields:

$$\dot{Q} = \frac{c_p \dot{m}_a}{1 - \chi_r} (T_e - T_a) \tag{1.4}$$

$$\dot{Q} = K (T_e - T_a) \tag{1.5}$$

Where K is the calibration factor, and can be determined experimentally. If there is a

heater in the chamber, equation 1.5 is still valid, T_a is replaced with a reference temperature. The reference temperature is the outlet gases steady state temperature while the radiant heaters are turned on. If the term χ_r is set to zero, then Equation 1.4 becomes Equation 1.6:

$$\dot{Q}_{conv} = c_p \dot{m}_a (T_e - T_a) \tag{1.6}$$

Where $\dot{Q}_{conv}$ now represents only the convective component of the heat released by the flame. If Equation 1.6 is used, then the heat release rate will be underestimated. So, including the term χ_r in Equation 1.6, leads to consider the heat losses to the surroundings. But the term χ_r is assumed to be constant and the same for the calibration fuel and for all fuels. This assumption has been proven to be wrong for the some fuels in the OSU calorimeter. Some authors have proven with the OSU calorimeter that the calibration constant depends on the material tested (Babrauskas, 1986; Tewarson, 2002; Filipczak et al., 2005) and is also time dependent (Filipczak et al., 2005; Evans and Breden, 1978; Lyon and Abramowitz, 1995). The use of this calibration constant in the calculations performed with the SCALA is discussed in section 2.8.

1.2.1.2 Oxygen consumption calorimetry

This section will explain the method to determine the heat release rate of a flame by knowing the oxygen consumed during the combustion reaction and the air flow involved. The concept of this method is that there is a constant energy released per unit mass of oxygen consumed. This relationship was found by Thornton (1917) for a list of organic materials. The energy constant is 13.1 kJ·g^{-1} for oxygen consumed and was found by Huggett (1980). The constant has a variability of ±5 % (Janssens, 1995; Biteau et al., 2008). This relationship is shown in Equation 1.7.

$$\dot{Q}_{OC} = E \Delta \dot{m}_{O_2} \tag{1.7}$$

Where E is the energy constant, $\Delta \dot{m}_{O_2}$ is the rate of oxygen consumed in the combustion

and $\dot{Q}_{OC}$ is the heat release rate. In incomplete combustion, some O_2 molecules react with carbon and form carbon monoxide. Thus, in incomplete combustion is it necessary to consider the amount of energy required to oxidize carbon monoxide into carbon dioxide. This amount of energy must be subtracted to the original equation (Biteau et al., 2008). Taking into account the amount of CO produced during combustion allows to have more accurate results. Parker (1984) proposed several equations to determine the heat release rate in different scenarios. Some of the variables considered in the equations to determine the heat release rate are:

- Oxygen concentration measurements
- Oxygen and carbon monoxide concentration measurements
- Oxygen, carbon monoxide and carbon dioxide measurements
- Trapping or neglecting the carbon dioxide in the apparatus
- Neglecting the presence of carbon monoxide
- Considering or not considering the water vapor presence in the entering air

These equations considers the presence of nitrogen, oxygen, carbon dioxide, carbon monoxide and water vapor in the air. Chow and Han (2011) made a compilation of equations for different species measurements and also include soot production into the equations. There are other relationships used to calculate the HRR by knowing the generation rates of carbon monoxide and carbon dioxide (ASTM E2058-03, 2003). The equation to calculate the heat release rate based only in the oxygen consumption is described in Section 2.2.2.1. The equation used to calculate the HRR based on oxygen consumption and carbon monoxide production is in Annex B.

1.2.1.3 Mas loss rate calorimetry

The heat release rate of a burning condensed phase material can be determined if the mass loss rate and the heat of combustion of the material are known. Equation 1.8 shows this relationship.

$$\dot{Q}_{MLR} = \chi \dot{m} \Delta h_c \tag{1.8}$$

χ is defined as a factor between 0 and 1 that indicates how complete the combustion reaction was, ΔH_c is the heat of combustion. For some materials the heat of combustion is known and tabulated, but for other more complex ones it must be determined using an oxygen bomb calorimeter. The mass loss rate $\dot{m}$ is defined as the rate of mass consumed in the combustion reaction divided by the time it takes to consume it. It is the slope of the equation that describes the relationship between the mass loss of the burning sample through time.

1.2.2 Standard Fire Calorimeters

Several fire calorimeters have been designed and built. In order to improve the design of the calorimeter built for this study, it was necessary to learn about other calorimeters and understand the advantages and disadvantages of their designs. All fire calorimeters have a heat source capable to produce a constant heat flux (kW$\cdot$ m^{-2}) on the specimen being tested. The incident heat fluxes vary depending on the calorimeter heat source design. Calorimeters can use natural inlet gas flows or they can have fans that provide the apparatus with constant air flows. Some calorimeters can be used to perform horizontal and vertical tests. All apparatuses usually have a pilot ignition system. Babrauskas (1992) describes calorimeters built for small and intermediate scale heat release rate tests. The first standard calorimeter was the FM Construction Materials Calorimeter (Developed at the Factory Mutual Research Laboratory in 1959 (Thompson and Cousins, 1959)). It uses the substitution method. A disadvantage of this calorimeter is that two runs are required for each test and the apparatus has to be cooled to ambient temperature before the second run. Then the FPL Calorimeter was developed by U.S. Forest Product Laboratories (FPL), with similar operating principles to the FM apparatus. This calorimeter had a maximum irradiance of 35 kW$\cdot$ m^{-2} over the specimen area, and the distribution of the incident heat flux in the specimen had variations of 40 %. Another standard calorimeter is the Ohio State University Rate of Heat Release

Apparatus (OSU). It was developed by Smith (1972). It uses the sensible enthalpy rise method. One advantage is that there is no need of gases analyzers in order to determine the heat release rate. This makes this technique more inexpensive. One disadvantage is that heat release rate magnitudes can be underestimated because of heat losses through the walls. Another standard apparatus is the Cone Calorimeter designed at the National Bureau of Standards (Babrauskas, 1984). It uses the oxygen consumption method. One disadvantage is that it assumes that for each gram of oxygen consumed in the reaction, a constant amount of energy is released, independent of the fuel type. This assumption can lead to errors while using more complex fuels like those with variable composition. Other standard apparatus is the Fire Propagation Apparatus (FPA). It was developed by the Factory Mutual Research Corporation. This apparatus uses carbon dioxide generation (CDG) and oxygen consumption methods to determine the heat release rate (Khan et al., 2016). With the FPA ignition, combustion and fire propagation tests can be performed (ASTM E2058-03, 2003). A disadvantage of this calorimeter is the high response time in the measurements due the gas analyzers characteristics and the gas sampling and filtering (Biteau, 2010). The calorimeter built for this study is designed based on the performance of the following three calorimeters described above:

- The Cone Calorimeter
- The Ohio State University Rate of Heat Release Apparatus (OSU)
- Fire Propagation Apparatus (FPA)

The following section will describe the main characteristics of the OSU and the Cone Calorimeter in order to understand how standard calorimeters are designed and how they work. Those calorimeters were selected because they use the same operating principle as the SCALA; the sensible enthalpy rise method (OSU) and the oxygen consumption method (Cone Calorimeter). The FPA uses the same method as the Cone Calorimeter, and the CDG technique is not used by the SCALA. So, in order to avoid redundancy, the FPA characteristics will not be detailed in this section. The calibration procedure of the Cone Calorimeter and the OSU will be also explained in this section, because the SCALA calibration procedure is based on them.

1.2.2.1 Cone calorimeter

The following information is obtained of the Standard Test Method for Heat and Visible Smoke Release Rates for Materials and Products Using an Oxygen Consumption Calorimeter (ASTM E1354-11b, 2011). As described above the Cone Calorimeter uses the oxygen consumption method to determine the heat release rate. With this calorimeter the ignitability (propensity to ignition), heat release rates, mass loss rates, effective heat of combustion and visible smoke development of materials and products can be determined. The specimens can be exposed to incident heat fluxes. The heat fluxes vary between 0 to 100 $kW \cdot m^{-2}$. It is possible to perform tests with vertical and horizontal orientation. The incident heat flux distribution on the specimen area has variations of ±2% respect to the central point of the 50×50 mm specimen area in the horizontal orientation and ±10% in the vertical orientation. The radiant heaters are monitored with thermocouples. The power of the heaters is controlled with a thyristor unit that can vary the current up to 25 A at 240 V. The main parts of the Cone Calorimeter are the following ones:

- Conical-shaped radiant electric heater
- Specimen holders
- Gas system with oxygen monitoring and flow measuring instrumentation
- Electric ignition spark-plug
- Data collection and analysis system
- Load cell (to measure the mass loss)

The exhaust system is capable of developing flows between 0.012 $m^3 \cdot s^{-1}$ and 0.035 $m^3 \cdot s^{-1}$. There is an orifice between the hood and the duct to promote mixing. Figure 1.2 shows the Cone Calorimeter with its respective dimensions. The analyzer is a paramagnetic sensor that measures the oxygen concentrations from 0 to 25 %. The analyzer drift is lower than ±50 ppm over a period of 30 min. The oxygen analyzer has a 10 to 90 % response time of less than 12 s. This time is not considering the time it takes the gases to reach the

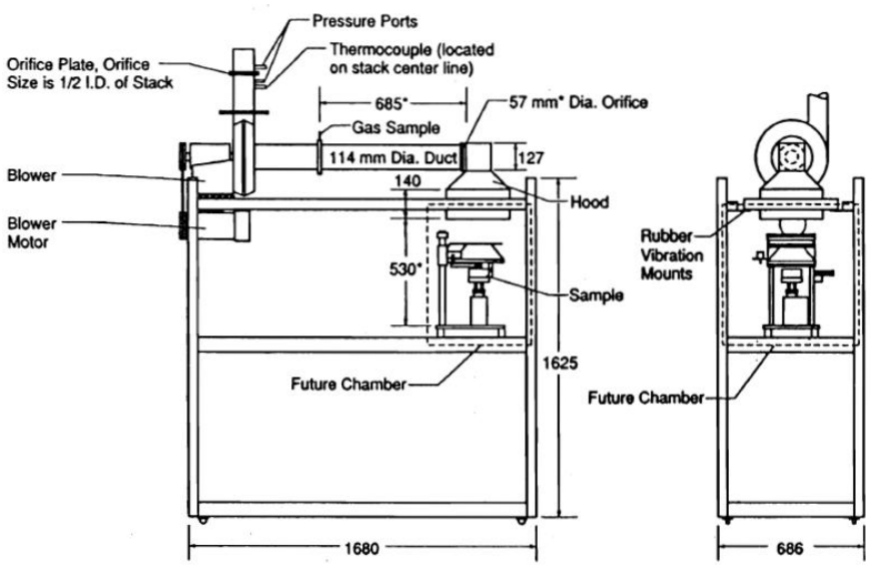

Figure 1.2: View of the Cone Calorimeter (ASTM E1354-11b, 2011)

analyzer. Equation 1.9 is applied to determine the HRR of a burning sample in the Cone calorimeter:

$$\dot{Q}_{cone}(t) = E1.1C\sqrt{\frac{\Delta P}{T_{om}}}\frac{X^0_{O_2} - X_{O_2}(t)}{1.105 - 1.5X_{O_2}(t)} \tag{1.9}$$

Where $\dot{Q}_{cone}(t)$ is the heat release rate in time t, E is the energy constant, 1.1 is the ratio of oxygen to air molecular weights, C is the calibration constant, ΔP is the orifice meter pressure differential, T_{om} is the absolute temperature of gas at the orifice meter, $X_{O_2}(t)$ is the oxygen analyzer reading at time t, and $X^0_{O_2}$ is the initial value of oxygen analyzer reading. The term $X_{O_2}(t)$ is corrected considering the delay times with Equation 1.10:

$$X_{O_2}(t) = X^1_{O_2}(t + t_d) \tag{1.10}$$

Where $X^1_{O_2}$ is the oxygen concentration before delay time correction, t_d is the oxygen analyzer delay time, and t is time.

1.2.2.2 Ohio State University Rate of Heat Release Apparatus (OSU)

The following information is obtained of the Standard Test Method for Heat and Visible Smoke Release Rates for Materials and Products Using a Thermopile Method (ASTM E906 / E906M-10, 2010). As described above the OSU calorimeter uses the sensible enthalpy rise method. The incident heat flux varies from 0 to 80 kW$\cdot$ m^{-2}. The power of the radiant heaters can reach 12.5 kVA. The uniformity of the incident heat flux is less than 5 %. The air entering the apparatus is approximately 0.04 ± 0.01 m$^3\cdot$ s^{-1} (0.01 m$^3\cdot$ s^{-1} flows through the environmental chamber and 0.03 m$^3\cdot$ s^{-1} flows through the pyramidal section). The temperature in the exhaust duct is controlled by a thermopile with 5 hot and 5 cold junctions. The hot junctions are located at the top of the duct. Tests can be performed in horizontal and vertical orientation. Pilot ignition is performed with a flame. The heat release rate is calculated using equation 1.5. The calibration constant is determined in the calibration procedure. But the calibration constant is not representative for all materials, because of the differences in the radiative heat losses of the fuels. Smith (1996) proposed a correction to this problem by including more constants that considers the radiation losses of the different fuels. This procedure is explained in Annex A. Figure 1.3 shows the OSU with its dimensions.

1.2.3 Calibration of the standard apparatuses

When using a calorimeter, the scientist would like to be assured that the results given by the apparatus are accurate. To ensure that the results of the calorimeter are correct, the standardized apparatuses use calibration methods that involve the use of materials with known properties to obtain calibration constants. These constants are introduced into equations to determine the heat release rate of burning samples with different properties. The calibration constants are subject to have an error below a determined limit, thus ensuring valid results. The OSU calibration procedures were taken from the ASTM E906 / E906M-10 (2010) and ASTM E1354-11b (2011).

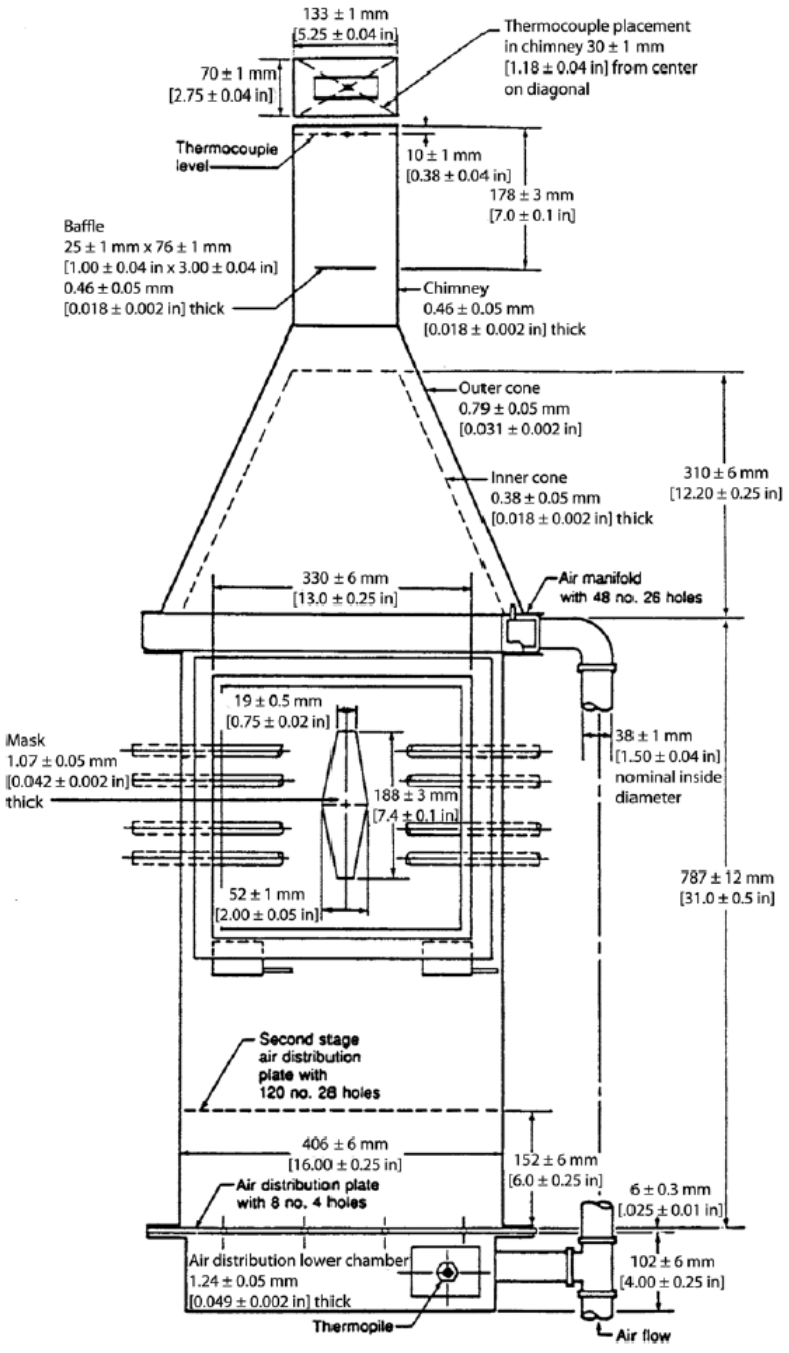

Figure 1.3: Dimensions of the OSU (ASTM E906 / E906M-10, 2010)

1.2.3.1 Calibration of the OSU

The OSU has two configurations; configuration A and configuration B. The first one is used by the Federal Aviation Administration for assessing materials for aircraft use, and

the second one is used for research and development purposes. Both configurations have different calibration procedure. Configuration A sets the radiant panelfor a $\dot{q}''_{inc} = 35$ kW·m^{-2}, and configuration B that uses no external heat flux and is suitable for various incident heat fluxes. In the following sections this 2 procedures will be explained.

Calibration A The OSU is calibrated with a burner using methane of at least 99 % purity. A wet test meter accurate to 0.2 L·min^{-1} is used to measure the gas flow rate. To control the calibration gas a manifold with 4 orifices with needle valves is used, allowing flow rates of 1, 4, 6 and 8 L·min^{-1}. For the calibration procedure, the baseline flow rate is set to 1 L·min^{-1}. Then, the thermopile baseline voltage is measured. After that the methane flow is set to 8 L·min^{-1} without recording the thermopile output. This is for preconditioning the chamber, so after a while the flow is decreased to the base line. Then the gas flow is increased to a higher flow and then decreased to the baseline flow rate. After 2 min burning at each rate, the thermopile reading is recorded and averaged for 10 s. The sequence of increasing and decreasing of the flow rate of methane is the following one:

1 – 4 – 1 – 6 – 1 – 8 – 1 – 6 – 1 – 4

The calibration constant is calculated for each upper value of the flow rate of methane with Equation 1.11:

$$k_h = 25.31 \frac{273}{T_a} \frac{(P - P_y)}{760} \frac{(F - F_0)}{V_1 - V_0} \tag{1.11}$$

Where F is the corrected upper flow rate of the methane (L·min^{-1}), F_0 is the corrected baseline flow rate of methane (L·min^{-1}), V_1 is the thermopile voltage at upper value (mV), V_0 is the thermopile voltage at baseline flow rate (mV), P is the ambient atmospheric pressure (mm Hg), P_y is the water vapor pressure of wet test meter (mm Hg), and T_a is the ambient temperature (K).

The standard deviation of the average of the five results obtained with equation 1.11

should be less than 5% to have a valid calibration constant. Then the average of the five results can be used as the calibration constant. If the standard deviation is greater than 5%, the calibration is repeated. To obtain the heat release rate is required the following equation:

$$\dot{Q}_{OSU} = k_h(V - V_0) \tag{1.12}$$

Where V_0 is the thermopile milivolt reading at the baseline, and V is the voltage of the thermopile. So, the OSU measures the heat release rate differences between baseline and the peaks. Then, the baseline becomes the temperature of the outlet gases at the steady state with the heaters turned on.

Calibration B The gas used in the burner in this configuration is at least 90% methane. There is no external heat flux during this calibration procedure. Two different gas flows are used: a high flow and a low flow. The gas flow is increased and decreased continuously to the high and to the low value for intervals of 4 minutes. This is repeated until the apparatus reaches steady state and no temperature variations in the thermocouples are observed (Compare the thermocouples value recorded during the last and the last minus 1 high flows, the same for the low flow). The difference of the high flow and the low flow is multiplied by the net heat of combustion, and the heat release rate of the methane flame is obtained. Then the high value recorded by the thermocouple and the low value are subtracted, and the heat release rate is divided by the result. This value is the calibration constant.

1.2.3.2 Calibration of the Cone Calorimeter

The calibration of this apparatus is done daily, and the difference obtained between two calibrations constants should be less than 5% to ensure good working. The radiant heater is not turned on for this procedure. Methane with purity of at least $99,5$ % is supplied to the calibration burner at a flow equivalent to 5 kW heat release rate (Considering the methane mass flow and the net heat of combustion). The calibration constant is calculated

from Equation 1.9, but replacing $\dot{Q}_{cone}(t)$ with 5 kW and E_{CH_4} with 12.54×10^3 kJ·kg^{-1}(for methane):

$$5 = (12.54 \times 10^3)(1.10)C\sqrt{\frac{T_e}{\Delta P}}\frac{1.105 - 1.5X_{O_2}}{X^0_{O_2} - X_{O_2}}$$

Solving for C:

$$C = \frac{5}{1.10(12.54 \times 10^3)}\sqrt{\frac{T_e}{\Delta P}}\frac{1.105 - 1.5X_{O_2}}{X^0_{O_2} - X_{O_2}}$$

The technique described above uses the same principles that will be used in the calibration of the SCALA; the use of a fuel with known and tabulated properties, provide a known power supply, and calculate the calibration constant using the amount of oxygen consumed during combustion.

1.2.4 Comparison of results obtained with different standard calorimeters

Several experiments have been performded in the past time in order to compare the results obtained with different calorimeters. Babrauskas (1986) performed experiments to obtain the HRR of low-flammability wall lining materials using the following techniques:

- Oxygen consumption calorimetry
- Carbon dioxide and carbon monoxide concentration measurements
- Flame height
- Sensible enthalpy rise calorimetry

The apparatuses used were the Cone Calorimeter, the FMRC Flammability Apparatus, the Flame Height apparatus, OSU/thermopile and OSU/O_2 (Modified version of the OSU that includes an oxygen analyzer) . With the Cone Calorimeter the HRR was determined

with the oxygen consumption technique. The FRMC Flammability Apparatus uses oxygen consumption measurements, supplemented with carbon dioxide and carbon monoxide measurements. The Flame Height apparatus uses a relationship between flame height and heat release rate. OSU/thermopile uses sensible heat and the OSU/O_2 uses oxygen consumption.

The Cone Calorimeter, Flammability Apparatus and the Flame Height apparatus showed similar results. The results varied in the range of ± 5% and in the worst cases they varied ± 25%. The standard deviation for the results given by the Cone Calorimeter was 8.4%, and for the other apparatuses were in the range of 5% to 10%. The values obtained with the OSU were approximately the half of the results of the others apparatuses used. The data obtained with OSU/O_2 was 10 to 20% higher than in the OSU/thermopile .

1.3 Present work

The SCALA was designed, constructed, calibrated, validated and then was used for Chilean biomass characterization. All elements required for the calorimeter operation were designed and constructed. Temperature sensors, an oxygen analyzer and a precision balance were incorporated to the apparatus. Radiant heaters were designed, constructed and incorporated to the main structure. An air supply system was included too. Elements and parts of the calorimeter were insulated and sealed respectively to improve the apparatus performance. The calibration procedure was defined. The infrastructure required for the calibration procedure was constructed. An experimental validation was carried out using PMMA. The PMMA heat release rate was determined using the three calorimetric methods used by the calorimeter. The results were compared between each calorimetric method and with results obtained with the Fire Propagation Apparatus. An error analysis was carried out for the oxygen consumption method and the sensible enthalpy rise method results. After the calorimeter experimental validation was finished, biomass tests were performed. The biomass was representative of the fuels used by the holding Celulosa Arauco S.A. in its power plant Arauco. Eight different biomass mixes were elaborated at three different

moisture contents. The performance of the different mixes, at different moisture content and imposed to different heat fluxes was studied. The critical incident heat flux for each biomass type was determined. The peak heat release rate, effective heat of combustion, ignition delay time and flaming time of the eight mixes at the three moisture content were determined. Finally, the performance of all the calorimetric methods at each test was studied.

This thesis work starts with the description, design, construction and validation of the SCALA. It is a whole chapter dedicated to the calorimeter development. Chapter 2 is about the characterization of the biomass used as feedstock for boilers in power plant Arauco. The chapter includes the experimental design, results and analysis of results obtained with the calorimeter. Chapter 3 is about the SCALA performance. It is discussed the apparatus behavior during tests performances. It also includes measurement limits calculations and other performance characteristics. Chapter 4 is about the conclusions of all work done and the future work.

2 | SCALA: The Sensible Heat Calorimetry Apparatus

The SCALA (Sensible heat CALorimetry Apparatus) is a calorimeter built for research purposes with the principal aim of characterizing Chilean biomass. This project is developed under the sponsorship of CONICYT. It is a part of the FONDECYT project n° 1130957: "Characterization of Chilean biomass fuels using calorimetric methods". In this section the main characteristics of the apparatus, principles of operation, main operating systems and instruments that integrate the calorimeter will be described. The calibration procedure will be defined and explained. At the end of this section there is an experimental validation of the methods used in the SCALA. To finish there is an error analysis of the results obtained with the calorimeter.

2.1 Features of the calorimeter

The SCALA is capable to work with solid fuels, liquid fuels and gases. It should not be used with explosive fuels. The shock waves could damage the structure of the calorimeter. The apparatus is composed of aluminum profiles that are joined together creating the main support structure. There are 4 windows at each face of the SCALA. Each window is composed of two glasses (High temperature resistance glasses). Between both glasses there is space that will be used in the future for air circulation. It will work as a cooling system. A plenum is located at the bottom of the aluminum structure. It is made of tin. The plenum connects an air supply system to the combustion chamber. A stainless steel bell shaped structure is located at the top of the calorimeter. It conducts the gases to the outside. An

air extractor above the apparatus drives the exhaust gases out of the laboratory. Figure 2.1 shows the apparatus from the inside and the outside. The view of the apparatus in the right picture represents the front of the SCALA. This point of view will be taken as reference to identify the parts of the apparatus, e.g. left window, right window, back window, front window, left radiant heater, right radiant heater.

Figure 2.1: Left: Inside of the SCALA. Right: Outside of the SCALA

The calorimeter requires three elements to work properly: air, heat and water. These three elements are supplied by the three main operating systems of the apparatus: the air supply system, the radiant heaters, and the scale insulation system respectively. The air supply system consists of a fan connected to the plenum through a pipe and an elbow. It provides different air flows to the combustion chamber. The air flow is regulated with a voltage regulator. The radiant heaters provide different incident heat fluxes above the specimen area. It is also regulated with voltage regulators. The scale insulation system is composed of an insulation box and a water cooling system. It is indispensable to maintain the scale temperature within the operating limits. Next to the apparatus is located the command station composed by a computer, a camera, and the DAQs of the measurement

instruments. The main operating principle of the SCALA is to use the heat produced by the radiant heaters to achieve a sustainable flame on the sample and use different systems to measure the heat release rate. The samples are located inside a sample holder (the sample holder is placed above the scale, which is protected with an insulation box) between both radiant heaters. Figure 2.2 shows the place of the sample in the calorimeter. In this case a biomass sample is being tested.

Figure 2.2: Position of the sample in the calorimeter

The calorimeter has novel aspects that differentiate it from other apparatuses: The oxygen concentration measurements are performed using Tunable Diode Laser Spectroscopy technique. There is full optical access to the combustion chamber. The delay times of the measuring instruments are low. There is high precision in the mass measurements.

2.2 Principle of operation

In section 1.2.1 the methods used by the SCALA to calculate the HRR have been mentioned and described. The main equations of each method have been presented. This section

shows the final equations used for each method to calculate the HRR.

2.2.1 Sensible enthalpy rise method (SER)

The temperature rise of the air flow that passes through the combustion chamber is measured by thermocouples positioned in the exhaust duct. Equation 1.5 is used to determine the rate of heat released, with the difference in the reference temperature used.

$$\dot{Q}_{SER} = \frac{\dot{m}c_p}{1-\chi_r}(T_e - T_{ss}) \tag{2.1}$$

$$\dot{Q}_{SER} = K_{SER}(T_e - T_{ss}) \tag{2.2}$$

The calibration constant K_{SER} is determined experimentally by performing the calibration procedure described later in Section 2.4.1. Variables T_e and T_{ss} are monitored by the same thermocouple at the exhaust duct. T_{ss} is the temperature at the steady state with the heaters turned on.

2.2.2 Oxygen consumption method

The apparatus uses a Tunable Diode Laser Absorption Spectroscopy (TDLAS) instrument to measure the oxygen concentration of the exhaust gases. At the moment only the oxygen analyzer is installed in the SCALA. A carbon monoxide analyzer will be installed shortly. With the carbon monoxide analyzer more accurate results will be obtained. The methodology to calculate the HRR including oxygen and carbon monoxide concentrations is explained in Annex B. Two methods are described to calculate the HRR with the oxygen consumption method: method A and method B. The first one is the method used in all calculations performed in this study, and it does not include a calibration constant. The second method includes a calibration constant and for the moment is not used in this study for reasons explained in Section 4.3.2.

2.2.2.1 Method A: Calculation with the oxygen consumption equation (OC)

As described above in Section 1.2.1.2, Parker (1984) proposed a method to determine the heat release rate by measuring the oxygen concentration of the exhaust gases for a Cone Calorimeter. Parker considers that only N_2, O_2, $CO2$ and CO_2 reach the oxygen analyzer. He considers that gases like water vapor, HCl and HCN are trapped out in the sampling line. He also considers that the inlet air is composed of N_2, O_2, CO_2 and H_2O. In this study it is considered that N_2, O_2, CO, CO_2, H_2O and soot reach the oxygen analyzer and that the inlet air is composed of N_2, O_2, CO_2 and H_2O. The terms $n^{\circ}_{N_2}$, $n^{\circ}_{O_2}$, $n^{\circ}_{CO_2}$ and $n^{\circ}_{H_2O}$ will be the molar flow rates of nitrogen, oxygen, carbon dioxide and water vapor respectively. The superscript "$\circ$" represents the gases in the incoming air. The following terms of concentrations are defined:

$$X^{\circ}_{O_2} = \frac{n^{\circ}_{O_2}}{n^{\circ}_{N_2} + n^{\circ}_{O_2} + n^{\circ}_{CO_2} + n^{\circ}_{H_2O}} \tag{2.3}$$

$$X^{\circ}_{N_2} = \frac{n^{\circ}_{N_2}}{n^{\circ}_{N_2} + n^{\circ}_{O_2} + n^{\circ}_{CO_2} + n^{\circ}_{H_2O}} \tag{2.4}$$

$$X^{\circ}_{CO_2} = \frac{n^{\circ}_{CO_2}}{n^{\circ}_{N_2} + n^{\circ}_{O_2} + n^{\circ}_{CO_2} + n^{\circ}_{H_2O}} \tag{2.5}$$

$$X^{\circ}_{H_2O} = \frac{n^{\circ}_{H_2O}}{n^{\circ}_{N_2} + n^{\circ}_{O_2} + n^{\circ}_{CO_2} + n^{\circ}_{H_2O}} \tag{2.6}$$

The terms $n^{\circ}_{N_2}$, $n^{s}_{O_2}$, $n^{s}_{CO_2}$, n^{s}_{CO}, $n^{s}_{H_2O}$ and n^{s}_{soot} will be the molar flow rates of nitrogen, oxygen, carbon dioxide, carbon monoxide, water vapor and soot in the exhaust duct. The superscript "s" represents the gases in the exhaust duct. The following term for the oxygen concentration in the analyzer is defined:

$$X^{A}_{O_2} = \frac{n^{s}_{O_2}}{n^{\circ}_{N_2} + n^{s}_{O_2} + n^{s}_{CO_2} + n^{s}_{CO} + n^{s}_{H_2O} + n^{s}_{soot}} \tag{2.7}$$

Parker calculates Equation 2.8 to obtain the HRR:

$$\dot{Q}_{OC} = E\rho_0 \frac{M_{O_2}}{M_{AIR}} X^{\circ}_{O_2} \phi \dot{V}_T \tag{2.8}$$

Where E is the energy released per mass of oxygen consumed in kJ$\cdot g^{-1}$, ρ_0 is the density of air, M_{O_2} and M_{AIR} are the molecular weights of oxygen and air respectively, $X^{\circ}_{O_2}$ is the initial oxygen volume fraction measured by the analyzer, $\dot{V}_T$ is the total volumetric flow rate of air into the system, and ϕ is the oxygen depletion factor. The last term is defined in the following equation:

$$\phi = \frac{n^{\circ}_{O_2} - n^{s}_{O_2}}{n^{\circ}_{O_2}} \tag{2.9}$$

Combining equations 2.3 and 2.7 with 2.9:

$$\phi = \frac{X^{\circ}_{O_2}(n^{\circ}_{N_2} + n^{\circ}_{O_2} + n^{\circ}_{CO_2} + n^{\circ}_{H_2O}) - X^{A}_{O_2}(n^{\circ}_{N_2} + n^{s}_{O_2} + n^{s}_{CO_2} + n^{s}_{CO} + n^{s}_{H_2O} + n^{s}_{soot})}{X^{\circ}_{O_2}(n^{\circ}_{N_2} + n^{\circ}_{O_2} + n^{\circ}_{CO_2} + n^{\circ}_{H_2O})} \tag{2.10}$$

In the burning of cellulosic materials and with an adequate air supply, the CO production can be neglected (Parker, 1984). Considering that the water vapors produced in the combustion reaction is neglected because it is small compared with the other gases concentrations and that there is no soot production and there is no carbon dioxide in the inlet air, then:

$$n^{s}_{O_2} + n^{s}_{CO_2} \approx n^{\circ}_{O_2} \tag{2.11}$$

$$n^{s}_{CO} = 0 \tag{2.12}$$

$$n^{\circ}_{H_2O} \approx n^{s}_{H_2O} \tag{2.13}$$

$$n^{\circ}_{CO_2} = 0 \tag{2.14}$$

Replacing Equations 2.12, 2.13, 2.14 and 2.14 into Equation 2.10 yields:

$$\phi = \frac{X^{\circ}_{O_2} - X^{A}_{O_2}}{X^{\circ}_{O_2}} \tag{2.15}$$

Substituting Equation 2.15 into Equation 2.8 yields:

$$\dot{Q}_{OC} = E\rho_0 \frac{M_{O_2}}{M_{AIR}} \left(X^{\circ}_{O_2} - X^{A}_{O_2}\right) \dot{V}_T \tag{2.16}$$

The output of the analyzer that measures the concentration of oxygen is in PPMM (Parts per million-meter). Thus, the following relationships should be incorporated to equation 2.16:

$$X^{\circ}_{O_2} = \frac{X^{0}_{PPMM}}{10^6 L}$$
$$X^{A}_{O_2} = \frac{X^{A}_{PPMM}}{10^6 L}$$

Where L is the optical path length of the laser beam (m). The final equation is:

$$\dot{Q}_{OC} = E\rho_0 \frac{M_{O_2}}{M_{AIR}} \frac{\left(X^{0}_{PPMM} - X^{A}_{PPMM}\right)}{10^6 L} \dot{V}_T \tag{2.17}$$

Equation 2.17 is used to calculate the heat release rate with the SCALA using the oxygen consumption method, without using a calibration constant.

2.2.2.2 Method B: Using a calibration constant (OC,K)

This method is used by Filipczak et al. (2005), and is based on the OSU calibration procedure for configuration A (ASTM E906 / E906M-10, 2010). With this method, the constants are grouped in one constant which is determined experimentally during the calibration procedure. With the calibration constant and the oxygen concentrations, the heat release rate can be calculated. This is expressed in Equation 2.18.

$$\dot{Q}_{OC,K} = K_{OC}\left(C^{A}_{O_2} - C^{0}_{O_2}\right) \tag{2.18}$$

Following Filipczak et al. (2005) the oxygen concentrations $C^{A}_{O_2}$ and $C^{0}_{O_2}$ are expressed as percentages, where the first term is the oxygen concentration at the analyzer during the test and the second term the is oxygen concentration at the beginning of the test (before ignition). The term K_{O_2} is the calibration constant determined experimentally. Replacing $C^{A}_{O_2}$ and $C^{0}_{O_2}$ with the variables $X^{A}_{PPMM} \cdot 10^{-4} \cdot L^{-1}$ and $X^{0}_{PPMM} \cdot 10^{-4} \cdot L^{-1}$ respectively, in Equation 2.18:

$$\dot{Q}_{OC,K} = K_{OC}\frac{\left(X^{A}_{PPMM} - X^{0}_{PPMM}\right)}{10^{4}L} \tag{2.19}$$

The differences between C_{O_2} and X_{O_2} is that the first one is in percentage, and the second one is the mole fraction (between 0 and 1). This distinction has been made with the purpose of comparing the calibration constant obtained in this study with the one calculated by Filipczak et al. The oxygen calibration constant represents an experimental way to calculate the constants showed in the method A. This method is discussed in section 4.3.2.

2.2.3 Mass loss rate method (MLR)

Equation 1.8 is used to calculate the heat release rate based on the mass loss rate method. It is assumed that complete combustion is achieved, this means that $\chi = 1$. The final equation becomes:

$$\dot{Q}_{MLR} = \dot{m}\Delta h_c \tag{2.20}$$

The mass loss is measured by the precision balance. To determine the mass loss rate of burning samples and minimize the noise of the measurements, the standard of the Cone Calorimeter proposes the following five-point numerical differentiation (ASTM E1354-11b,

2011):

$$\dot{m} = -\frac{dm}{dt} \tag{2.21}$$

For the first scan ($i = 0$):

$$-\frac{dm}{dt}_{i=0} = \frac{25m_0 - 48m_1 + 36m_2 - 16m_3 + 3m_4}{12\Delta t} \tag{2.22}$$

For the second scan ($i = 1$):

$$-\frac{dm}{dt}_{i=1} = \frac{3m_0 + 10m_1 - 18m_2 + 6m_3 - m_4}{12\Delta t} \tag{2.23}$$

For the i scan, where $1 < i < n - 1$ and n is total number of scans

$$-\frac{dm}{dt}_{i} = \frac{-m_{i-2} + 8m_{i-1} - 8m_{i+1} + m_{i+2}}{12\Delta t} \tag{2.24}$$

For the second to last scan ($i = n - 1$)

$$-\frac{dm}{dt}_{i=n-1} = \frac{-3m_n - 10m_{n-1} + 18m_{n-2} - 6m_{n-3} + m_{n-4}}{12\Delta t} \tag{2.25}$$

For the last scan ($i = n$)

$$-\frac{dm}{dt}_{i=n} = \frac{-25m_n + 48m_{n-1} - 36m_{n-2} + 16m_{n-3} - 3m_{n-4}}{12\Delta t} \tag{2.26}$$

2.3 Components of the SCALA

The components of the SCALA are divided in three groups: The main operating systems, the measuring system and the secondary components. The first one provides the calorimeter with air streams, heat fluxes and cooling water flows. The second one provides the SCALA with the instruments necessary to measure different parameters. The last system provides the calorimeter with the rest of elements necessary to its proper performance.

2.3.1 Main operating systems of the calorimeter

The main operating systems of the calorimeter are the air supply system, the radiant heaters and the scale insulation system. These systems provide the calorimeter the possibility of performing different experimental scenarios. The air supply system provides the possibility of different air flows, the radiant heaters different incident heat fluxes and the insulation system makes it possible to use high incident heat fluxes. Without the insulation system the use of the radiant heaters would be very limited, because the mass balance would reach the maximum operating temperature.

2.3.1.1 Air supply system

The air supply system consists of a fan connected to a pipe that is joined to the plenum of the calorimeter. The fan provides the total air supply for the apparatus. The fan is a Turbo 250 manufactured by Blauberg. The specifications of the fan are in table 2.1.

Table 2.1: Fan specifications

Speed	Power, W	Capacity, $m^3 \cdot h^{-1}$	r.p.m.
max	188	1350	2690
min	140	1160	2360

The fan has two speeds by factory settings, but it has been fitted with a voltage regulator. The air supply can thus be regulated by changing the input voltage. The pipe that connects the fan with the apparatus has an external diameter of 3″. A reduction section had been fabricated to connect the fan with the pipe. The choice of the fan was determined principally

by the operation flow, besides other variables. The operation flow rate was determined by analyzing the flows of the standard apparatuses. The OSU uses 0.01 $m^3 \cdot s^{-1}$ of internal flow, the FPA has an exhaust flow rate between 0.035 and 0.364 $m^3 \cdot s^{-1}$, and the Cone Calorimeter has an exhaust flow rate between 0.012 and 0.035 $m^3 \cdot s^{-1}$. Finally, with the system curve and different fan performance curves, the fan was selected in order to achieve a flow of 0.048 $m^3 \cdot s^{-1}$. This value was selected by overestimating the flow rates of the Cone Calorimeter and the OSU, and it is above the minimum flow rate of the FPA. The system curve and the fan performance curve are plotted in Figure 2.3. The real air flow is calculated empirically during each calibration procedure. The system curve do not consider the radiation shield and the air diffuser described in Section 2.3.3. These two elements are not definitive, their design will be changed and improved in the future. The system curve corresponds to the unchangeable structure of the calorimeter. Is the maximum achievable flow using the Turbo 250 fan.

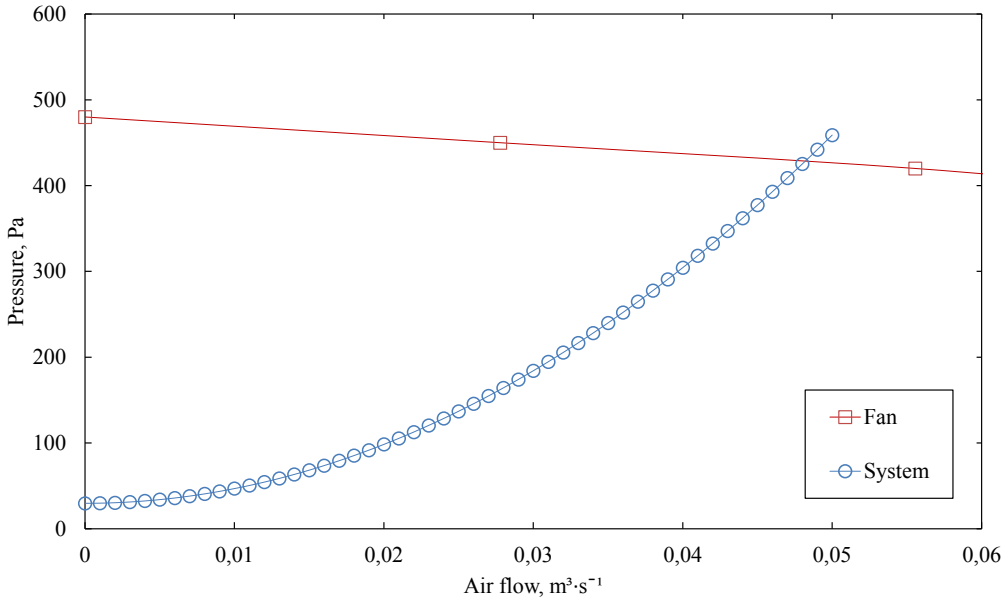

Figure 2.3: Graph of the system curve and the fan curve

Flow measurement methodology The flow measurements are performed with a Pitot tube. This is a temporary method, as it will be later performed with an orifice plate. The measurements are conducted in the final section of the pipe, letting the flow develop its

velocity profile along the pipe. The cross section is divided in 7 points along the z axis. The Pitot tube is set in the position of each point and records the velocity for 10 seconds. Figure 2.4 shows the cross section with the 7 points. The recorded velocities should be time averaged and then multiplied by the corresponding area. The sum of the flows gives the total flow.

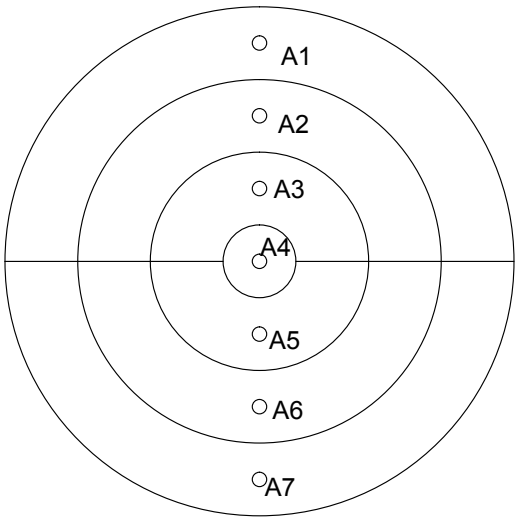

Figure 2.4: Cross section of the pipe with the positions for flow measurements

Along 3 months in different days, the flow was calculated with the methodology described above. The average air flow is 0.051 $m^3 \cdot s^{-1}$, with a relative standard deviation of 1.63 %. Note that the measured air flow is higher than the calculated design flow (0.048 $m^3 \cdot s^{-1}$). Figure 2.5 shows the velocity profile of the measurements. The error bars in the figure correspond to the standard deviation of the measurement performed.

Variation of the air flow due modifications of the apparatus The air flow decreased due the pressure drops generated because of the addition of new elements inside the ducts and because of air losses to the surroundings. Two elements have been added: An air diffusor in the inlet of the plenum, and a radiation shield in the inlet of the exhaust duct. These two elements were not considered to calculate the design flow rate, because they are provisionally in the machine. With the design improvements of these two elements and by improving the sealing of the calorimeter, the air flow is expected to increase. All the

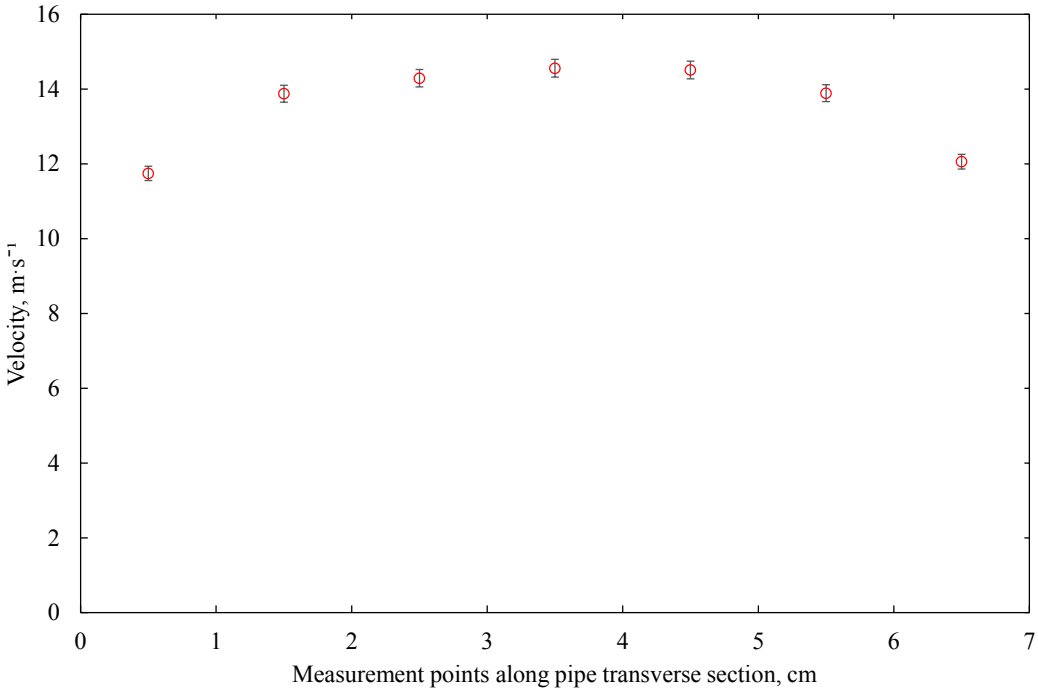

Figure 2.5: Velocity profile of the air flow through the pipe

experiments discussed in this work were performed with an air flow rate of 0.013 $m^3 \cdot s^{-1}$.

2.3.1.2 Radiant heaters

Calorimeters have radiant heat source systems, capable of providing external incident heat fluxes on the specimens under study. The heat source of the SCALA is capable to provide a heat flux between 0 and 50 $kW \cdot m^{-2}$ on the specimen area. Table 2.2 compares the heat source and power capacity of standard calorimeters with the SCALA.

Table 2.2: Rediant heat source systems of different calorimeters

Calorimeter	External heaters	External heat flux, kW/m^2
SCALA	Electrical resistance elements	0 – 50
OSU	Electrical resistance elements	0 – 80
Fire Propagation Apparatus	Tungsten-quarz	0 – 110
Cone Calorimeter	Electrical coils	0 – 100

The SCALA has 2 radiant heating panels made of 4 U-Type silicon carbide (SiC) heating elements each one. The SiC heating elements are manufactured by Zhengzhou

LEPE Refractory Materials Co., LTD. Figure 2.6 shows 4 of the resistances described above. The nominal resistance is 4.1 ohms. This is calculated by measuring the voltage and the current of the elements when they achieve a surface temperature of 1000°C. Annex refsicelements shows the calculations performed to determine the nominal resistance of the heating elements. A K-type thermocouple is attached to the surface of the heating elements to monitor the surface temperature.

Figure 2.6: U-type silicon carbide resistences

The structure of the heaters was designed with the Autodesk Inventor software. The drawings are attached in annex D.1. Figure 2.7 shows the design in Inventor. The aim of the design was to hold the heating elements without applying to much pressure to them and to direct the heat to only one direction. This was achieved by using refractory ceramic fiber blanket and ceramic fiber boards. Both types of ceramic fiber have a thickness of 25 mm. The ceramic fiber blanket is Kaowool HP 1260. It has a density of 96 $kg \cdot m^{-3}$ and a thermal conductivity of 0.15 $W \cdot m^{-1} \cdot K^{-1}$ (CarboChile, 2015b). The board is manufactured by Morgan Thermal Ceramics. The model is Ceraboard 100. It has a density of 310 $kg \cdot m^{-3}$ and a thermal conductivity at 1000 °C of 0.2 $W \cdot m^{-1} \cdot K^{-1}$ (CarboChile, 2015a). Both types allows a maximum temperature of 1260 °C.

The structure of the heaters is made of 2 mm thick stainless steel. Each heater consists of one principal structure that supports the heating elements, one plate used for holding them to the principal structure with 4 cap screws, and ceramic fiber to insulate the SiC

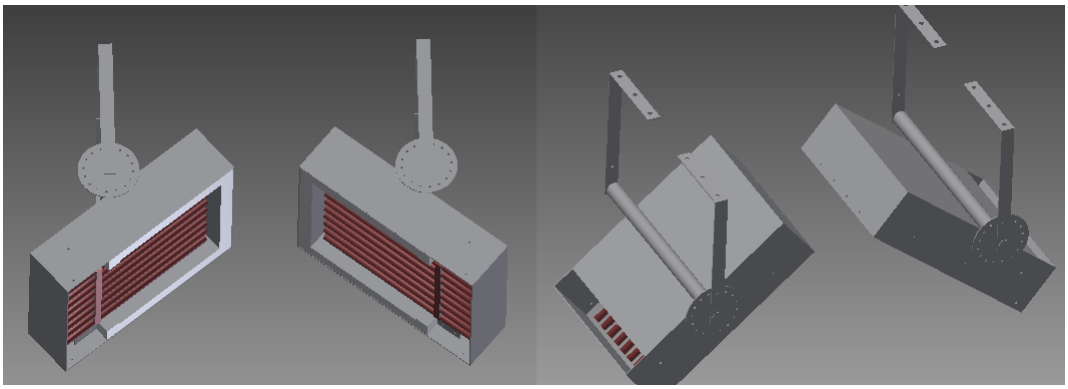

Figure 2.7: Design of the heaters

elements. Figure 2.8 shows the parts of the heater.

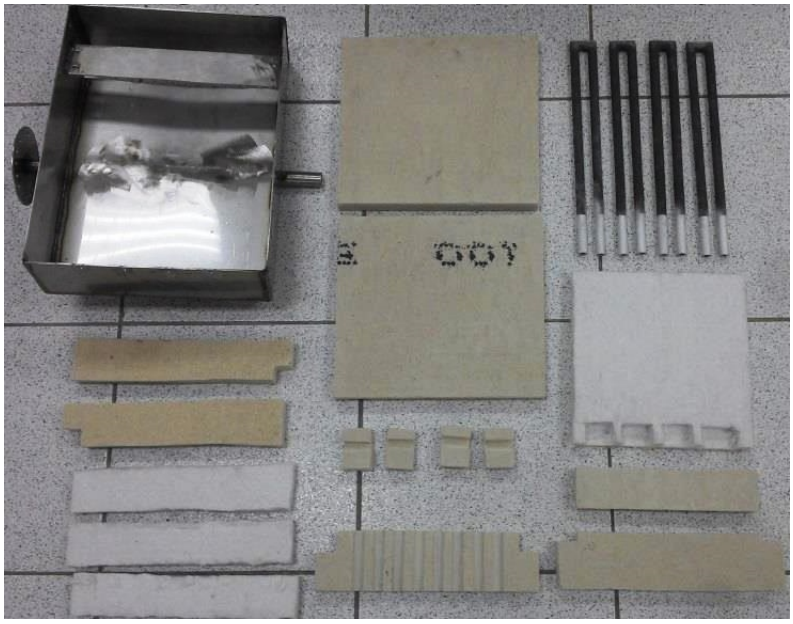

Figure 2.8: Heater elements

The electrical connection of the heating elements is made with high temperature resistance materials. The connection with the SiC heating elements is done with connecting braids specially made for them. These connecting braids endure high temperature and do not oxidize nor deteriorate along time. The detailed assemble of the radiant heaters is specified in annex D.3.

The total power supply of the heaters is 9.59 kW. By controlling the surface temperature

of the heating elements, the incident heat flux is controlled. The surface temperature is controlled by regulating the power of the heaters. This is done by using a voltage regulator. Each pair of resistances is in serial connection and is linked to a voltage regulator and then plugged to the power supply. Thus the incident heat flux on the specimen is regulated by varying the voltage in the voltage regulator (See figure 2.9). The screen shows a scale between 0 to 100 of the total voltage, where 0 corresponds to 0 volts, and 100 is the total voltage of 220 volts. The relationship between the voltage and the scale of the regulator is not linear. It was determined experimentally.

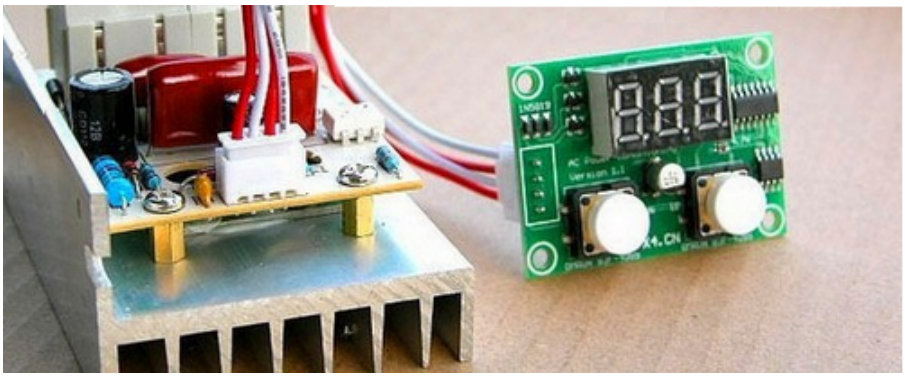

Figure 2.9: Voltage regulator

Figure 2.10 shows the relationship between the total current supply of the heaters and the incident heat flux on the specimen (See equation 2.8). There is a linear relationship between both variables in the range of 35 A and 68 A with R^2 = 99.38 %. Figure 2.10 also shows the relationship between the power supply of the heaters and the incident heat flux on the specimen. There is a linear relationship between both variables in the range of 1.9 kW and 9.6 kW with R^2 = 99.09 % Equation 2.28 shows this relationship.

$$I_{supply} = 0.97\dot{q}''_{inc} + 20.10 \tag{2.27}$$

$$P_{supply} = 0.21\dot{q}''_{inc} - 1.36 \tag{2.28}$$

Where $\dot{q}''_{inc}$ is the incident heat flux on the specimen (kW·m^{-2}), P_{supply} is the power supply (kW), determined experimentally by measuring the voltage and current of the heaters,

and I_{supply} is the total current consumed by the heaters (kW). Both equations should be used as a reference, for design purposes.

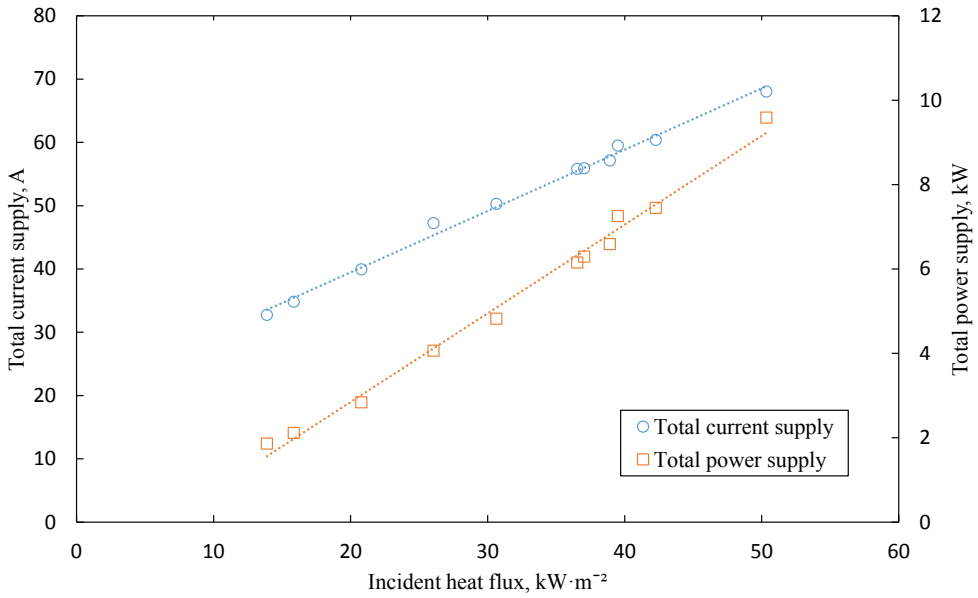

Figure 2.10: Total power and total current supply at of the heaters at different incident heat fluxes

Since the nominal resistance value has a variability because of fabrication errors, the values of the voltage regulator screen are not the same for all the pairs of SiC heating elements to produce the same power. Therefore the voltage regulator values and the incident external heat flux were experimentally determined and tabulated (See table 2.3). The voltage of each SiC heating element pair has been regulated so that all SiC elements pairs power are as similar as possible between them. This is done at each level of incident heat flux. The resistance of the elements changes with temperature variations, therefore the resistance of each element pair was calculated at each power supply level. The standard deviation and the average of the resistances at each power supply level was calculated. The highest relative standard deviation of all the levels was 12.74 %.

The nomenclature (x, y, z, w) in the "Regulator Value" cells in table 2.3 correspond to:

- x: voltage regulator of the pair of resistances located in the front of the apparatus, left heater.

Table 2.3: Voltage regulator values for different heat fluxes

Regulator Value, %	Power, kW	Current, A	Incident heat flux kW·m^{-2}
(63, 57, 62, 58)	9.6	68.1	50.3
(57, 53, 55, 53)	7.4	60.4	42.3
(56, 52, 54, 52)	7.3	59.5	39.5
(53, 50, 52, 50)	6.6	57.2	38.9
(52, 49, 51, 49)	6.3	55.9	37.0
(52, 48, 50, 48)	6.2	55.8	36.6
(46, 43, 44, 43)	4.8	50.3	30.6
(40, 37, 40, 39)	4.1	47.2	26.1
(36, 33, 35, 33)	2.8	39.8	20.8
(32, 30, 32, 30)	2.1	34.8	15.9
(29, 28, 29, 31)	1.9	32.8	13.9

- *y*: voltage regulator of the pair of resistances located in the back of the apparatus, left heater.
- *z*: voltage regulator of the pair of resistances located in the front of the apparatus, right heater.
- *w*: voltage regulator of the pair of resistances located in the back of the apparatus, right heater.

These values should be used as a reference, as the values could change over time. To achieve better results, the incident radiation is always measured before each test. For a better uniformity in the heat flux distribution at the specimen area, the voltage and current of each heater is measured. Then the voltage regulator is adjusted to achieve similar power at each heater.

2.3.1.3 Scale insulation system

The scale insulation is required for maintaining the scale temperature below the maximum operating temperature. It is made of two main parts: an insulation box and a water cooling system.

Insulation box The insulation box has two main purposes. The first one is to insulate the precision balance from the high heat fluxes emitted by the heaters. It also works as a

structure to hold the water supply system. The second main goal of the box is to avoid the entrance of air flows to the area where the sample holder is positioned on the scale. The high accuracy of the precision balance exposes it to measurement perturbations when air flows around the sample holder.

The main structure of the box is a stainless steel plate that holds the rest of the components. Below the metal sheet there are ceramic fiber blankets and ceramic fiber boards. The properties of both types of ceramic fiber are described above, in section 2.3.1.2. Figure 2.11 shows the structure of the insulation box.

Figure 2.11: Insulation box

The boards are glued to each other and to the metal sheet using high temperature silicone (up to 300°C). The blankets are held between the boards and the metal plate. Two ceramic fiber blankets are placed on the top surface of the box to increase the insulation of the scale. The total insulation thickness is about 150 mm on the top, 50 mm on the sides and 25 mm on the bottom of the box.

Water cooling system Inside the insulation box there is a system of copper pipes, with coil shape. Figure 2.12 shows the system. Through the pipe flows water that comes from the faucet. The cooling water passes first through the Schmidt-Boelter radiometer and then through the insulation box.

The box has a hole to let the metal tube of the sample holder pass to the outside. The metal tube acts like a thermal bridge, increasing the temperature at the inside. Aluminum sheets wrap the pipes to improve the heat transfer. It has been determined experimentally

Figure 2.12: Insulation box with the copper pipes system

that both systems are necessary to maintain the operating temperature of the scale within the allowable limits.

2.3.2 Measuring systems

The measuring systems are all systems that perform measurements or that their outputs are used to make measurements (e.g. the photos taken by an Axis camera can be used to measure the flame height and subsequently calculate the heat release rate of the flame). The measuring systems are the precision balance, the thermocouples with its data acquisition system, the TDLAS instrument and the Axis camera.

2.3.2.1 Precision balance

The aim of the scale is to measure the mass of the sample during a test. Thus the mass loss of solid and liquid burning fuels can be obtained. The mass loss rate can be calculated, and by this the heat release rate of the burning fuel (if the net heat of combustion is known).

The scale is a PS 1000/X manufactured by RADWAG. It has a resolution of 1 mg and a capacity of 1000 g. Table 2.4 shows the scale characteristics presented in the SCALA, Cone Calorimeter and Fire Propagation Apparatus. It works in a temperature range of 10°C and 40°C, with an ambient humidity between 35% and 80% (RADWAG, 2011). Figure 2.13 shows the dimensions of the scale. The pan has attached a metal tube that holds the sample holder.

The scale communicates with the computer using RS-232 ports. A Matlab code is

Table 2.4: Scale characteristics presented in the SCALA Cone Calorimeter and Fire Propagation Apparatus (Babrauskas, 2016; ASTM E2058-03, 2003).

	SCALA	Cone Calorimeter	Fire Propagation Apparatus
Load cell capacity (g)	1000	500	1000
Load cell resolution (g)	0.001	0.005	0.1

used to establish the communication. The output data are the mass measured and the corresponding time of the measurement. A Visual Basic code is used to process the data. The Visual Basic code is in Annex E.1.

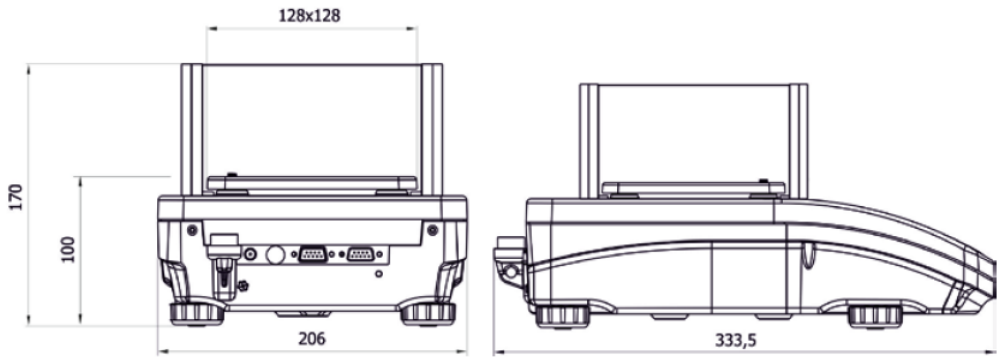

Figure 2.13: Scale dimensions (RADWAG, 2011)

The scale is placed inside the calorimeter. Thereby the maximum operation temperature is a significant parameter considering the high temperatures inside the chamber. It should be monitored during the test. Over the scale the insulation box with the cooling system is placed. This avoids that the temperatures inside the box increase above the operating limit. If the temperature inside the box approaches the maximum operating value, the test should be concluded.

When the scale is plugged to the power supply, it immediately makes an internal calibration. After that and before the first 10 minutes of being powered, it will do a second calibration. Until it has done the two calibrations, no mass should be set on the pan. The balance should not do more automatic calibrations.

Problems and solutions with the precision balance: There are some common reasons by which the scale can give spurious measurements. If the mass of the sample starts to increase instead of decreasing, the pan has probably been moved out of its position. The heaters should be turned off, and then the pan should be set to its right position. If the pan is in its right position and there is no response of the scale, the balance is probably doing an internal calibration. If so, the mass should be removed from the pan and it should be replaced after the calibration is over. Sometimes the precision balance send meaningless symbols. The Visual Basic code will not take into account those strings.

2.3.2.2 Thermocouples

K-type thermocouples of 0.5 mm diameter are adhered to specific zones of the apparatus. Three PVC insulated thermocouples are positioned at the top of the exhaust duct, in the same axis, parallel to the longest side of the duct, with one of the thermocouples at the center. There is a flat temperature profile in the exhaust duct. Thus only the center thermocouple is used to monitor the temperature of the exhaust gases and calculate the heat release rate with the SER method.

One thermocouple is positioned inside the insulation box, as mentioned before, to monitor the temperature near the scale. One more is attached to the external metal wall of the exhaust duct at the same level of the TDLAS, and at the top of the apparatus. This thermocouple has two aims:

- To know the influence of the metal temperature on the exhaust gases and the 3 thermocouples at the top. If the temperature of the metal duct is higher than the temperature of the exhaust gases and hence the temperature of the 3 thermocouples, the temperature of the gases and of the stack thermocouples will increase. In other words, if an experiment is being executed and the metal wall is heated to high temperatures and then the heat release rate of the sample decreases, then the duct thermocouple readings will decrease slower than the decrease in HRR. This is because of the thermal inertia of the metal walls and leads to wrong HRR calculations.

- To know the temperature near the TDLAS sensors, to make sure they are within the operating range.

There are also thermocouples attached to other metal parts, glass windows and to aluminum profiles of the SCALA structure. One thermocouple is positioned at the air inlet. Two thermocouples are attached to the electrical resistances of the radiant heaters. They are fiberglass insulated to endure higher temperatures, and have a diameter of 1 mm. The aim of these two thermocouples is to monitor the temperature at the surface of the heating elements, and thus make relationships between the heater temperature, heater power and incident heat flux on the sample.

The thermocouples are attached to miniature thermocouple connectors and plugged to DAQs. There are 2 DAQs: one suitable only for thermocouples, and an universal DAQ. The DAQs are QuantumX modules manufactered by HBM. The software used as interface is the Catman Easy. Figure 2.14 shows the interface of the software. The software plots the data in real time. The data then is exported in .xlsx format and is processed in with the software Microsoft Excel.

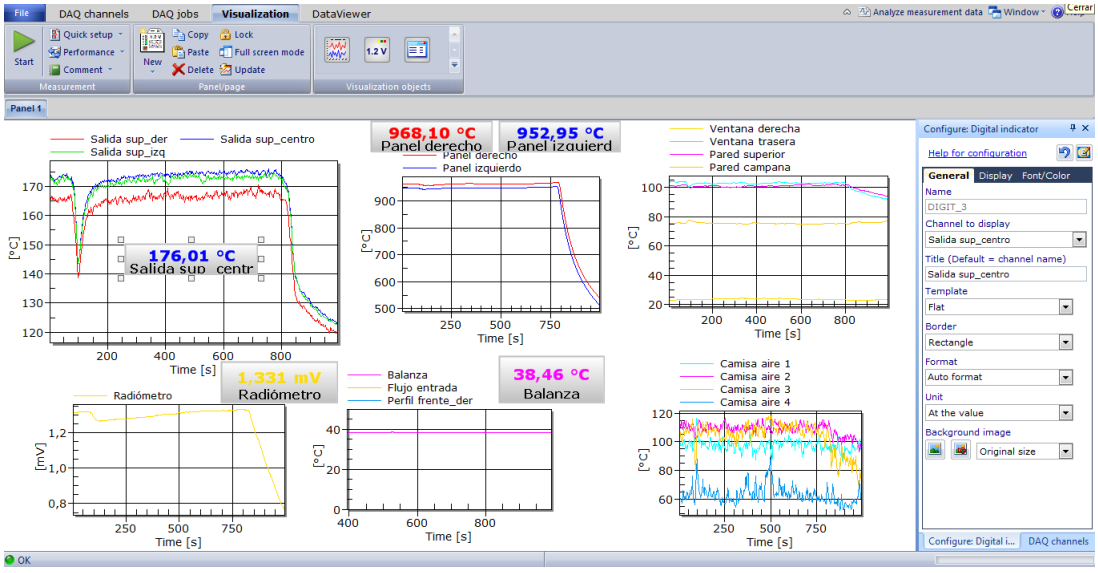

Figure 2.14: Catman Easy: software of the QuantumX modules

2.3.2.3 Tunable Diode Laser Absortion Spectroscopy (TDLAS) instrument

The TDLAS technique is based on light extinction by gaseous species that are present in the exhaust gases. There are two modules that work with two different species: oxygen and carbon monoxide. The carbon monoxide module is not available for the moment, but it will be made operational in the future. The TDLAS apparatus is a Spectra-1 manufactured by PKL Technologies Inc. The TLDAS module consists of the DAQ and two more modules, one that generates the laser beam and the receiver of the laser beam (Figure 2.15). These two modules are mounted in the stack. Specifically, the laser is generated within the DAQ, and then it goes to the emitting module through the fiber optics. The technique of the TDLAS is based on the Beer-Lambert law (John R. Howell, 2016) presented in equation 2.29

$$I_\lambda(L) = I_\lambda(0)e^{-\kappa(\lambda)L} \tag{2.29}$$

Where λ is the wavelength of the light source, $I_\lambda(0)$ is the initial intensity of the radiation, $I_\lambda(L)$ is the intensity of the radiation after it passes through the distance L, and $\kappa(\lambda)$ is the absorption coefficient of the medium.

The Spectra-1 software is used to start and stop recording, and for visualization of the data. Figure 2.16 shows the interface of the software. The signal intensity of the laser should be in the range of 30% and 80% (PKL Technology Inc., 2015). It can be regulated by moving 3 different screws in the back of the laser transmitter module to align the laser beam with the photodiode.

There is the option to record the data in ppm and in ppmm. The relationship between both is in Equation 2.30:

$$PPM = \frac{PPMM}{L} \tag{2.30}$$

L is calculated experimentally by letting the Spectra-1 recording for determined time in

Figure 2.15: Spactra-1 module (PKL Technology Inc., 2015)

different occasions. Then the values are averaged and divided by the PPM of oxygen. The calculated value is $L = 0.322$ with a RSD (Relative Standard deviation) of 0.87 %.

2.3.2.4 Network camera

An Axis network camera is positioned in front of the calorimeter, pointing to the specimen area. It takes photos in variable intervals. The photos have the computer time included. So, with the photos it can be determined the time when the sample enters the chamber, the time to ignition, time to extinction, and also the flame behaviors can be compared with measurements recorded by the TDLAS, precision balance or with the thermocouples. With the photos the height of the flame can be determined , and thus the heat release rate of the flame can be estimated.

2.3.2.5 Radiometer

A Schmidt-Boelter heat flux sensor is used to determine the incident heat flux above the specimen area. The radiometer is water cooled. It is capable of measuring heat fluxes from 0 to 100 kW·m^{-2}. The radiometer is placed at the center of the specimen area and the incident heat flux is measured before each test. This is performed manually. In the future,

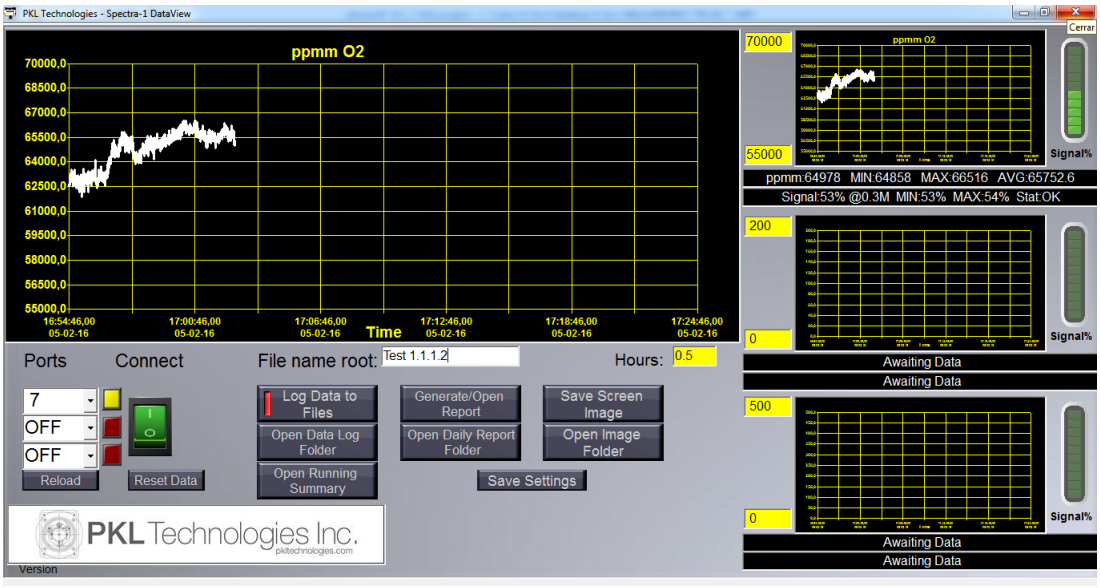

Figure 2.16: Spactra-1 interface of the software

the radiometer will be attached to a mechanical arm that will place the sensor in the right position.

2.3.3 Secondary components

This section is about components of the SCALA that are operative, but their design should be improved to achieve better results. The function of each component is important for the proper behavior of the calorimeter.

2.3.3.1 Sample holder

The sample holder is necessary to hold the specimen during all the duration of the test. It should resist high heat fluxes without deforming. The sample holder has a bolt placed at the bottom of it. The screw should be introduced into the hole of the metal rod embedded to the pan of the scale. The screw was sanded to avoid becoming trapped with the metal rod. The sample holder is shown in figure 2.17.

There is a piece of ceramic fiber board at the bottom of the specimen holder. This is to minimize the conduction heat from the sample holder to the metal rod, and thus to avoid the heating of the inside of the insulation box and also ensure that the boundary condition at the back of the specimen is adiabatic. If the sample size is too low, and the height of the

Figure 2.17: Sample holder

sample is lower than the height of the sample holder , then ceramic fiber blankets are used to increase its height and make sure that the top of the sample is at the same height as the rim of the sample holder. The specimen holder is made of a mesh with a porosity of 41%. The diameter is 100 mm.

2.3.3.2 Insulation cube

The insulation cube is a small cube made of ceramic fiber board and ceramic fiber blanket. This shield is set above of the metal rod of the pan. Its aim is to avoid heat transfer from the heaters to the metal rod. Great part of the heat that enters the insulation box is because of the metal rod. it is the only part of the insulation box that do not have permanent insulation. The insulation shield is used until the apparatus reach the steady state. The height of the cube with the radiometer on it, is the same as the height of the sample holder, so it is also used to measure the radiation before the test.

2.3.3.3 Radiation shield

The radiation shield is a metal piece with many holes placed in the inlet of the exhaust duct. It is above the flames. Its aim is to prevent the flame radiation affect the thermocouple readings. The holes let the air flow and combustion gases pass to the exhaust duct. It creates a considerable pressure drop, but it also serves as a flow straightener to ensure that the

temperature and concentration profiles at the top of the exhaust duct are flat.

2.3.3.4 Air difusser

The air diffuser is a metal piece with many holes placed at the inlet of the plenum, at the end of the elbow that joints the air supply duct with the SCALA. The aim of this component is to realign the air flow and to distribute it in all directions. At the moment, there are greater air flows in specific directions. This will be improved in the future. The air diffuser will be redesigned with the aim of achieving an homogeneous air distribution. It crates a considerable pressure drop.

2.4 Calibration

In the following sections the calibration procedures of the sensible enthalpy rise method and the oxygen consumption method will be described.

2.4.1 Sensible enthalpy method calibration

There are two calibration procedures: The daily and weekly calibration procedure. Both methods should give similar calibration constants. A Bunsen burner is used in both calibration procedure. The calibration fuel is ethylene.

2.4.1.1 Daily calibration

This procedure is similar to the OSU calibration in configuration B. There is no external heat flux during this calibration procedure. Two different gas flows are used: a high flow and a low flow. The gas flow should increase and decrease continuously to the high and to the low value for intervals of 4 minutes respectively. This should be repeated until the apparatus temperatures reach steady state and no temperature variations in the thermocouple are seen for each gas flow (Compare the thermocouple value recorded during the last and the second to last high flows, the same for the low flow). The difference of the high flow and the low flow is multiplied by the net heat of combustion, and the heat release rate of the methane flame is obtained. Then the high value recorded by the thermocouple and the

low value are subtracted, and the heat release rate is divided by the result. This value is the calibration constant. This is expressed in the following equation:

$$K_{SER,D} = \frac{(\dot{m}_{high} - \dot{m}_{base})\Delta h_c}{T^{ss}_{high} - T^{ss}_{base}} \tag{2.31}$$

2.4.1.2 Weekly calibration

This calibration procedure is based on the OSU configuration A calibration (ASTM E906 / E906M-10, 2010). The gas used for calibrating the calorimeter is ethylene, with a net heat of combustion of 47.2 MJ·kg^{-1}, ρ = 1.19 kg·m^{-3} (The Engineering ToolBox, 2016). The heaters are set to a 20 kW·m^{-2} incident heat flux.

The first step is to turn on the heaters and wait until the apparatus reaches steady state. Then the ethylene flame is turned on and set to a flow of 1 L·min^{-1}. This is the base line. The ethylene flow is increased to higher levels and subsequently decreased to the base line. The flows and HRR used in the calibration are described in Table 2.5.

Table 2.5: HRR and flow variation for the calibration procedure

Time interval, min	0	2	4	6	8	10	12	14	16	18
Flow, L·min^{-1}	1	3	1	5	1	5	1	4	1	3
HRR, kW	0.94	2.81	0.94	3.74	0.94	4.68	0.94	3.74	0.94	2.81
Effective HRR, kW	0	1.87	0	2.81	0	3.74	0	2.81	0	1.87

The effective HRR is the HRR calculated with the baseline 0.94 kW (1 L·min^{-1}) as reference (see Table 2.5). Each gas flow setting should last for 2 minutes, and the temperature at the exhaust duct thermocouple should be recorded and averaged for the last 10 seconds of each interval. Then, applying equation 2.32, the calibration constants K_i are calculated:

$$(\dot{m}_i - \dot{m}_{base})\,\Delta h_c = K_{SER,i}\,(T_i - T_{base}) \quad i \in (3,4,5,4,3) \tag{2.32}$$

Finally, the five calculated constants K_i are averaged and the average becomes the calibration constant K_{SER}:

$$K_{SER,W} = \frac{\sum_{i=1}^{5} K_{SER,i}}{5}$$

According to the OSU standard the relative standard deviation of the 5 constants should be less than 5%. Figure 2.18 shows the behavior of the measured heat release rate during the calibration. The weekly and daily calibration constants should be of similar magnitude.

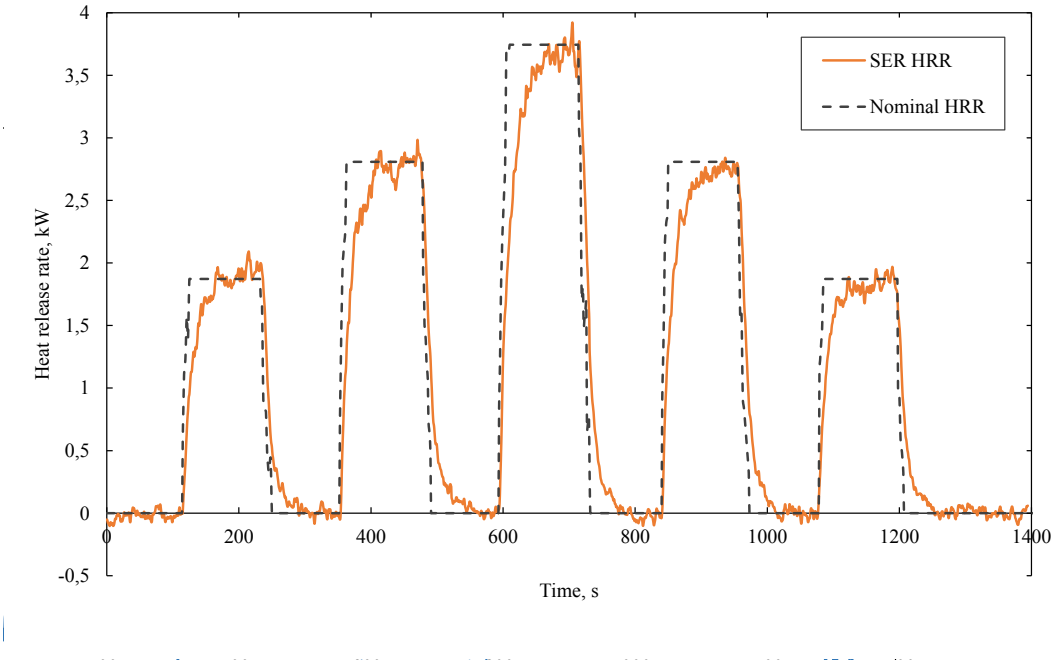

Figure 2.18: Sensible heat method calibration

2.4.2 Oxygen consumption calibration with calibration constant

In the oxygen consumption calibration procedure, as in the SER calibration procedure, there is also a daily and weekly method.

2.4.2.1 Daily calibration

The calibration methodology is the same to the sensible heat daily calibration. The oxygen concentrations should have no variations between the base heat release rates. This, because those variations in the thermocouples are explained by the thermal inertia of the apparatus, and the time it takes to reach steady state. With the oxygen consumption method there is no decrease in the oxygen concentration at a constant heat release rate. The same interval as that the SER method is considered to calculate the calibration constant.The following equation is used:

$$K_{OC,D} = \frac{(\dot{m}_{high} - \dot{m}_{base})\Delta h_c}{C_{high} - C_{base}}$$

Where C_{high} is the oxygen concentration in percentage at the high ethylene flow, C_{base} is the oxygen concentration in percentage at the base flow of ethylene.

2.4.2.2 Weekly calibration

This methodology is the same as the sensible heat weekly calibration procedure. It uses the sequence described in Table 2.5. The equations used to calculate the calibration constant are the following:

$$(\dot{m}_i - \dot{m}_{base})\,\Delta h_c = K_{OC,i}\,(C_i - C_{base}) \quad i \in (3,4,5,4,3) \tag{2.33}$$

$$K_{OC,W} = \frac{\sum_{i=1}^{5} K_{OC,i}}{5} \tag{2.34}$$

The calibration constant calculated in one calibration procedure is -2.683 kW·$\%_{O_2}^{-1}$. The calibration constant calculated for the OSU (Modified OSU with an oxygen analyzer) by Filipczak et al. (2005) is -2.5358 kW·$\%_{O_2}^{-1}$. Figure 2.19 shows the behavior of the heat release rate during the calibration of the oxygen consumption method. The weekly and daily calibration constants should be of similar magnitude.

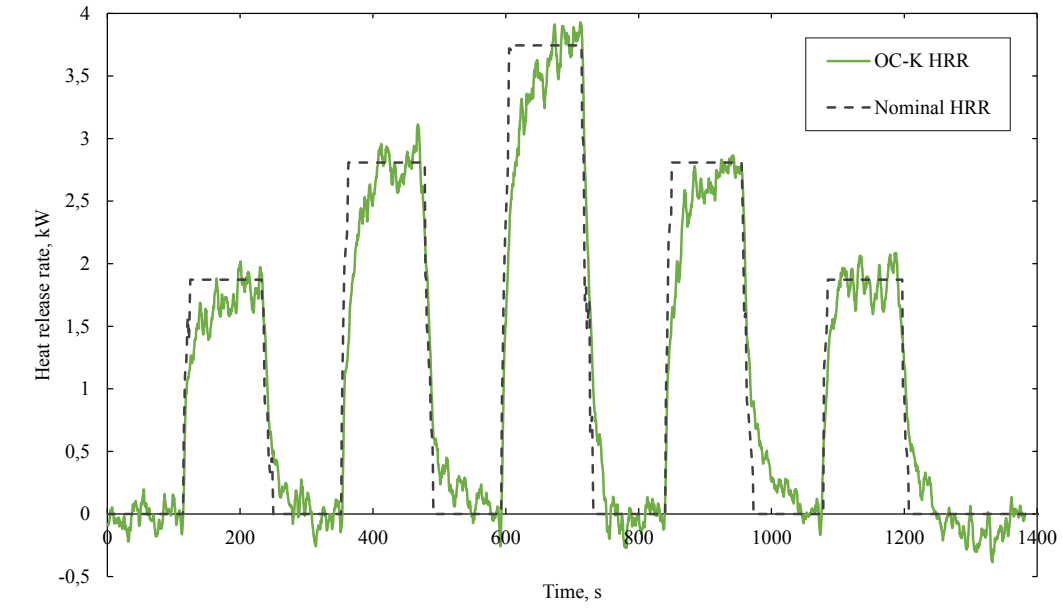

Figure 2.19: Oxygen consumption method weekly calibration

2.4.3 Oxygen consumption calibration without calibration constant

This calibration involves no calibration constant calculation. It is just a comparison between the heat release rate calculated with equation 2.17 of some burning fuel, and the known HRR of that fuel. Ethylene is used for this purpose. The nominal HRR used in sections 2.4.1.2 and 2.4.2.2 is plotted with the HRR calculated with equation 2.17.

The calculated HRR of ethylene is underestimated with the OC method. This could be explained because of the air losses through the walls of the calorimeter. The air losses can lead to differences in the mixing of air and combustion gases between different flame heights.

2.4.4 Precision balance calibration

The calibration of the mass loss measurement system is basically the internal calibration of the precision balance. The scale comes with a user guide that explains in detail all calibration procedures. It comes with 3 fixed weights that should be weighted before the

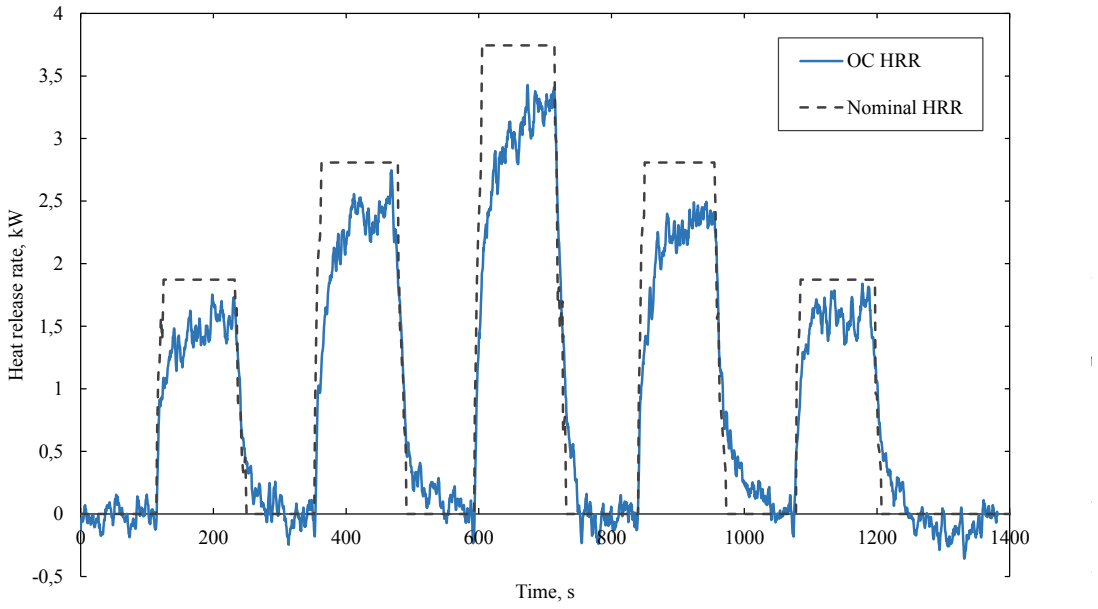

Figure 2.20: Oxygen consumption method calibration without calibration constant

tests to ensure its good performance. The weight of the loads are 1 g, 50 g and 200 g. The precision balance should be calibrated before performing experiments. It should calibrate automatically, so there is no need to do it manually.

2.5 Experimental validation with PMMA

Experiments with PMMA were performed using the SCALA with the purpose of comparing the results with tests performed with other calorimeters. PMMA was selected because of its wide use in fire tests along history. There is an extensive literature of PMMA burning rates and other characteristics of the fuel, performed with different standard calorimeters. The results of the PMMA tests are compared with the results obtained by Biteau et al. (2008). Those tests were performed using the Fire Propagation Apparatus with different calorimetric techniques.

2.5.1 Description of the tests

The tests were performed with an imposed heat flux of 30 $kW \cdot m^{-2}$. The selection was based on the experimental conditions of Biteau et al. Piloted Ignition was used in Biteau test. In contrast, in these tests there was used spontaneous ignition. Seven tests were performed in three different days. The net heat of combustion of the PMMA considered is 25 $kJ \cdot g^{-1}$ (Walters et al., 2000).

2.5.2 Experimental methodology

The PMMA samples have dimensions of $100 \times 100 \times 5$ mm. The PMMA samples were manufactured by Norglas S.A. A PMMA holder is used with a cercamic fiber blanket to increase the height of the external surface of the PMMA specimen. The air supply system is activated and the extractor is turned on. The cooling system is activated, the insulation cube is set on the metallic rod, and then the heaters are set to 30 $kW \cdot m^{-2}$ of external heat flux. The instruments are turned on, and their respective software are started. After about 1 hour, the apparatus reaches the steady state. This is controlled by checking the temperature of the central thermocouple in the exhaust duct. Before the test, the incident radiation at the specimen area is measured. After that, the insulation cube is removed, and the experiments are performed.

2.5.3 Experimental results

The results are plotted first for each experiment in a different graph. Figure 2.21 shows the heat release rate determined by the 3 different calorimetric methods in the same graph. The negative values with the SER method in the first 50 seconds of the test are caused by the door opening. The door is opened to insert the specimen in the combustion chamber. This causes a temperature decrease. Figure 2.22 shows the rest of the experimental results. Figure 2.23 shows HRR results with SER and MLR method. The oxygen consumption method has a great variability. Therefore a Savitzky-Golay filter was applied to the data (Savitzky and Golay, 1964) . Figure 2.24 shows the filtered HRR data obtained with the OC method.

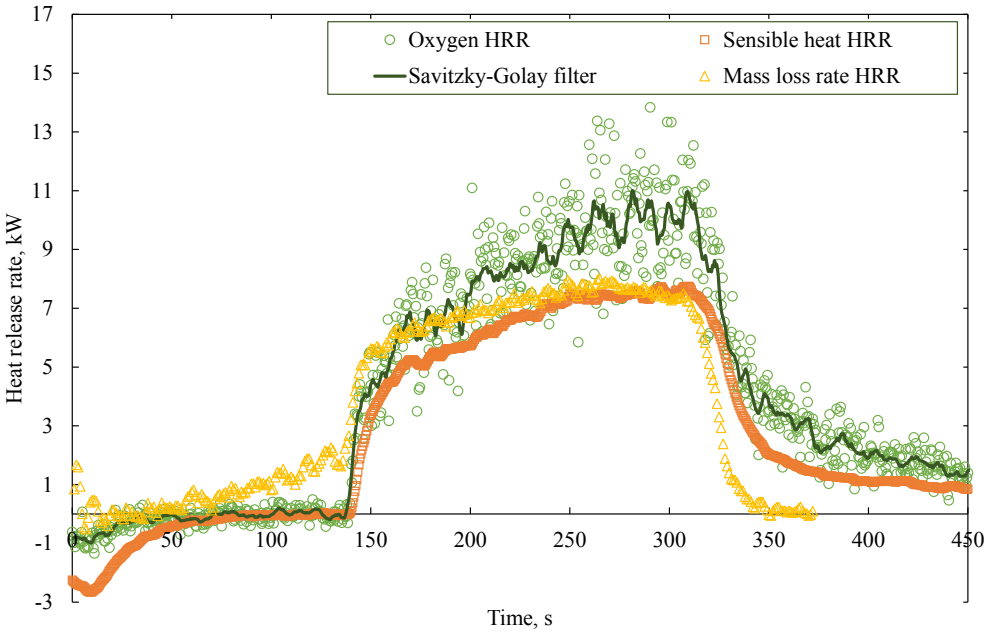

Figure 2.21: Heat release rate of PMMA at 30 kW·m^{-2}

Comparing the results obtained with the three calorimetric methods (See Figure 2.21 and 2.22) it can be seen that there is good agreement in their behavior. Table 2.6 shows the average peak HRR of all tests for each calorimetric method.

Table 2.6: Average peak HRR of all tests for each calorimetric method

	MLR method	SER method	OC method
Average peak HRR, kW	8.29 ± 0.56	7.12 ± 0.55	10.95 ± 1.5

Taking the MLR method average peak HRR as reference, the percentage difference of the OC and SER method have been calculated. The OC method results are 32 % higher than the MLR method results, and the SER method results are 14 % smaller than the MLR method results. Figures 2.21 and 2.22 show that $\dot{Q}_{OC}$ and $\dot{Q}_{SER}$ increased almost at the same time. Then at the flame extinction there is some delay in the HRR decrease of both methods. The delay times are explained in the SER method by the thermal inertia of the apparatus. The walls temperature increase with the HRR of the specimen. When the HRR of the sample starts to decrease, the walls temperature decrease at a slower rate and keep heating the product gases. For the OC method there are three possible reasons of the delay

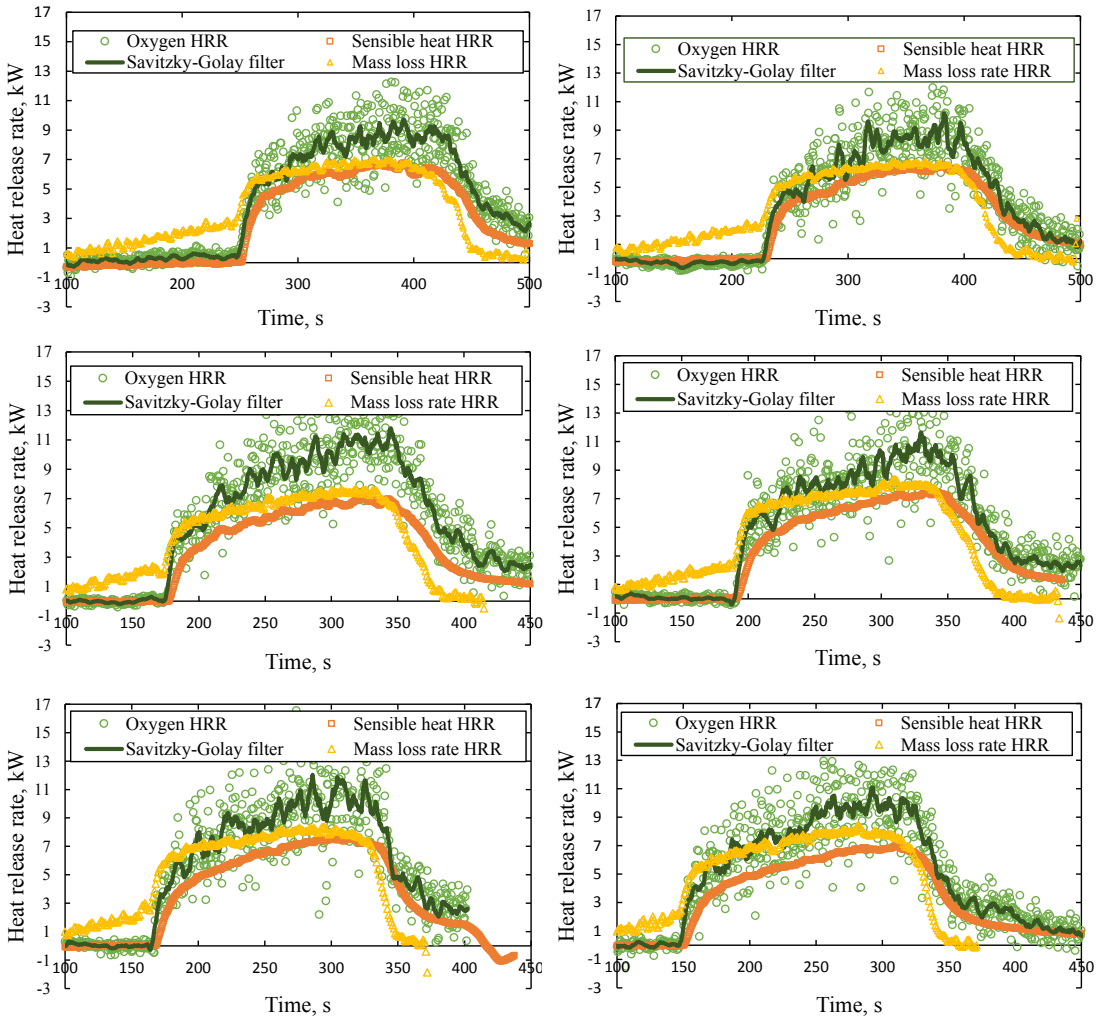

Figure 2.22: Heat release rate of PMMA at 30 kW·m^{-2} of all the tests

at the flame extinction. The first one is that part of the product gases accumulate in the combustion chamber. When the flame is extinguished, part of the product gases could keep flowing through the duct. The product gases accumulation was seen after the tests were concluded, when the window of the calorimeter was opened (Product gases got out of the calorimeter). This will be considered in the future work in section 5.1. The other possibility is that there was an unexpected drift in the oxygen measurements. The oxygen measurement drifts are explained in section 4.3.1. The third option is that the temperature changes in the exhaust gases influence the oxygen concentrations measurements. It was seen that the oxygen concentrations measurements decrease when the outlet gases temperature increases,

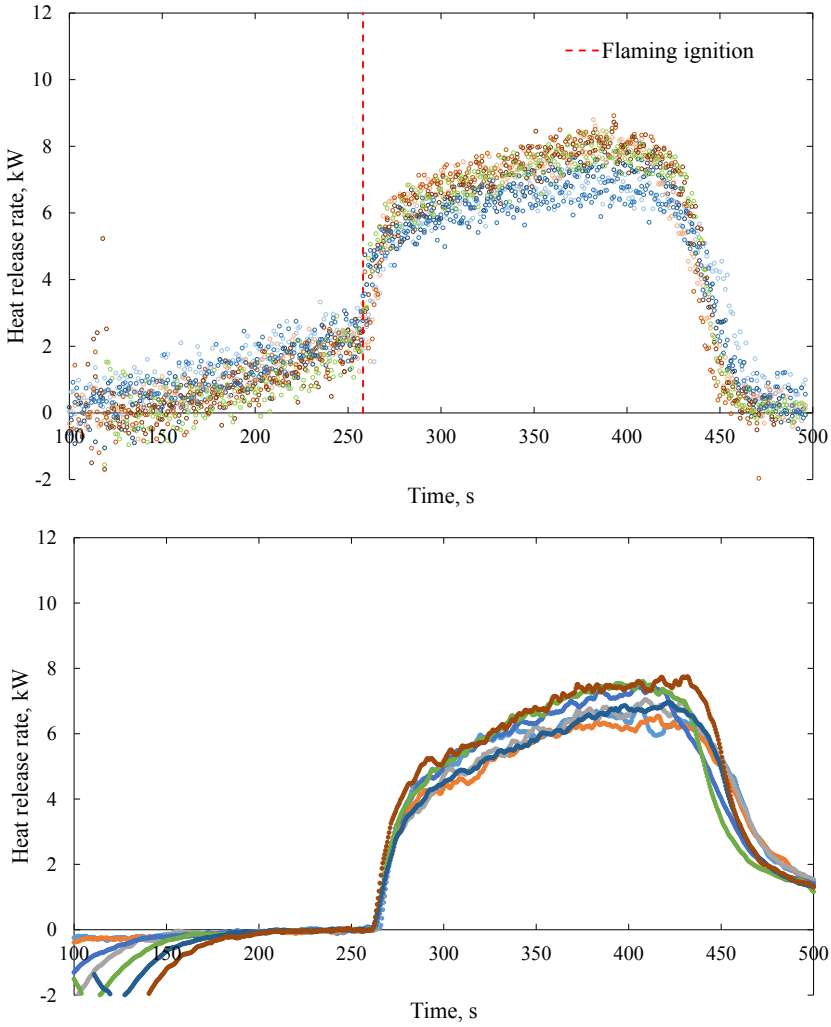

Figure 2.23: Top: HRR results with MLR method. Bottom: HRR results with SER method

and they increase when the outlet gases temperature decreases. This was seen in the heating of the calorimeter with the radiant heaters (and in the cooling of the calorimeter when the heaters were turned off). This could also explain the apparent oxygen concentrations decrease, when the window of the calorimeter was opened. The temperature differences can also explain why in the calibration procedure (Section 2.4.2.2) the HRR calculated with the OC method was underestimated and in the PMMA experiments it is overestimated. High temperatures could lead to higher influences on the oxygen concentrations measurements. Also it is known that there is a temperature dependence on the absorption coefficient in Equation 2.29 (Equation used to calculate the oxygen concentrations). This problem could

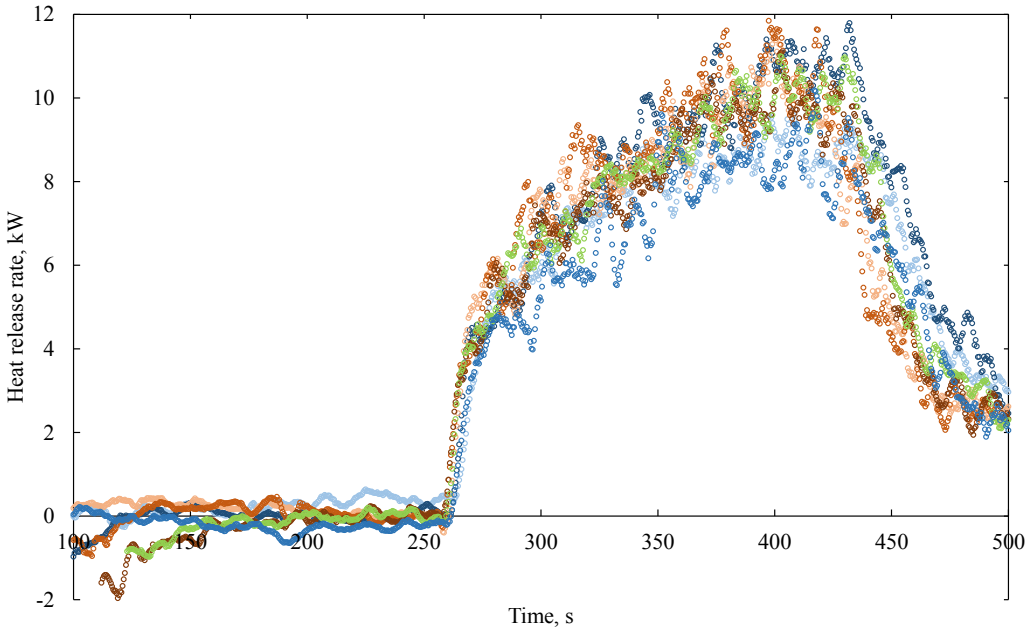

Figure 2.24: Savitzky-Golay filtered OC method results

be solved by correcting the absorption coefficient by temperature. The MLR method is taken as reference because it gives instantaneous responses about the flame behavior. This is because the use of the precision balance. The magnitude of $\dot{Q}_{MLR}$ should be taken as an upper limit, because the PMMA net heat of combustion is used. This last considered that there is complete combustion in the reaction. At the beginning of the test, the HRR calculated with the MLR method seemed to increase at a constant rate. But the first minutes there was no flaming ignition. So, the first HRR increase is actually attributed to the pyrolysis of the fuel. Flaming ignition occurs at the point where the slope of the curve increases.

The SER method uses the calibration constant determined in the calibration procedure using ethylene. If the term χ_r (fraction of the total heat release rate that is lost by radiation, see section 1.2.1.1) is not fuel independent, and in the PMMA flame is similar to the χ_r in the ethylene flame, then the calibration constant will be appropriate for the PMMA tests. At the moment there is no study of the influence of the fuel type in the χ_r term with the SCALA, but comparing the curves in the graphs it can be seen that there is good agreement

between the both terms. Comparing the behavior of each method in different tests (Figure 2.23 and Figure 2.24) it can be seen that there is good agreement between all tests.

All PMMA tests have shown that there is repeatability in the SCALA and the results are consistent. The calorimeter is validated using the three calorimetric methods. The following section compares results obtained with the SCALA with results obtained with other calorimeters.

2.5.4 Comparation with other authors

The results obtained with the SCALA are compared with the results obtained by Biteau et al. (2008) with the Fire Propagation Apparatus. The effective heat of combustion has been calculated using the mass loss rate and the HRR with the SER and the OC method (The effective heat of combustion calculation methodology and its conceptual definition is in Section refsubsec:ehc). It is compared with the net heat of combustion calculated by Walters et al. (2000). The $\dot{Q}_{MLR}$ of all the tests performed with the SCALA are compared with the $\dot{Q}_{MLR}$ of Biteau et al. test. Then the test which its $\dot{Q}_{MLR}$ behavior was more similar to the one obtained by Biteau et al was selected. The ignition times of both tests were matched. The results are compared in figure 2.25. There is good agreement between the $\dot{Q}_{SER}$ obtained with the SCALA and the $\dot{Q}_{MLR}$ calculated with both calorimeters. The $\dot{Q}_{SER}$ of the SCALA has a better agreement to $\dot{Q}_{MLR}$ (Of both calorimeters) than the $\dot{Q}_{SER}$ of the FPA. This can be explained due the calibration constant characteristics used by the SCALA. It considers the heat losses to the surroundings. The HRR calculated with the SER method by Biteau et al. considers only the convective component. The thermal inertia seemed to have greater influence in the FPA measurements than in the SCALA. The SCALA $\dot{Q}_{OC}$ magnitude is greater than heat release rates obtained with all the other calorimetric methods. But it has the same behavior. The SCALA is validated with the FPA results obtained by Biteau et al. The SER method of the SCALA gives more appropriate results than the SER method of the FPA. The OC method of the SCALA gives overestimated results, but the behavior is the same as the other methods.

Table 2.7 shows the effective heat of combustion calculated with the mass loss rate

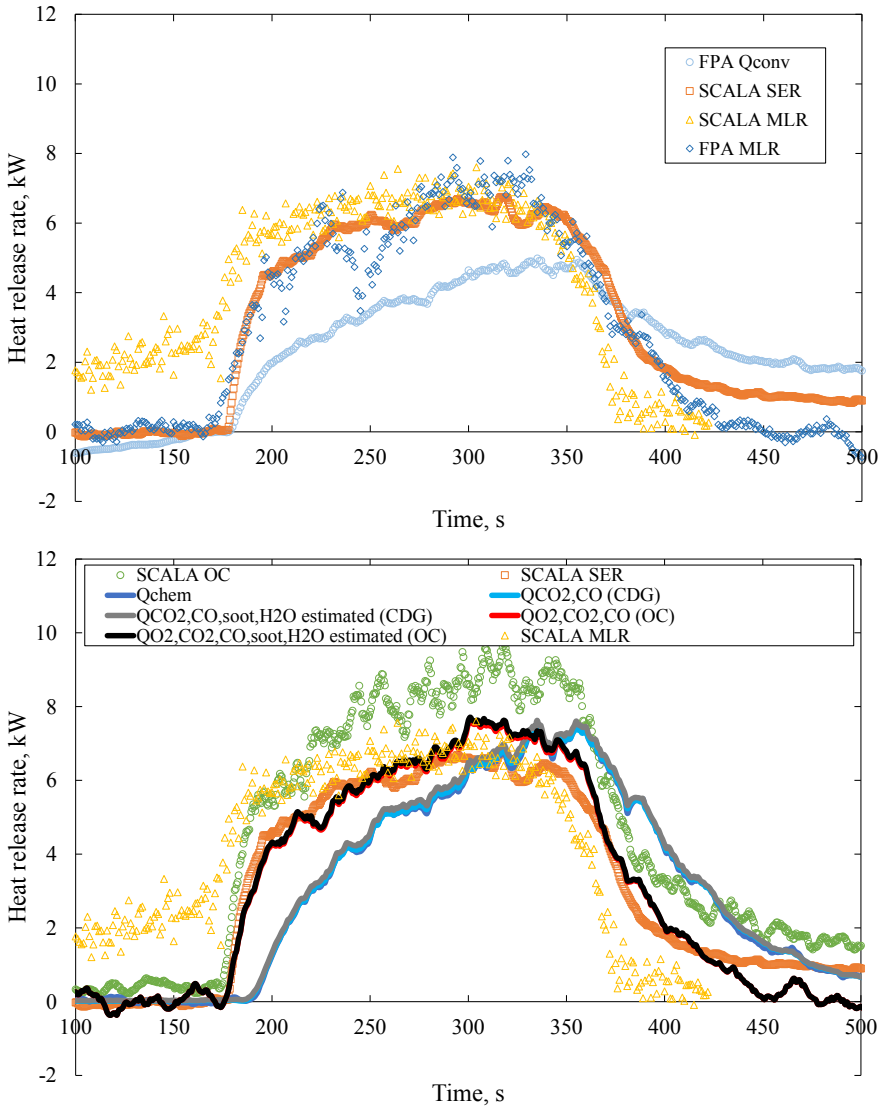

Figure 2.25: Top: Comparison of $\dot{Q}_{MLR}$ and $\dot{Q}_{SER}$ between results of Biteau et al. and this study. Bottom: Comparison of the results with all methods used by Biteau et al. and all methods used in this study

and the HRR obtained with the SER and OC method. The uncertainty correspond to the standard deviation. It is compared with the net heat of combustion calculated by Walters et al.

Table 2.7: Calculated heat of combustion of PMMA

	Walters et al	SER method	OC method
Heat of combustion, kJ·g^{-1}	25	22.42 ± 1.55	23.34 ± 1.16

Taking Walters et al. net heat of combustion calculation as reference, the heat of combustion percentage variation for the SER and OC results has been determined. For the SER and the OC method, the heat of combustion is 10 and 7 % lower than the net heat of combustion calculated by Walters et al. respectively. The effective heat of combustion calculated for the OC method, was determined considering only values that were not overestimated. In other words, only values below $\dot{Q}_{MLR}$ were considered.

2.6 Error analysis

The uncertainty of the measurements performed with the SCALA. Equation 2.35 is used to calculate the uncertainty of a function of several variables (Taylor, 1997)

$$\delta q \leq \left|\frac{\partial q}{\partial x}\right| \delta x + \cdots + \left|\frac{\partial q}{\partial z}\right| \delta z \tag{2.35}$$

Where q is the function with an uncertainty of δq, and $x, ..., z$ are the variables measured with uncertainties $\delta x, ..., \delta z$. The variables can be dependent or independent. The uncertainties can be calculated standard deviations and also values found in the literature.

2.6.1 Uncertainty of the sensible enthalpy method measurements

The uncertainty of the heat release rate measurements with the sensible enthalpy rise method is calculated by applying equation 2.35 to equation 2.2. The last equation has 3 variables with uncertainties that have to be determined; the calibration constant K_{SER}, the temperature at the steady state T_{ss}, and the temperature of the outlet gases during the test T_e.

$$\dot{Q}_{SER} = K_{SER}(T_e - T_{ss}) \tag{2.36}$$

The calibration constant uncertainty is obtained from the weekly calibration procedure

(cf. Section 2.4.1.2). It is the standard deviation of all calibration constants calculated at different ethylene flows. The relative standard deviation is calculated, by dividing the standard deviation with the average of the 5 calibration constants. In order to calculate the thermocouple uncertainty, the temperature was recorded during 10 minutes while the apparatus was in the steady state (All operating systems were turned on). The thermocouple uncertainty is calculated as the relative standard deviation of all these values. So, the uncertainty of both temperature variables are assumed to be the same as the thermocouple uncertainty. Table 2.8 shows the relative uncertainty of each variable.

Table 2.8: Relative uncertainty of the variables used to determine the HRR with the SER method

	Relative uncertainty, %
Calibration constant K_{SER}	2.64
Temperature T_e	0.43
Temperature T_{ss}	0.43

The uncertainty of $\dot{Q}_{SER}$ is calculated using Equation 2.38.

$$\delta\dot{Q}_{SER} \leq \left|\frac{\partial\dot{Q}_{SER}}{\partial K_{SER}}\right|\delta K_{SER} + \left|\frac{\partial\dot{Q}_{SER}}{\partial T_e}\right|\delta T_e + \left|\frac{\partial\dot{Q}_{SER}}{\partial T_{ss}}\right|\delta T_{ss} \tag{2.37}$$

$$\delta\dot{Q}_{SER} \leq (T_e - T_{ss})\delta K_{SER} + K_{SER}(\delta T_e + \delta T_{ss}) \tag{2.38}$$

Where the calibration constant considered is the obtained with the calibration procedure, this is 0.0717. The temperatures are varied in order to show the error at different magnitudes of heat release rate. T_{ss} (Temperature at the stack) is fixed to 163°C. This value is calculated as the average temperature registered at different incident heat fluxes. Figure 2.26 shows the total relative uncertainty, and the contribution of each variable uncertainty. The % Error is with respect to the heat release rate.

The peak heat release rates of the PMMA experiments varied between 6.8 kW and 7.7 kW. For this case, the error for the SER measurements is 5%. Biteau (2010) estimates a relative uncertainty of 7 % for the convective heat of the OSU, considering the absolute uncertainty of the constant C of the orifice plate, the pressure differential uncertainty of the orifice plate and the temperature uncertainty at the orifice plate. But this error is not

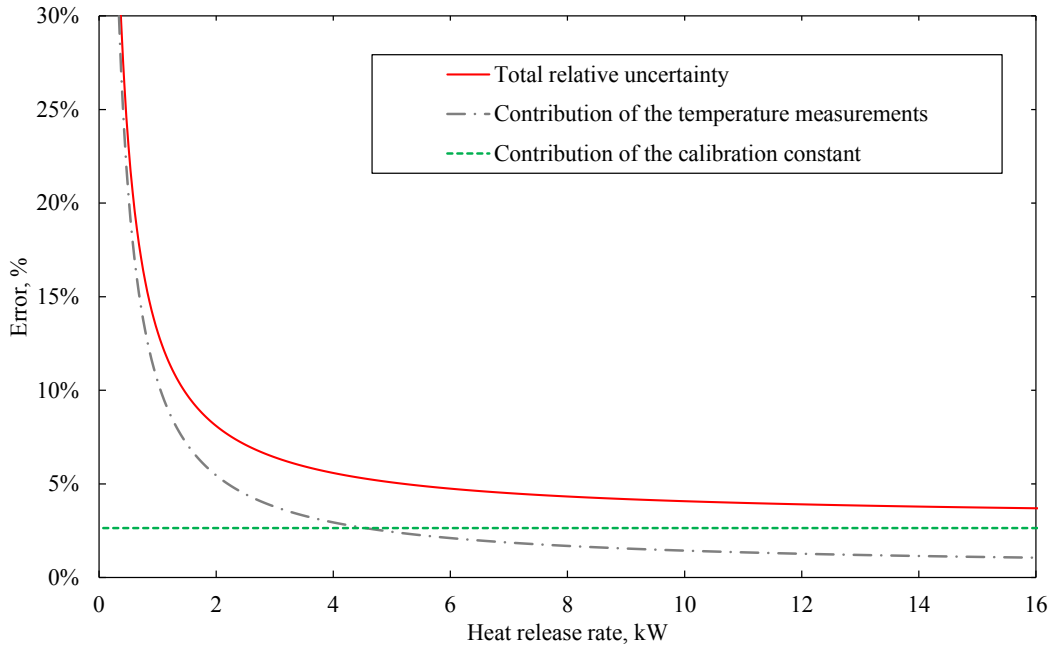

Figure 2.26: Uncertainty of the SER method at different heat release rates

considering the heat losses through the walls of the apparatus. Tewarson (2002) estimates the χ_r factor for different materials. Based on the variation of χ_r, Biteau estimates the uncertainty of the sensible enthalpy method considering the heat losses. Using the standard deviation of the χ_r values, and a 95% of confidence, Biteau estimates an uncertainty of 77 %. In spite of this big uncertainty calculated by Biteau, the good agreement of the HRR results with different calorimetric methods indicate that the calibration constant obtained with ethylene is adequate for PMMA. Tewarson demonstrated that the calibration constant is fuel dependent at the OSU calorimeter (By calculating the different χ_r factor for different materials), but the calibration factor depends also on the calorimeter design and construction materials. So, for the moment the ethylene and PMMA results have shown that for the SCALA the χ_r for both fuels is similar. But, a deeper analysis should be carried out in order to corroborate the validity of the calibration constant using different fuels.

2.6.2 Uncertainty of the oxygen consumption method measurements with calibration constant

The uncertainty of the heat release rate obtained with Equation 2.19 is calculated. The variables K_{O_2}, X^A_{PPMM}, X^0_{PPMM} and L have an associated uncertainty that has to be determined.

$$\dot{Q}_{OC,K} = K_{O_2}\frac{(X^A_{PPMM} - X^0_{PPMM})}{10^4 L} \tag{2.39}$$

The uncertainty of the calibration constant is obtained with the weekly calibration procedure, like in the sensible enthalpy calibration. The relative standard deviation is calculated, by dividing the standard deviation with the average of the 5 calibration constants. The uncertainty of variables X^A_{PPMM} and X^0_{PPMM} were obtained by letting the apparatus record data about two and a half hours. The relative standard deviation of this data set correspond to the relative uncertainty. L corresponds to the path length that separates the transmitter and the receiver. It was calculated with the amount of oxygen in the air and the data recorded by the TDLAS (Section 2.3.2.3). The relative standard deviation of this data is the relative uncertainty. Table 2.9 shows the calculated relative uncertainties.

Table 2.9: Relative uncertainty of the variables used to determine the HRR with the OC method with a calibration constant

	Relative uncertainty, %
Calibration constant K_{OC}	2.35
Oxygen concentration X^A_{PPMM}	0.46
Oxygen concentration X^0_{PPMM}	0.46
Beam path length L	0.87

The following equation is used to calculate the uncertainty of $\dot{Q}_{OC,K}$.

$$\delta\dot{Q}_{OC,K} \leq \left|\frac{\partial\dot{Q}}{\partial K_{O_2}}\right|\delta K_{O_2} + \left|\frac{\partial\dot{Q}_{OC,K}}{\partial L}\right|\delta L + \left|\frac{\partial\dot{Q}_{OC,K}}{\partial X^A_{PPMM}}\right|\delta X^A_{PPMM} + \left|\frac{\partial\dot{Q}_{OC,K}}{\partial X^0_{PPMM}}\right|\delta X^0_{PPMM}$$

$$\delta\dot{Q}_{OC,K} \leq \frac{X^A_{PPMM} - C^0_{PPMM}}{10^4 L}\delta K_{O_2} + \frac{K_{O_2}(X^A_{PPMM} - C^0_{PPMM})}{10^4 L^2}\delta L + \frac{K_{O_2}}{10^4 L}(\delta X^A_{PPMM} + \delta X^0_{PPMM})$$

Where the calibration constant has a value of −2.683, L has a magnitude of 0.322 m, and the oxygen concentrations are varied correspondingly to obtain different values of heat release rate. Figure 2.27 shows the total relative uncertainty, and the contribution of each variable uncertainty.

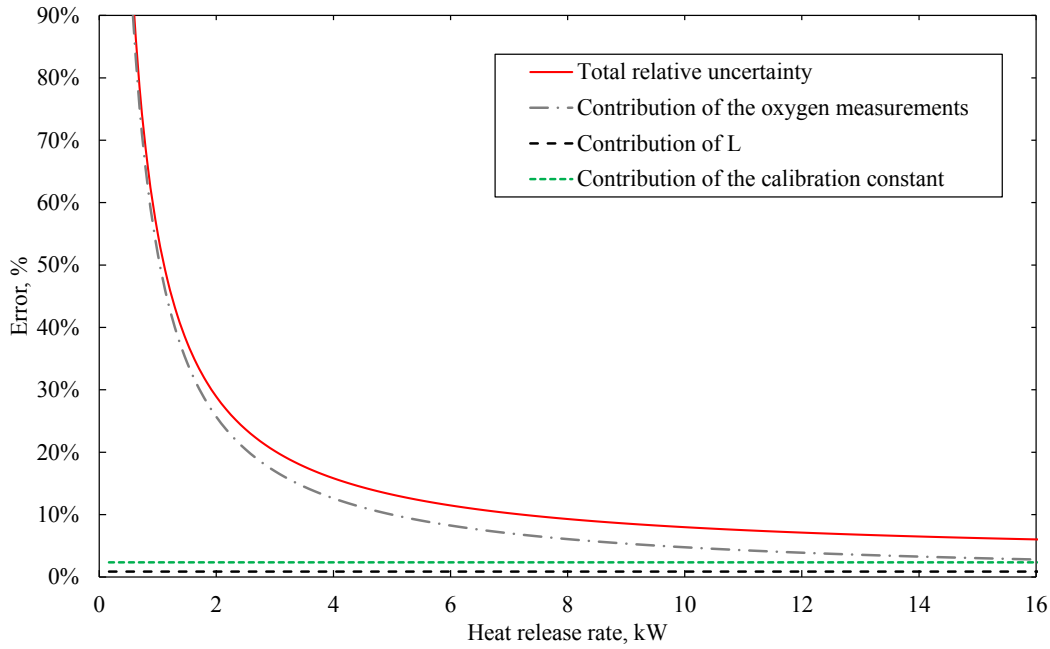

Figure 2.27: Uncertainty of the oxygen consumption method with a calibration constant (Method B) at different heat release rates

2.6.3 Uncertainty of the oxygen consumption method without calibration constant

The uncertainty of equation 2.17 is calculated. The variables with an associated uncertainty are the air flow $\dot{V}_T$, the path length L, the oxygen concentrations X^0_{PPMM} and X^A_{PPMM} and the energy constant E.

$$\dot{Q}_{OC} = E\rho_0 \frac{M_{O_2}}{M_{AIR}} \left(\frac{X^0_{PPMM} - X^A_{PPMM}}{10^6 L} \right) \dot{V}_T$$

The uncertainty of the air flow is calculated by measuring the air flow in different days

through 3 months. The relative standard deviation of these values is will be considered as the uncertainty of the air flow. The uncertainty of the oxygen measurement is the same as that calculated above in Section 2.6.2 (For variables X^0_{PPMM} and X^A_{PPMM}). The uncertainty of L was also calculated in Section 2.6.2. The uncertainty of the oxygen energy constant was obtained by Brohez (2005). Biteau et al. (2008) uses the same energy constant uncertainty. Table 2.10 shows the relative uncertainty of all variables described above.

Table 2.10: Relative uncertainty of the variables used to determine the HRR with the OC method with a calibration constant

	Relative uncertainty, %
Oxygen concentration X^A_{PPMM}	0.46
Oxygen concentration X^0_{PPMM}	0.46
Beam path length L	0.87
Volumetric air flow $\dot{V}_T$	1.63
Energy constant E	5

The following equation is used to calculate the uncertainty of $\dot{Q}$:

$$\delta\dot{Q}_{OC} \leq \left|\frac{\partial\dot{Q}_{OC}}{\partial E}\right|\delta E + \left|\frac{\partial\dot{Q}_{OC}}{\partial L}\right|\delta L + \left|\frac{\partial\dot{Q}_{OC}}{\partial X^0_{PPMM}}\right|\delta X^0_{PPMM} + \left|\frac{\partial\dot{Q}_{OC}}{\partial X^A_{PPMM}}\right|\delta X^A_{PPMM} + \left|\frac{\partial\dot{Q}_{OC}}{\partial\dot{V}_T}\right|\delta\dot{V}_T$$

$$\begin{aligned}\delta\dot{Q}_{OC} \leq\ & \rho_0\frac{M_{O_2}}{M_{AIR}}\left(\frac{X^0_{PPMM}-X^A_{PPMM}}{10^6 L}\right)\dot{V}_T\delta E + E\rho_0\frac{M_{O_2}}{M_{AIR}}\left(\frac{X^0_{PPMM}-X^A_{PPMM}}{10^6 L^2}\right)\dot{V}_T\delta L \\ &+ E\rho_0\frac{M_{O_2}}{M_{AIR}}\frac{\dot{V}_T}{10^6 L}(\delta X^0_{PPMM}+\delta X^A_{PPMM}) + E\rho_0\frac{M_{O_2}}{M_{AIR}}\left(\frac{X^0_{PPMM}-X^A_{PPMM}}{10^6 L}\right)\delta\dot{V}_T\end{aligned}$$

The air flow is 0.013 $m^3 \cdot s^{-1}$, the length L is 0.322 m and the energy constant is 13.1 $kJ{\cdot}g^{-1}$. The variable X^0_{PPMM} is fixed to the concentration of oxygen at atmosphere conditions, and X^A_{PPMM} is varied in order to determine error at different the heat release rates. Figure 2.28 shows the total uncertainty of the heat release rate measurements with the oxygen consumption method, and the single contribution of each variable.

The values obtained with the oxygen consumption method are influenced by other variables not considered in the error analysis. As seen in equation 2.10, the oxygen depletion factor assumes that there is complete combustion in the reaction. It also assumes that there is no soot production and that there is no water vapor generated in the reaction. So, if there

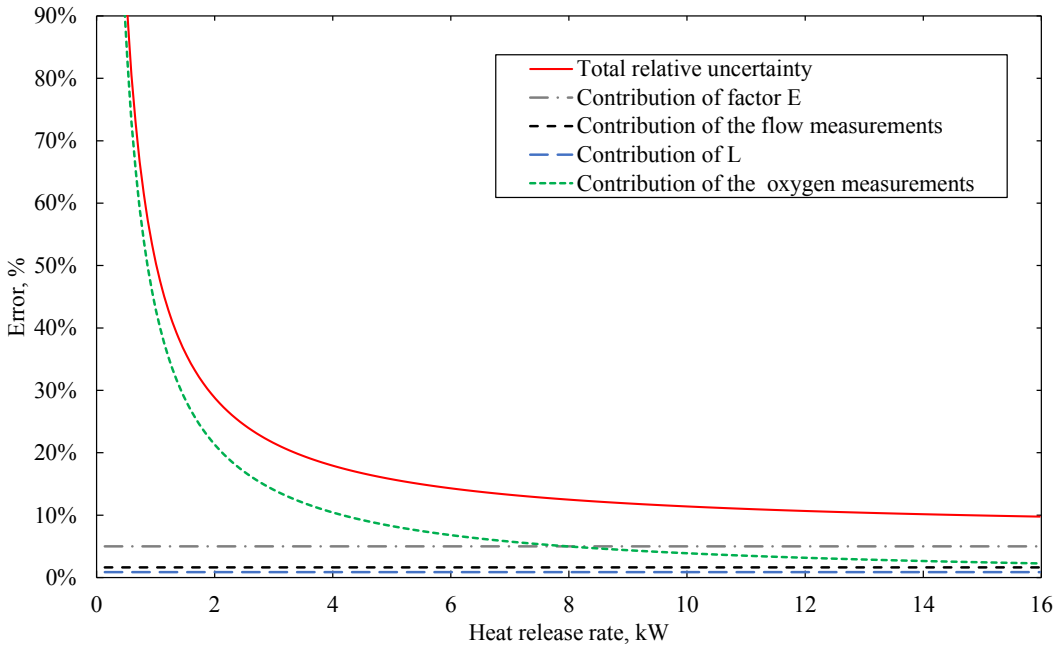

Figure 2.28: Uncertainty of the oxygen consumption method without calibration constant (Method A) at different heat release rates

is some of these variables presented in the reaction then the heat release rate calculated will be overestimated. Other important factor is that the absorption coefficient of the medium $\kappa(\lambda)$ in equation 2.29 depends on the species temperature. So the measurements performed by the TDLAS instrument have to be corrected by temperature. These corrections will not be done in this study.

The relative uncertainty calculated with Method A and Method B are compared with the relative uncertainty calculated for the Cone Calorimeter by Brohez (2005) in Table 2.11. The uncertainties calculated by 2.11 are in function of the percentage of oxygen consumed in the reaction. So, the uncertainties in Table 2.11 are shown for two values of oxygen consumed: 1 % and 10 %.

The number in brackets is the HRR corresponding to the relative uncertainty and the percentage of oxygen consumed. The relative uncertainty in the SCALA methods decrease in function of the HRR. Contrary, the relative uncertainty in the Cone Calorimeter increase when the HRR increase. This is explained by contribution of the combustion expansion

Table 2.11: Relative uncertainties for the oxygen consumption methods of the SCALA and the Cone Calorimeter, %

Method (Calorimeter)	1 % oxygen consumed	10 % oxygen consumed
OC method (SCALA)	27 (@ 2.22kW)	9 (@ 22.22kW)
OC,K method (SCALA)	21 (@ 2.83kW)	5 (@ 26.83kW)
OC method (Cone Calorimeter)	12	13

factor used by the Cone Calorimeter (Brohez, 2005). The expansion factor is used by calorimeters that measure the air flow in the exhaust duct. This is not the case for the SCALA. The air flow is measured in the air inlet.

2.6.4 Uncertainty of the peak heat release rate results

In section 2.5.4, the average peak heat release rate of the PMMA tests with each calorimetric method was calculated. In the sections above, the uncertainty of the HRR measurements were calculated. But there are other error sources in fire test results that should be considered in order to achieve a more complete analysis. Janssens (2007) quantified the uncertainty of fire test results and identifies three sources of error :

- **Uncertainties of the measurements to quantify how the specimen responds in the test ($\mathbf{u}_1$)**: These are the uncertainties calculated before. The measurements to quantify how the specimen respond are those of the heat release rate (e.g. for SER method: temperature readings and calibration constant).

- **Uncertainties associated with the specimen being tested ($\mathbf{u}_2$)**: These uncertainties are related with characteristics of the sample, and can be seen by repeating an experiment and see the variations between results. These uncertainties are calculated as the standard deviation from all the measurements.

- **Uncertainties in the test conditions ($\mathbf{u}_3$)**: An example of this source of error is the error in the heat flux. If the test consist in varying the incident heat flux, the error in the incident heat flux reading should be considered (e.g. the error of the Schmidt-Boelter gauge, if this type of radiometer was used). This source of error is not considered in this analysis because there is no incident heat flux variations.

To obtain the standard uncertainty is necessary to combine the three components. Applying the law of propagation of uncertainty yields to:

$$u_T = \sqrt{u_1^2 + u_2^2} \tag{2.40}$$

Where u_T is the standard uncertainty of the test results, u_1 is the standard uncertainty of the heat release measurement and u_2 is the standard uncertainty due to specimen variation. So, Table 2.12 shows the uncertainty of the average peak heat release rate calculated in section 2.5.4:

Table 2.12: Average peak HRR of all tests for each calorimetric method

	MLR method	SER method	OC method
Average peak HRR, kW	8.29	7.12	10.95
Uncertainty HRR (u_1), kW	-	0.32	1.23
Standard deviation (u_2), kW	0.56	0.45	0.85
Total uncertainty (u_T), kW	0.56	0.55	1.5
Total relative uncertainty, %	7	8	14

2.6.5 Uncertainty results analysis

The relative uncertainties of $\dot{Q}_{SER}$, $\dot{Q}_{OC,K}$ and $\dot{Q}_{OC}$ at different heat release rates were calculated and shown in Figures 2.26, 2.27 and 2.28 respectively. In this section the uncertainties of these three methods will be compared. Figure 2.29 shows for each calorimetric method the absolute uncertainty at different heat release rates. It can be seen that the absolute uncertainty increases with the heat release rate magnitude. Above 2 kW HRR, the OC method without calibration constant (Method A) shows the highest absolute uncertainty, then the OC method with calibration constant (Method B) and the smallest magnitude correspond to the SER method. Below the 2 kW, the absolute uncertainty in Method A is lower than in Method B. This is because at lower heat release rates, the error is dominated by the high magnitude of the calibration constant (in method B). Then at higher HRR, the uncertainty contributed by the energy constant and the air flow in method A become higher, overcoming the influence of the calibration constant magnitude in Method B. The

absolute uncertainty in Method B is lower than in Method A, basically because it considers less variables for the HRR calculation. Therefore there are less variables subjected to uncertainties.

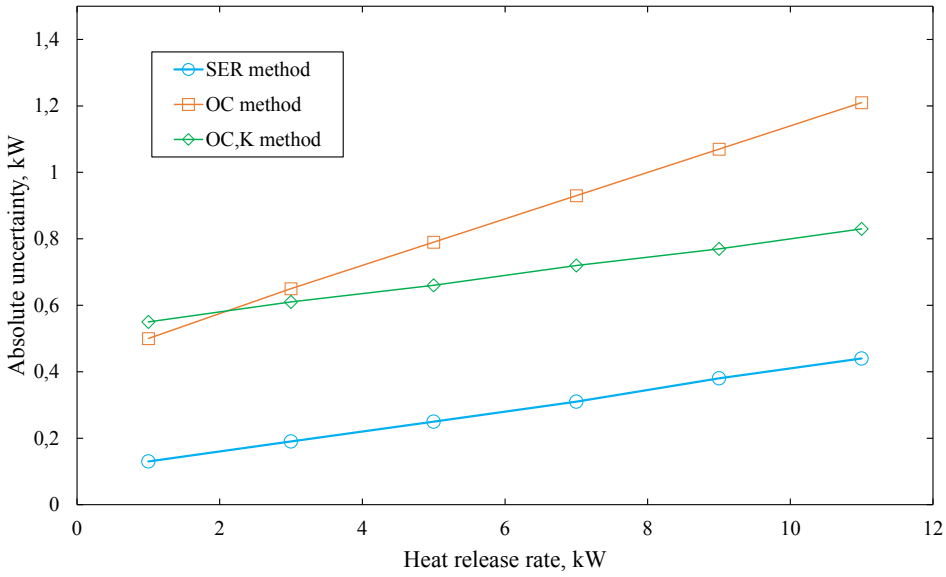

Figure 2.29: Absolute uncertainty for each calorimetric method at different heat release rates

2.6.5.1 Error influence on the PMMA results

Figure 2.21 showed the results obtained with the three calorimetric methods at the same experimental conditions. Magnitude differences are evidenced in the graph. In order to know if the magnitude differences are explained by the uncertainty of each method, a results analysis is carried out. Figure 2.30 shows the results the same results as in Figure 2.21, but with error bars in some points. The MLR HRR results are taken as the reference, because it is the upper limit considering complete combustion. Some points are inside the uncertainty intervals calculated for the SER and the OC method. But there are values whose magnitude differences are not explained by the random uncertainty of the measurements. The differences between the SER and the MLR methods can be explained by two reasons. The first one is that the calibration constant calculated for the SER method, is not so representative for all the HRR measurements, because of the thermal inertia influence. This can be seen for example in the first part of the experiment after ignition, where the values

are underestimated. The second option is that there was no complete combustion during the reaction. The differences between the SER and the MLR methods can be explained by the temperature dependence of the absorption coefficient. Other variables that could have influenced in the results are the soot production, water vapor presence in combustion gases and incomplete combustion.

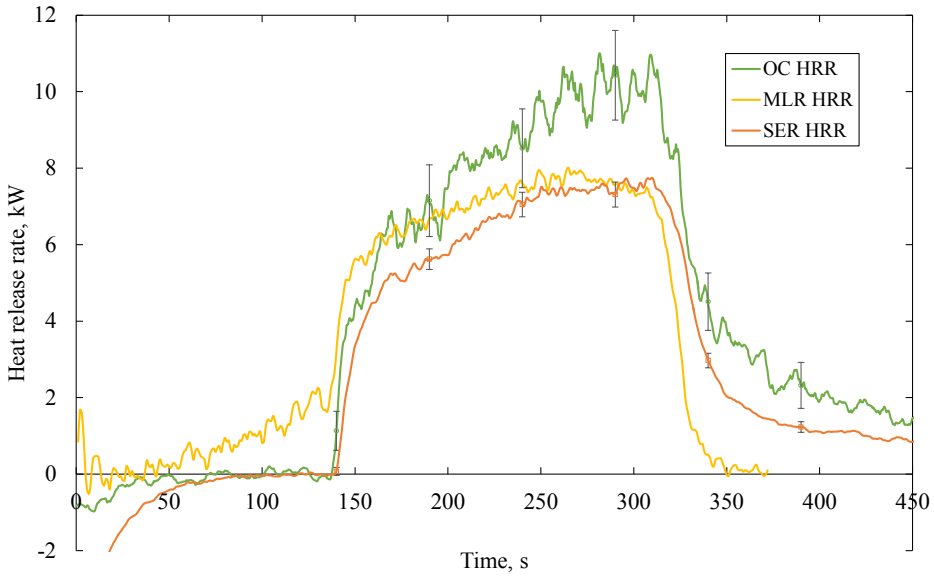

Figure 2.30: PMMA results with 3 calorimetric methods and the uncertainties of OC and SER method

3 | Characterization of biomass species used as feedstock for boilers in Chile

The results of the PMMA experiments have shown that the SCALA is suitable to be used with this kind of fuels. The heat release rate determined by each method of the SCALA results in the same behavior. There were magnitude differences between each method, but all of them fall within an acceptable range. The second part of this project is to test biomass fuels with the calorimeter. As described in the Introduction, the biomass comes from a biomass power plant and is commonly used as feedstock in boilers to produce electricity. There are significant differences between biomass and PMMA. PMMA is a synthetic polymer with a higher heat of combustion than biomass, and it has no porosity. Biomass is a more complex fuel. It is a celullosic fuel, with variable porosity. The water absorption of PMMA is between the range 0.3 and 0.4 % by weight. The moisture content of biomass can exceed the 100 by weight (dry basis). In the following chapters the main and specific goals will be defined, the fuel characteristics will be explained, following by the experimental design and finally the experimental results and analysis.

3.1 Main goals

The following tests were developed for two main purposes. The first one is to characterize biomass and predict boiler performance using a fire calorimeter. The second aim of this study is to analyze the performance of the calorimeter, under the use of biomass as fuel and know if there is also good agreement in the HRR results obtained with different methods.

3.2 Specific goals

The following goals have been defined to characterize biomass:

- Create mixes with different proportions of biomass types and compare the heat release rate of each mix at different moisture contents. Identify the mix or group of mixes that produce more power than the rest. Study this at each moisture content level.
- Assess the influence of the fuel moisture content in the heat release rate of each biomass mix. This will be done by comparing the peak HRR of each mix at different moisture contents.
- Compare the ignition delay times and the flaming duration of each biomass mix at each moisture content level and between each moisture content level.
- Compare the time to ignition and flaming duration of each biomass type at different incident heat fluxes.
- Compare the results obtained with the SER and the OC method and analyze the performance of each method.

3.3 Characteristics of the biomass feedstock

Celulosa Arauco S.A. uses different biomass types to supply their boilers. All power plants of the Celulosa Arauco S.A. holding provide in total 160 MW to the principal electric power transmission system in Chile (Comisión Nacional de Energía, 2016). The biomass mix used in the principal boilers in year 2012 by the Arauco unit is shown in Figure 3.1. This mix is representative of the power plants located in Arauco. They provide 24 MW to the SIC (Comisión Nacional de Energía, 2016).

For this study, Bioforest S.A. (Research unit of Celulosa Arauco S.A.) provided 3 types of biomass of the original mix presented in Figure 3.1. So, part of the mix in Figure 3.1 will

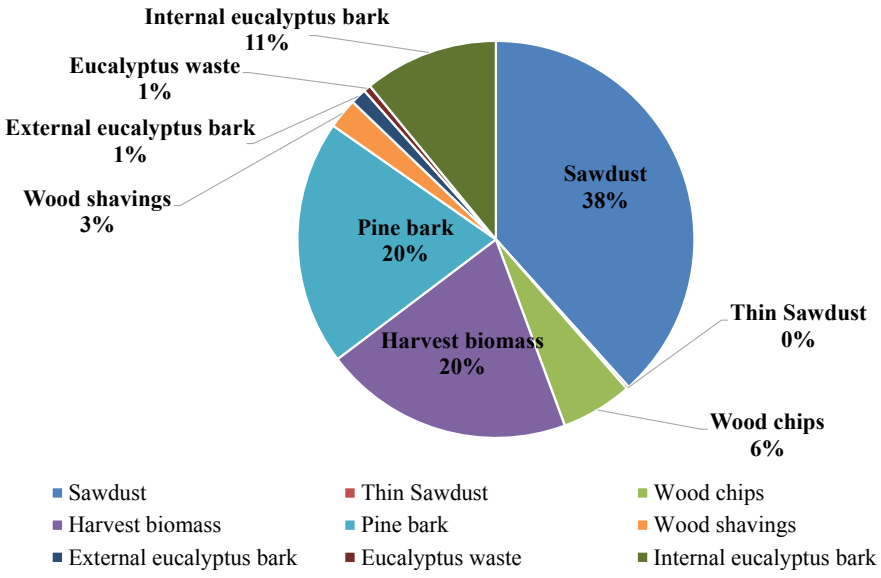

Figure 3.1: Biomass mix used in Celulosa Arauco boilers in year 2012

be considered as representative of the complete mix used in the Arauco unit. The biomass proportions will be kept as the originals. The biomass types are the following:

- Sawdust
- Pine bark
- Wood chips

The three types of biomass are shown in Figure 3.2. These biomass types are used in the plants located in Arauco. Each type of biomass was shipped in closed plastic bags, preserving the original moisture content. This is important, because the aim is to study the biomass under its original conditions.

The weather in the south of Chile is rainy, so the biomass typically has high levels of moisture content. Three different levels of moisture content are considered in this work. The first level, which will be called the Arauco moisture content from now on, is the original moisture content of the biomass. The second moisture content level is defined as the one in which the biomass is left 1 day out of the plastic bag at atmospheric conditions. This level will be named 1-Day moisture content. The third moisture content level is defined as

Figure 3.2: Left: Sawdust, Center: Pine bark, Right: Wood chips

the one in which the biomass is left 2 days out of the plastic bag at atmosphere conditions. This will be called the 2-Day moisture content.

The following terms will be used in the next sections: The term MC means moisture content, the subindex OD means ovendry basis, and GB means green basis. In Section 3.3.1 the difference between both basis is explained , and why both are used in this work. Table 3.1 shows the moisture content at each level.

Table 3.1: Moisture content of the biomass species at different levels using ovendry and green basis

Ovendry basis	Arauco	1-Day	2-Day
Pine bark	86%	52 %	29 %
Wood chips	117 %	67 %	39%
Sawdust	155 %	101 %	49 %
Green basis	Arauco	1-Day	2-Day
Pine bark	46%	34 %	22 %
Wood chips	53 %	40 %	28%
Sawdust	61 %	50 %	33 %

3.3.1 Moisture content measurement

The moisture content of the biomass is determined using an oven to dry the specimens. The samples are weighed before placing them in the oven. The moisture content is calculated using the dry weight as reference and also using the total weight as reference. It is calculated using equations 3.1 and 3.2 respectively.

$$MC\%_{OB} = \frac{mass\ of\ water}{mass\ of\ dry\ wood} \tag{3.1}$$

$$MC\%_{GB} = \frac{mass\ of\ water}{mass\ of\ water + mass\ of\ dry\ wood} \tag{3.2}$$

The moisture content was calculated for the same sample at different times. For this purpose a good choice is to use equation 3.1, because the reference is the same, in spite of the water lost. But in the industries that work with biomass, it is common practice to use Equation 3.2; it is simpler to know for example the amount of usable fuel, with the total weight and the moisture content.

The oven-drying method specifies a constant temperature of 103°C ± 2°C (ASTM D4442-07, 2007). The endpoint is achieved when the weight of the sample does not change in intervals of 4 hours. At 103°C some thermal decomposition was observed. Therefore, the temperature was set to 90°C to avoid any mass loss of the dry mass. In 24 hours the sample reached the endpoint. The biomass was kept in plastic bags to avoid water loss over time. The moisture content was calculated each day, to know if there is any water lost. The results showed that there were no significant variations in the moisture content over time, thus for simplicity, the averaged values are considered to characterize each level of moisture content.

3.4 Experimental design

The variables considered in this study are the moisture content, the mix composition and the incident heat flux imposed to the specimen. This study is looking to replicate the conditions at the Arauco boiler and to analyze other scenarios where the moisture content is lower than the original conditions. The moisture content in the Arauco plant is measured using green basis. Therefore the weight of each sample in this study is in green basis. In other words, each sample of biomass is prepared and weighed at the Arauco moisture content. Thus, the mixes with 1-Day moisture content will weight less than the ones of Arauco level,

Table 3.2: Composition of the biomass mixes

Biomass type	Mix 1	Mix 2	Mix 3	Mix 4	Mix 5	Mix 6	Mix 7	Mix 8
Sawdust	100 %	0 %	0 %	60 %	33, 3 %	60 %	20 %	20 %
Pine bark	0 %	100 %	0 %	30 %	33, 3 %	20 %	60 %	20 %
Wood chips	0 %	0 %	100 %	10 %	33, 3 %	20 %	20 %	60 %

and the biomass at 2-Day level will weight less than the ones of 1-Day level, due to the water losses. But all of them had the same weight at the beginning. The dry mass weight of the biomass stays the same at all moisture content levels. Each sample has an initial weight of 50 g at green basis.

With the 3 types of biomass, 8 different mixes are elaborated. Table 3.2 shows the composition of each biomass mix. The first three mixes (Mix 1, Mix 3 and Mix 3) consist of only one type of biomass. Therefore, the characteristics of each biomass type can be studied separately. The composition of Mix 4 is based on the mix actually used by Celulosa Arauco. These three types of biomass are not the only types used to produce power in Celulosa Arauco. In Figure 3.1 the complete biomass mix used in the boilers is described. Mix 4 has the same biomass proportions than Celulosa Arauco mix. Mix 5 is made of the three species of biomass with the same quantity. Mix 6, Mix 7 and Mix 8 have all one predominant biomass type, and other two types of biomass with the same amount of mass. In Mix 6 the sawdust is predominant, in Mix 7 the pine bark, and in Mix 8 the wood chips. This can be graphically seen in figure 3.3.

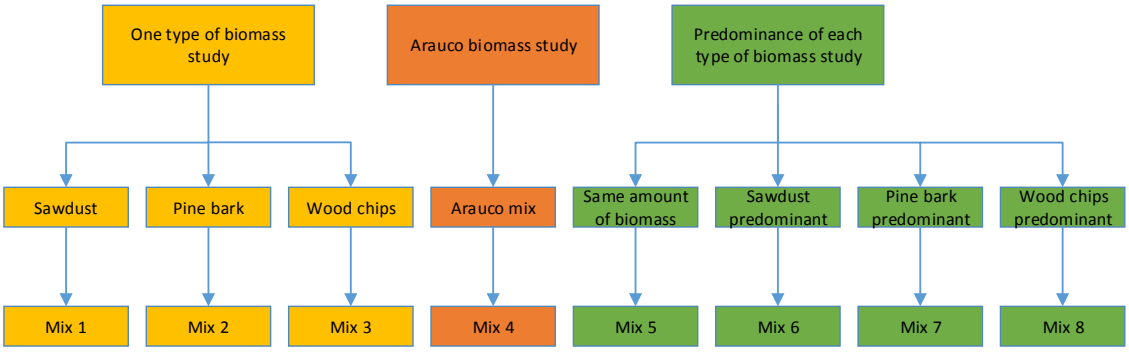

Figure 3.3: Biomass mixes

The heat fluxes imposed on the specimens in the ignition tests were: 25 kW$\cdot$ m^{-2}, 30 kW$\cdot$m^{-2}, 37 kW$\cdot$ m^{-2}, 40 kW$\cdot$ m^{-2} and 48 kW$\cdot$ m^{-2}. These heat fluxes were imposed to Mix 1, Mix 2 and Mix 3. The goal of these tests is to determine the influence of the incident heat flux on the ignition delay time of the three biomass types and determine the critical heat flux to achieve ignition with spontaneous ignition. With this study it can also be determined which biomass type achieve ignition faster at different heat fluxes, and thus find which biomass type acts like an accelerant in the combustion reaction. These tests are performed only to each type of biomass alone, in order to avoid the influence of the other biomass types in the ignition delay time. The selection of the heat fluxes was determined during experimentation, these tests helped to select the incident heat fluxes used in the rest of the tests. Each test was repeated three times. An additional repetition was carried out because of the following causes:

- The time to ignition between test repetitions had great magnitude differences
- Flaming ignition occurs after the peak mass loss rate was achieved
- No flaming combustion is attained

Spontaneous ignition tests were carried out. The tests were performed in a random order. The mixes were placed in the sample holder with its upper surface at the same plane than the top of the sample holder. That is the plane where the incident radiation is measured. If the external surface of the sample was at a lower position, a ceramic fiber blanket wrapped into aluminum was used to raise it.

3.4.1 Experimental conditions

The first part of the experiments consisted in ignition test for incident heat flux variations. These tests were performed at Arauco moisture content. The ignition tests also helped to select the incident heat flux that will be used in the other tests (With fixed heat flux). The tests are performed at the heat fluxes named in section 3.4, and also at 2 kW$\cdot$ m^{-2} lower than the last heat flux that the specimen made ignition. This is to ensure that the biomass

do not ignite at lower heat fluxes.

The second tests were calorimetric tests for each mix of biomass at different moisture content. The incident heat flux has to be high enough to achieve spontaneous ignition. But for better performance of the calorimeter, the sample should ignite passed a minimum time since the beginning of the test (See section 4.4.2 for a deeper explanation). The sample should ignite after the stack thermocouple readings return to the steady state temperature (the temperature at the stack decrease because of the window opening). The ignition delay time depends on the fuels characteristics, porosity, moisture content and the incident heat flux. In order to maintain the ignition delay time high enough to achieve valid results, the incident heat flux was set to lower values, when the moisture content of the sample decrease. Therefore, not all tests were performed under the same incident heat flux. Table 3.3 shows the incident heat flux used for the second tests.

Table 3.3: Incident heat flux at each type of calorimetric test (kW$\cdot$ m^{-2})

Moisture content	Mix 1	Mix 2	Mix 3	Mix 4	Mix 5	Mix 6	Mix 7	Mix 8
Arauco	40	37	37	37	37	37	37	37
1-Day	37	37	37	37	37	37	37	37
2-Day	30	30	30	30	30	30	30	30

The tests performed with Mix 1 at Arauco moisture content did not achieved flaming ignition at 37 kW$\cdot$ m^{-2}. Therefore the incident heat flux was increased to 40 kW$\cdot$ m^{-2}. Ideally all tests should have been performed at the same incident heat flux in order to compare the ignition delay times of each mix between different moisture content levels. If the incident heat flux of two tests is different, then the ignition delay time can not be compared (Ignition delay times of 2-Day can not be compared with the other levels). 2-Day moisture content samples were tested with an incident heat flux of 30 kW$\cdot$ m^{-2} in order to avoid flaming ignitions before the outlet gases temperature returned to the steady state.

The variables under study in these tests were:

- Peak HRR
- Effective heat of combustion

- Ignition delay times
- Flaming duration

3.5 Experimental results and analysis

A total of 135 tests were performed, of which 33 tests did not achieve ignition. The mass loss rate and the HRR with OC and SER method for each test was obtained. Some tests do not have the mass loss rate measurements, because the precision balance failed to record data. It was afterwards discovered that the scale stops recording data when the pan gets out of its position. The sensible enthalpy method gives consistent results in all tests. The oxygen consumption method gives consistent results in some tests, but in other ones the data shows an evidently inaccurate behavior. This will be discussed later in section 4. Therefore all tests have thermocouple readings, but not all of them have oxygen concentration and/or mass loss rate readings. For this reason, all tests were compared using the SER method. All results of the moisture content and mix variations are presented in Annex C.2. Not all mass of the samples was consumed during combustion. The average final mass (including the ashes and the mass not burnt) at moisture contents Arauco, 1-Day and 2-Day were 4.6, 3.1 and 2.2 g respectively. Table C.5 in Annex C.1 shows the final mass weights of each mix at each moisture content.

3.5.1 Critical incident heat flux for ignition

This is the first part of the tests. The incident heat fluxes were set to 25 kW$\cdot$ m^{-2}, 30 kW$\cdot$ m^{-2}, 37 kW$\cdot$ m^{-2}, 40 kW$\cdot$ m^{-2} and 48 kW$\cdot$ m^{-2}. For the pine bark (Mix 2) the heat flux was set also to 28 kW$\cdot$ m^{-2}, and for the wood chips (Mix 3) and the sawdust (Mix 1) the heat flux was set also to 23 kW$\cdot$ m^{-2}. Figure 3.4 shows the ignition delay times of each type of biomass at the different incident heat fluxes.

The error bars of the graph correspond to the standard deviation of the test repetitions. The critical incident heat flux for ignition for sawdust (Mix 1), pine bark (Mix 2) and wood

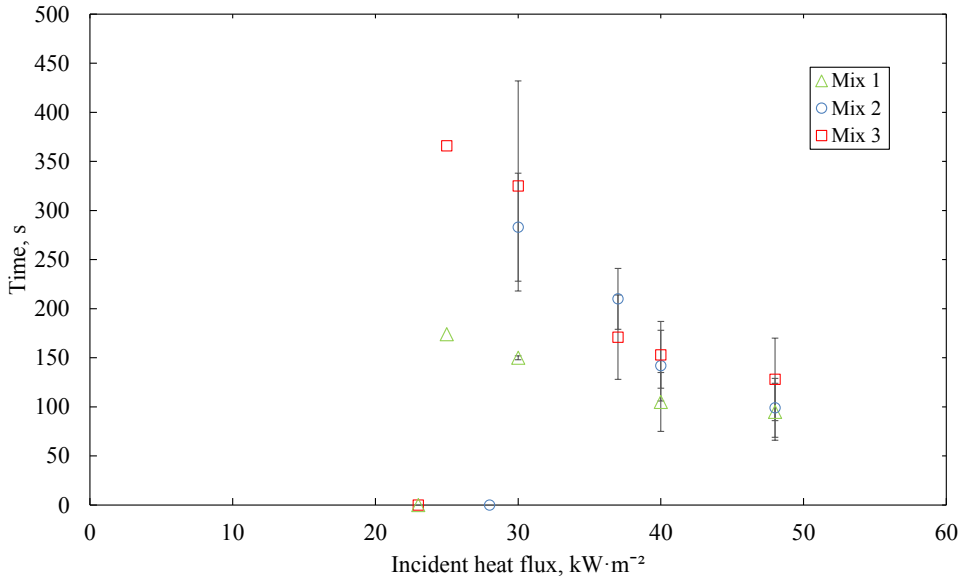

Figure 3.4: Ignition delay times at different incident heat fluxes

chips (Mix 3) at Arauco moisture content level is 25 kW· m^{-2}, 30 kW· m^{-2} and 25 kW· m^{-2} respectively. It can be seen that sawdust achieved ignition faster than the other biomass types, but due to the high moisture content, the number of times it achieved ignition was to low. At 37 kW· m^{-2} there was no ignition. Just at incident heat fluxes above or equal to 40 kW· m^{-2} it starts to make ignition more times.

3.5.2 Peak heat release rate with SER method

The first parameter analyzed is the peak heat release rate obtained with the SER method. The peak heat release rate is the highest heat release rate generated by the sample through the test. The results are shown in three different graphs; Figure 3.5 shows the results at Arauco moisture content, Figure 3.6 shows the results at 1-Day moisture content and 3.7 shows the results at 2-Day moisture content (Table C.1 in Annex C collects all the results shown in the graphs, but with the exact value). These values are an average of the three results obtained per experimental condition. Some cases have two valid results, and other ones just one. Table C.2 in Annex C can be used as a complement for the analysis. It shows the minimum and maximum peak heat release rates obtained for each mix at each moisture content level. The highest values are highlighted with yellow. When there is only one value

at the center of the minimum and the maximum it is because of there is only one valid result for that experimental condition.

3.5.2.1 Influence of the mix composition in the peak HRR at different moisture contents

This first analysis will be performed by comparing the peak HRR at each of the three moisture contents; Arauco, 1-Day and 2-Day. It will be analyzed if there are biomass species that increase the power generation when they are combined with other biomass types.

Peak HRR with Arauco moisture content This analysis is based on Figure 3.5. At this moisture content there is an average of 0.84 kW with a standard deviation of 0.18 kW (Relative standard deviation (RSD) = 21.4 %) of all the peak HRR of all the mixes. The highest averaged value was achieved by Mix 3 (100 % wood chips) with 1.1 kW. The maximum HRR was also achieved by Mix 3 with 1.46 kW (See table C.2 in Annex C). Mix 6 and Mix 7 were the mixes with the lowest HRR, 0.65 and 0.49 kW respectively. At this level of moisture content, wood chips have an outstanding performance. Mix 2 (100 % pine bark) showed also a good performance, with the second highest average peak heat release rate.

Peak HRR with 1-Day MC level Figure 3.6 shows the peak HRR of all mixes at this moisture content. The average HRR of all the results is 1.36 kW and the standard deviation is 0.2 kW (RSD = 14.6 kW %). The highest value was obtained by Mix 8 with 1.69 kW, and the maximum peak heat release was achieved by Mix 8 too, with 1.93 kW. This mix is mostly composed of wood chips. Other two mixes that generated high HRR were Mix 2 and then Mix 7. Mix 2 is composed only of pine bark, and Mix 7 is composed mostly of pine bark. This time Mix 3 did not performed better than the other mixes. So, the mix composed only of pine bark and the two mixes composed mostly of wood chips and pine bark each one, reported the best performance.

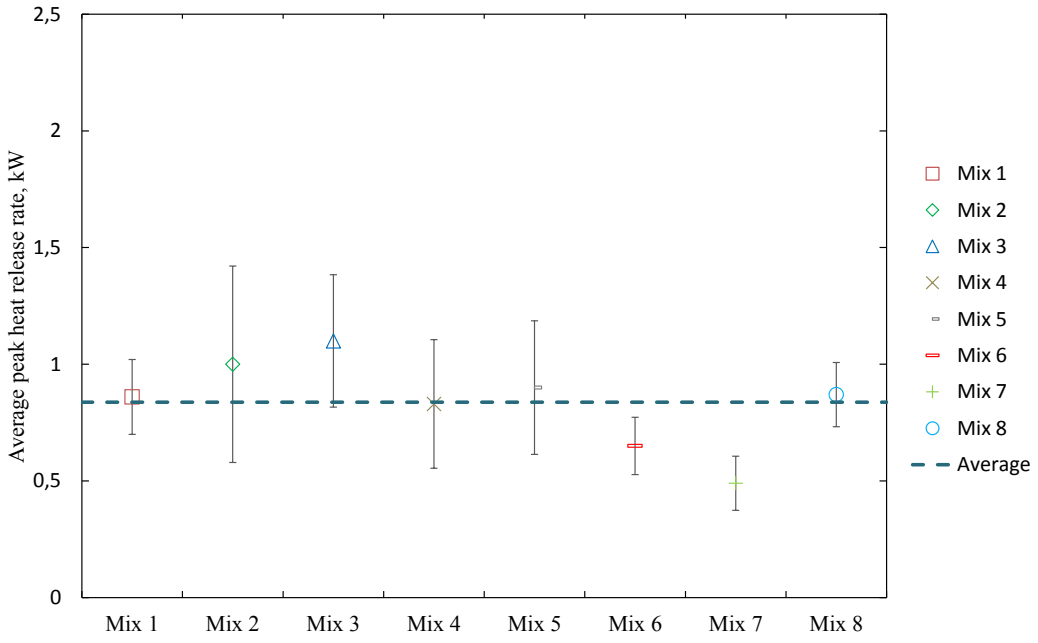

Figure 3.5: Peak HRR of all mixes at Arauco moisture content level

Peak HRR with 2-Day MC level Figure 3.7 shows the peak HRR of all mixes at this moisture content level. The averaged peak heat release rate of all mixes is 1.54 kW and the standard deviation is 0.21 kW (RSD = 13.4 kW %). The highest HRR was generated by Mix 3 with 2.00 kW, and the highest value was also achieved by Mix 3 with 2.32 kW (See table C.2 in the annexes). Wood chips generated more power than the other mixes. Mix 7 is the second mix with the highest peak HRR.

The average peak HRR of all mixes at 1-Day moisture content overcomes the average at Arauco moisture content in 0.52 kW. Day-2 moisture content average peak HRR overcomes 1-Day moisture content in 0.18 kW. With less moisture content level, the average peak HRR becomes higher. Wood chips generated more power than all the others combinations of biomass types at Arauco and 2-Day moisture content. When wood chips are combined with the other biomass types at 1-Day moisture content, they produce the highest HRR. The pine bark generates great power at Arauco and 1-Day moisture content too.

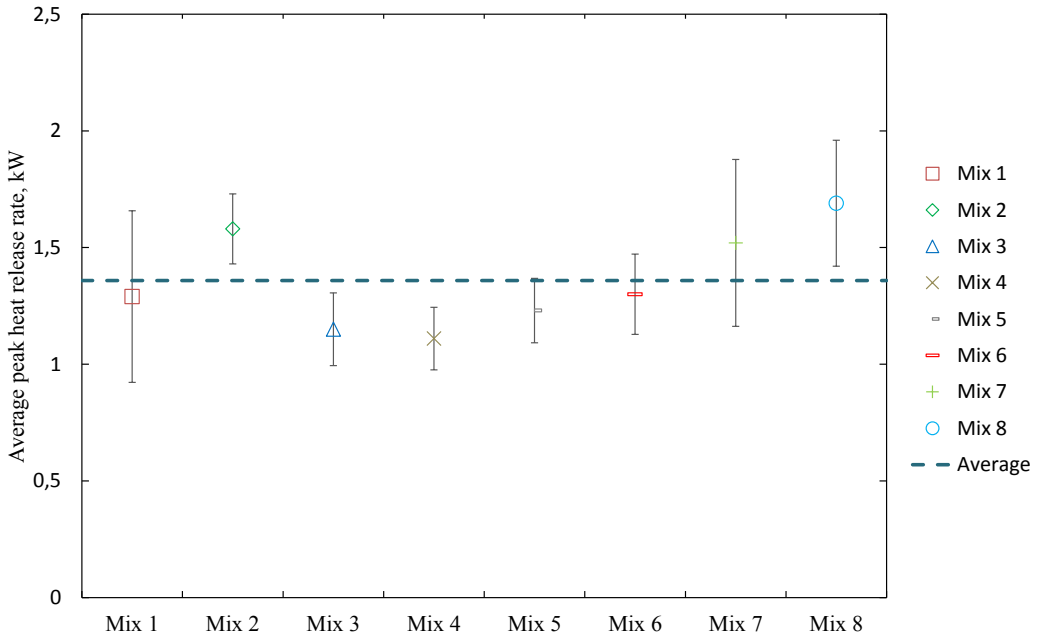

Figure 3.6: Peak HRR of all mixes at 1-Day moisture content level

3.5.2.2 Influence of the moisture content on the peak HRR of each biomass mix

In this analysis, the peak HRR of each mix will be compared at the three different moisture content level. All the mixes, except the Mix 3, have improvements higher than 0.3 kW from Arauco moisture content to 1-Day moisture content (Compare Figure 3.5 with Figure 3.6). This means that less moisture content results in higher HRR. Only Mix 3 gives no significant difference between those two moisture contents. Mix 7 had the highest variation of the group. This mix is mostly composed of pine bark. Due to the moisture content variation, pine bark (Mix 2) increased its HRR in 0.58 kW. Pine bark combined with sawdust and wood chips (Mix 7) increased its HRR in 1.03 kW. Sawdust increased its HRR in 0.43 kW, and combined with pine bark and wood chips, the HRR increased in 0.65 kW. In conclusion, pine bark and sawdust have considerable power improvements due to the decrease of their moisture content. Wood chips have considerable improvements too, but only when it is combined with sawdust and pine bark.

Due to the moisture content decrease from 1-Day to 2-Day (Compare Figure 3.6 with

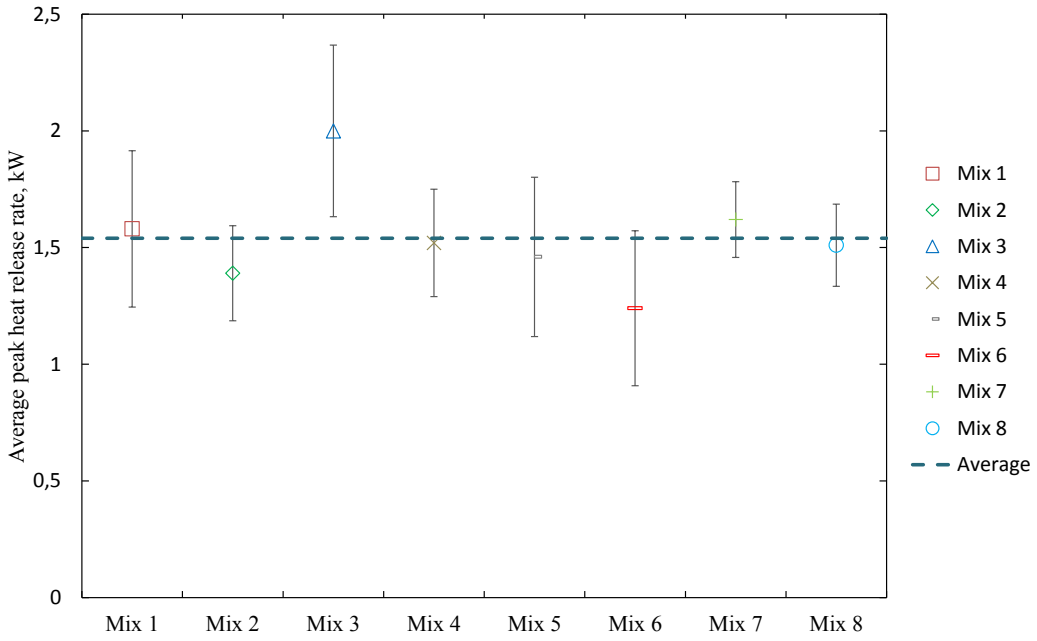

Figure 3.7: Peak HRR of all mixes at 2-Day moisture content level

Figure 3.7), Mix 3 reported the highest increment in power (0.85 kW). Mix 1 and Mix 4 had high increments too; 0.29 kW and 0.41 kW respectively. Both mixes are mostly composed of sawdust. Mix 2, Mix 6, Mix 7 and Mix 8 had no significant variations. Some of them decreased the power generated, but in magnitudes smaller than 0.18 kW. The greatest variations occur from Arauco to 1-Day moisture content with an average increase of 0.5 kW. The variations from level 1-Day to 2-Day have an average increase of 0.2 kW. There is an increase of 60 % in the average peak heat release rate from Arauco MC to 1-Day MC. This means that there would be a boiler efficiency increase, due the heat release rate increase. There is an increase of 80 % in the average peak HRR from Arauco MC to 2-Day MC. Finally, from 1-Day to 2-Day, there is an increase of 13 %.

3.5.3 Effective heat of combustion (EHC)

The heat of combustion (Δh_c) is a thermodynamic property measured with an oxygen bomb calorimeter. It can also be calculated from fuel elements concentrations (García et al., 2014). The heat of combustion is obtained under complete combustion and all the

fuel mass is consumed in the process. The oxygen bomb calorimeter gives the gross heat of combustion, which means that all water in the combustion products is in liquid state (Rivera et al., 2012). If the gross heat of combustion is used to characterize the biomass types used for energy generation in this study, the values will be overestimated. This is because the biomass boilers used by Celulosa Arauco do not use the energy stored in the combustion products. The heat consumed in evaporating the water should be subtracted from the gross heat of combustion. This is called the net heat of combustion. The net heat of combustion can not be determined experimentally. There are relationships in the literature used to calculate it. The net heat of combustion also considers that there is complete combustion and that the fuel is completely consumed. This is not the case in the biomass boilers. A parameter more adapted to the reality is the effective heat of combustion (EHC). Dyken et al. (2010) define the effective heat of combustion as the net heat of combustion subtracting the energy of evaporating the moisture content of the biomass. The Cone Calorimeter Standard defines the EHC as "the amount of heat generated per unit mass lost by a material, product or assembly, when exposed to specific fire test conditions". It can be a constant value if the specimen is homogeneous and has a single mode of degradation. If the material is not homogeneous or is a composed of various materials or if it has more than one mode of degradation than the EHC can be variable (ASTM E1354-11b, 2011). Wood burns by first pyrolyzing and then charring. Mostly flaming combustion is fed by pyrolysis. Char oxidation becomes more dominant after the flaming ceases. The EHC tends to increase in the char oxidation process (Babrauskas, 1990). In summary, the EHC is not a thermodynamic property, it depends on the experimental conditions, it does not necessary consider complete combustion, not all the mass has to be consumed in the combustion reaction and it does not has to be constant. In this study, the heat of combustion of the sawdust, pine bark and wood chips was determined with an oxygen bomb calorimeter. Furthermore the effective heat of combustion was determined experimentally with the SCALA. Table 3.4 shows the gross heat of combustion of all biomass mixes studied in this work.

The combustion efficiency as defined in Section 1.1.1 is the the ratio of the effective heat of combustion to the net heat of combustion. There is no direct procedure to obtain the net

Table 3.4: Gross heat of combustion of all mixes

	Mix 1	Mix 2	Mix 3	Mix 4	Mix 5	Mix 6	Mix 7	Mix 8
Δh_c, kJ·g^{-1}	18.96	18.61	20.73	19.01	19.41	19.25	19.06	19.94

heat of combustion. It is commonly calculated from the fuel elements compositions based on the gross heat of combustion. This leads to obtain net heat of combustion dependent of the method used to calculate it. In order to avoid this dependence, the gross heat of combustion was used to calculate the combustion efficiency. The gross heat of combustion is also the upper limit of the energy release by the biomass. So, Equation 3.3 is used to calculate the combustion efficiency (η):

$$\eta = \frac{EHC}{\Delta h_c} \tag{3.3}$$

The EHC is calculated with the heat release rate (obtained with the SER method) and the mass loss rate. The heat release rate is divided by the mass loss rate and plotted in function of time. So, the EHC is calculated in function of time with equation 3.4:

$$EHC(t) = \frac{\dot{Q}_{SER}(t)}{\dot{m}(t)} \tag{3.4}$$

Figure 3.8 shows the EHC of wood chips at 2-Day moisture content level. The graph shows also the gross heat of combustion. This is an example of the performance of the EHC when is calculated with equation 3.4. To calculate the EHC as a single value, some of the results are averaged. It can be seen in figure 3.8 that the EHC increases at the flame ignition, then remains constant for a while and finally it starts to increase. At the end can be seen that the EHC values are ridiculously high. This occurs because $\dot{Q}_{SER}$ does not return to zero when the flame is extinguished (See section 4.4.1 for deeper explanation) and the mass loss rate approximates to zero. Then the EHC tends to the infinite. The HRR determined with the OC method was not used to calculate the EHC. This was because some tests had no valid oxygen concentration measurements due unexpected drifts (See Section

4.3.1). Therefore there would be less valid EHC calculations.

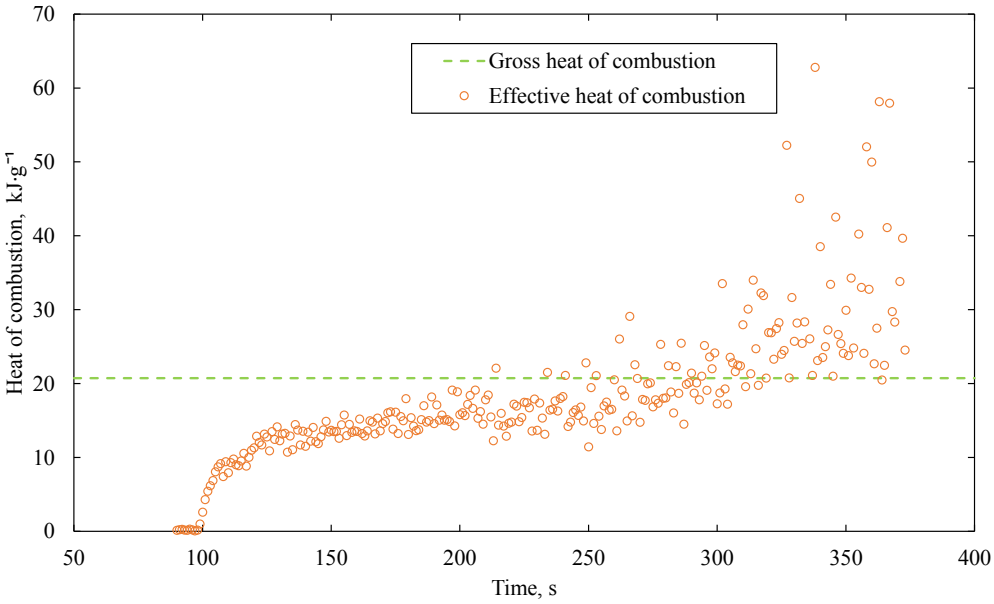

Figure 3.8: Example of effective heat of combustion of wood chips at 2-Day level

The single value EHC is obtained averaging the data located after ignition during the time lapse where the EHC remains approximately constant. Some tests shows no constant EHC, but an increasing EHC. These tests were not considered in the EHC calculation. All tests of the three different moisture content levels with a valid EHC (Based on the criteria just described) are plotted in figure 3.9. The peak HRR is plotted in function of the EHC.

This graph does not consider the influence of the mix composition. It can be seen that the peak HRR increases when the EHC increases. The samples with Arauco moisture content level have in general lower EHC than the other ones. The 1-Day moisture content samples have in general higher EHC than the ones at Arauco level and lower EHC than the 2-Day moisture content level. So, the EHC increases when the moisture content decreases. The efficiency is calculated and shown in Table 3.5, where the values are presented with their respectively standard deviation.

Finally, Table 3.6 shows all effective heat of combustion calculated for all mixes at each moisture content level. Each value comes with its respective standard deviation. The values with no standard deviation means that there is only one data available. This is because of

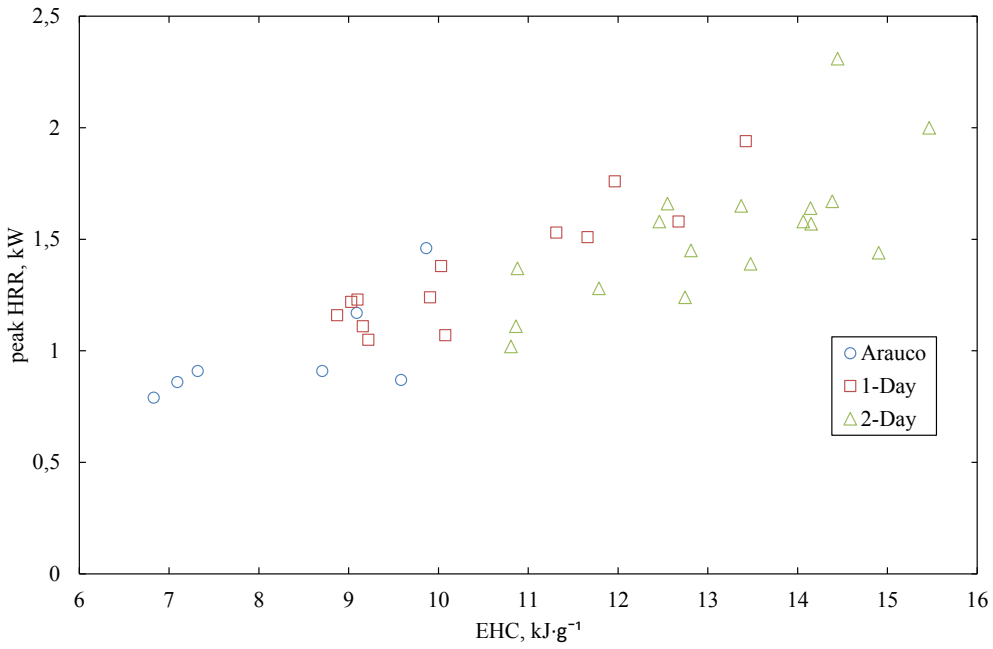

Figure 3.9: Peak HRR in function of the EHC of biomass mixes of different moisture content level

Table 3.5: Combustion efficiency of all mixes at each moisture content

Moisture content	Mix 1	Mix 2	Mix 3	Mix 4
Arauco	46	49	41 ± 9	32
1-Day	54 ± 8	68	45 ± 3	48
2-Day	62 ± 7	63	70 ± 5	73 ± 2
Moisture content	Mix 5	Mix 6	Mix 7	Mix 8
Arauco	47			40 ± 7
1-Day	47	52	63	63 ± 6
2-Day	70 ± 6	62 ± 10	70 ± 6	69 ± 9

precision balance operation problems. The highest average effective heat of combustion correspond to Mix 3 at 2-Day moisture content with 14.4 ± 1 kJ· g^{-1}. Mix 2 and Mix 8 reported high EHC at 1-Day MC, with 12.7 and 12.5 ± 1.3 kJ· g^{-1} respectively. In Arauco MC, mixes have similar EHC. Just Mix 4 presented low EHC. It can be seen in Table 3.6 that the EHC in most cases increases when the moisture content decreases. This means that the lower the moisture content, the better will be the biomass performance in the boiler.

Table 3.6: EHC of all mixes at each moisture content level (kJ· g^{-1})

Moisture content	Mix 1	Mix 2	Mix 3	Mix 4
Arauco	8.7	9	8.5 ± 2	6.1
1-Day	10.3 ± 1.5	12.7	9.3 ± 0.7	9.2
2-Day	11.8 ± 1.4	11.8	14.4 ± 1	13.8 ± 0.5
Moisture content	Mix 5	Mix 6	Mix 7	Mix 8
Arauco	9			7.9 ± 1.5
1-Day	9.1	10 ± 0.1	12	12.5 ± 1.3
2-Day	13.6 ± 1.2	11.9 ± 1.9	13.4 ± 1.1	13.7 ± 1.7

3.5.4 Ignition delay time

One of the problems when carrying out spontaneous ignition tests, is that some tests do not achieve flaming ignition. Those tests are useless for this study. Table 3.7 shows the percentage of valid tests where ignition was achieved at each mix and at each moisture content level. Mix 3 (100 % wood chips) achieved ignition in all tests. Mix 8 is the second mix that achieves ignition more times (60 % wood chips). So, the mixtures with wood chips improved their ignition rate. Wood chips improve the conditions to achieve ignition.

Table 3.7: Percentage of valid tests that made ignition

Moisture content	Mix 1	Mix 2	Mix 3	Mix 4	Mix 5	Mix 6	Mix 7	Mix 8
Arauco	0	67	100	50	75	67	34	100
1-Day	67	34	100	34	34	67	67	100
2-Day	100	67	100	67	100	100	50	50

Figure 3.10 shows the ignition delay times of each mix at Arauco MC level. With 37 kW·m^{-2} of imposed heat flux, Mix 4 is the first to ignite with 127 ± 54 s (See table C.3 in the annexes to see the exact numbers). The second one that achieves ignition is Mix 5. This mix, is composed mostly of sawdust, it has the same sawdust proportion than Mix 4. Mix 1 have the lowest ignition time, but it was performed under 40 kW·m^{-2}. So, sawdust has lower time to ignition compared with the other biomass species. The slowest is Mix 7, and then the second slowest is Mix 2. Both mixes are composed mostly by pine bark.

Figure 3.11 shows the ignition delay time of all mixes at 1-Day MC. All tests were performed under 37 kW·m^{-2} incident heat flux. Mix 2 has the lowest time to ignition of all the mixes with 63 s (See Table C.3 in Annex C to see the exact values). Then comes

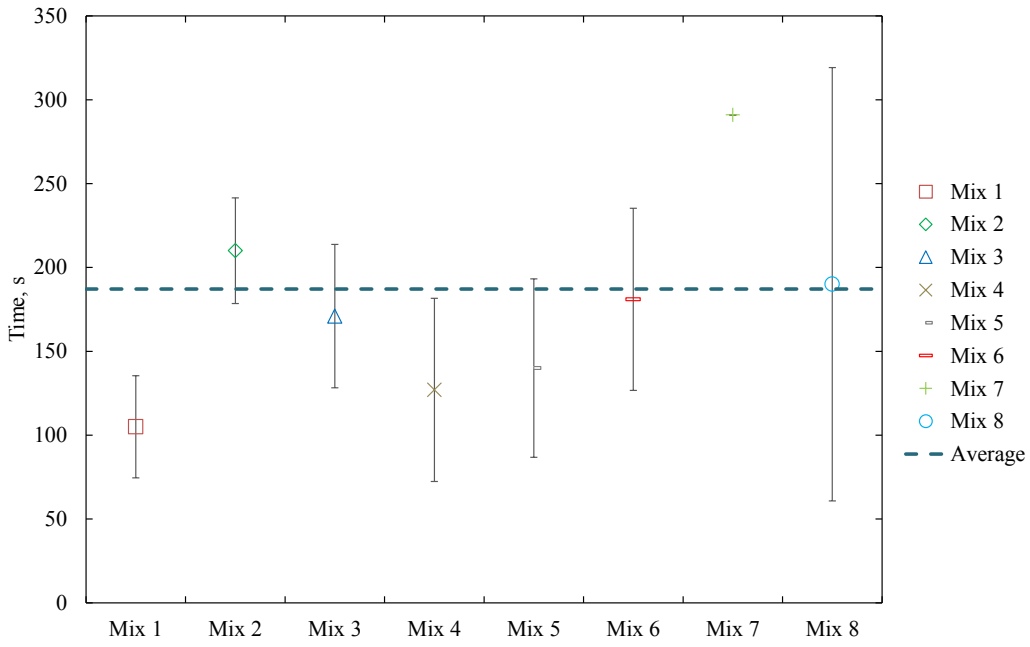

Figure 3.10: Ignition delay time of all mixes at Arauco moisture content

Mix 7. Mix 2 is composed only of pine bark, and Mix 7 is composed mostly of pine bark. Therefore, at this moisture content, pine bark is the biomass type with the lowest ignition delay time. Pine bark also reduces the ignition delay times of other mixes (Based on Mix 7 results). Figure 3.4 showed that at different incident heat fluxes and at Arauco MC, sawdust reported the lowest ignition delay times. This occur instead of that the amount of mass of water present in the sawdust was higher than in the pine bark (at Arauco MC). So, the pine bark ignition delay time change from Arauco MC to 1-Day MC is probably due the combination of different variables like the moisture content decrease, the porosity and the particle size. Pine bark characteristics (like high porosity and great particle size) could lead to reduce the ignition delay time, but above a specific moisture content.

Figure 3.12 shows the ignition delay time of all mixes at 2-Day moisture content. All these tests were performed with 30 $kW \cdot m^{-2}$ of imposed incident heat flux. The lowest ignition delay times are from Mix 7 with 41 ± 4 s and Mix 2 with 45 ± 0 s (See table C.3 in the annexes for the exact values). At this level the pine bark is again the fastest to achieve ignition.

At 1-Day MC and 2-Day MC pine bark required less energy to achieve ignition. At

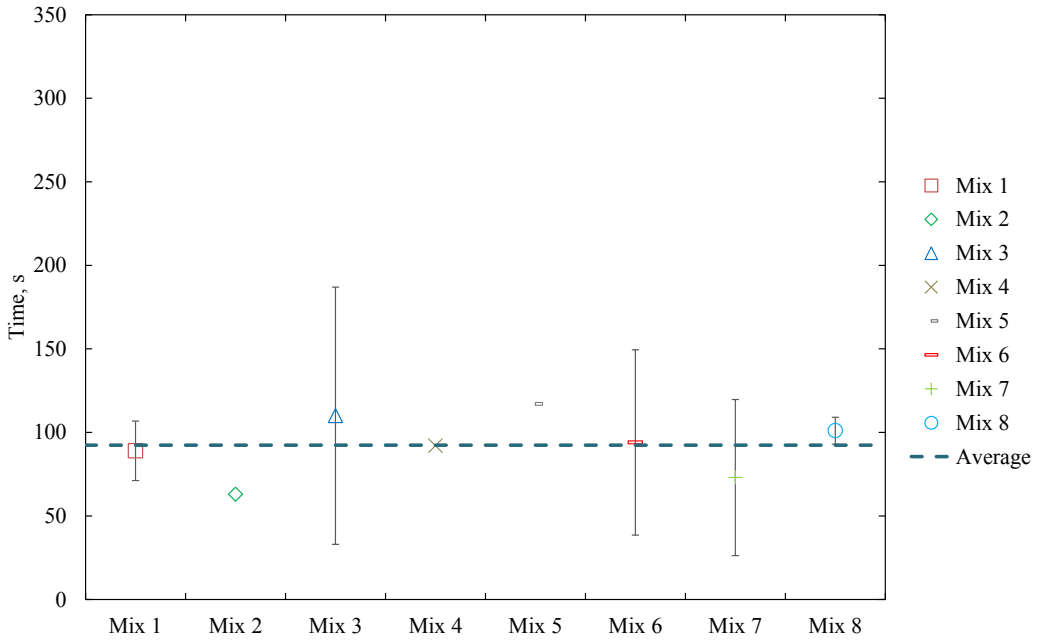

Figure 3.11: Ignition delay time of all mixes at 1-Day moisture content

Arauco MC, sawdust reduced the amount of energy that the mixes required to achieve ignition. The average time to ignition of all the mixes at Arauco MC is 187 ± 54 s, and at 1-Day level it is 92 ± 17 s, so there is a mean decrease in the energy required to achieve ignition from moisture content level Arauco to 1-Day. The mixes mostly composed of pine bark have the highest ignition delay time at Arauco level, and then have the lowest ignition delay time when the moisture content decrease. It shows great performance improvements when it looses moisture from Arauco to 1-Day level. The average time to ignition at 2-Day MC is 87 ± 41 s, so there is almost no variation from 1-Day MC to 2-Day MC. But is important to note that the incident heat flux used in 1-Day MC was 37 $kW \cdot m^{-2}$, and at 2-Day MC it was 30 $kW \cdot m^{-2}$. This difference have an influence on the ignition delay time, so both values can not be compared. With the moisture content decrease from Arauco to 1-Day, the ignition delay time decrease in 50 %. This means that less energy is required to produce the samples ignition, increasing the efficiency in the boiler. This energy could be used to produce steam instead of heating the fuel, which means financial benefits. All this benefits are explained by the moisture content decrease. Smaller ignition delay times means shorter residence time of the fuel in the boiler.

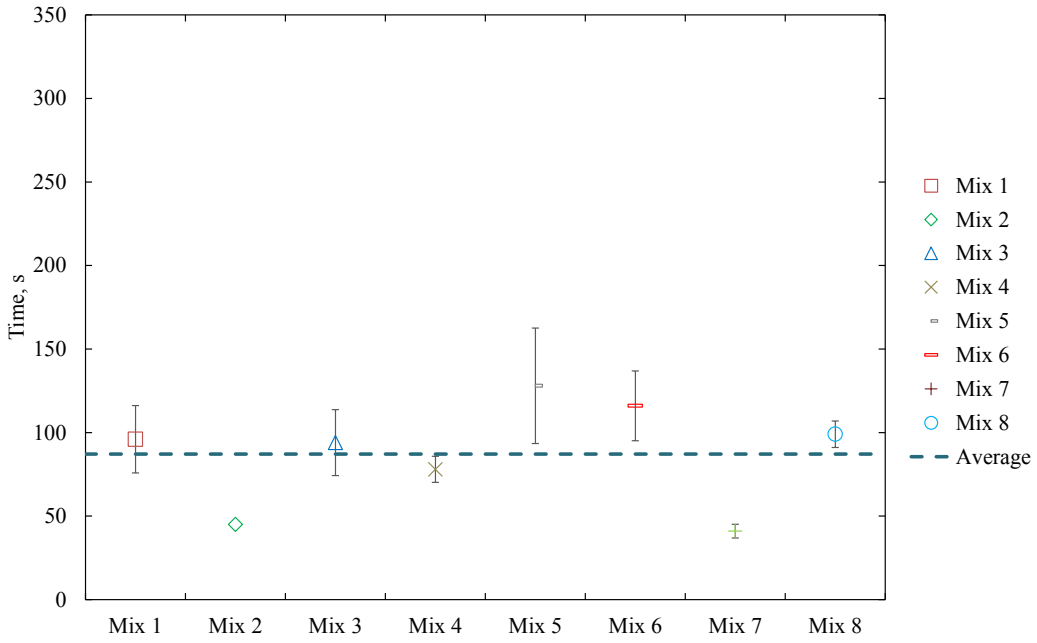

Figure 3.12: Ignition delay time of all mixes at 2-Day moisture content

3.5.5 Flaming time

The flaming time is defined as the time between flame ignition and flame extinction. Table C.4 in Annexe C shows the average flaming time of the tests at each moisture content. Figure 3.13 shows the flaming time of all mixes at Arauco moisture content level, Figure 3.14 at 1-Day level, and Figure 3.15 at 2-Day level. The variability of the flaming time is higher in almost all the tests at Arauco moisture content level than at the other levels. Only Mix 3 has less variability at the first moisture content level. There is no significant difference between the variability of 1-Day tests and 2-Day tests. It can be seen that with less moisture content the flaming time tends to be more stable. There is more repeatability between experiments.

There is no mix with a predominant high flaming time at all the moisture content levels. At Arauco MC level, Mix 3 have the highest flaming time (See Figure 3.13). At 1-Day level, Mix 5 has the highest flaming time, and near it comes Mix 6 (See Figure 3.14). At 2-Day level , Mix 7 has the highest flaming time (See Figure 3.15).

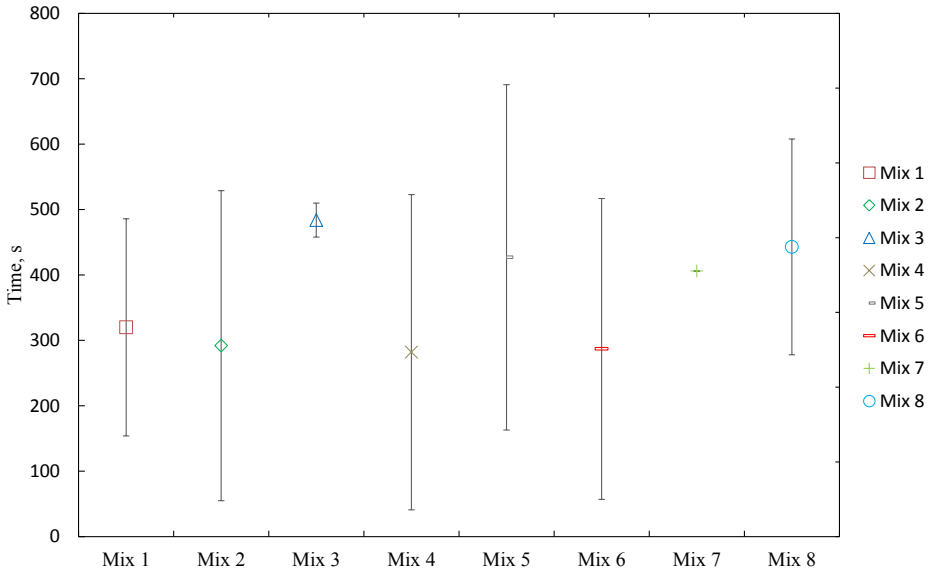

Figure 3.13: Flaming time of all mixes at Arauco moisture content level

3.6 Summary

The critical incident heat flux for ignition for sawdust, pine bark and wood chips at Arauco moisture content level is 25 kW·m^{-2}, 30 kW·m^{-2} and 25 kW·m^{-2} respectively. Sawdust reported the lowest ignition delay time in the variable incident heat flux test. The peak HRR increases when the EHC increases. The peak HRR and the EHC increases when the moisture content decreases.

Mix 3 (100 % composed of wood chips) has the highest average peak HRR and the highest peak HRR of all individual tests at Arauco moisture content. It has also the highest flaming time at this moisture content. Mix 3 has also the better ignition rate. The averaged Effective heat of combustion of Mix 3 was not the highest at Arauco moisture content, but presented the highest individual EHC. Mix 2 (100 % composed of pine bark) also presented high averaged peak HRR at Arauco moisture content.

At 1-Day moisture content Mix 8 (Mostly composed of Wood chips) has the highest

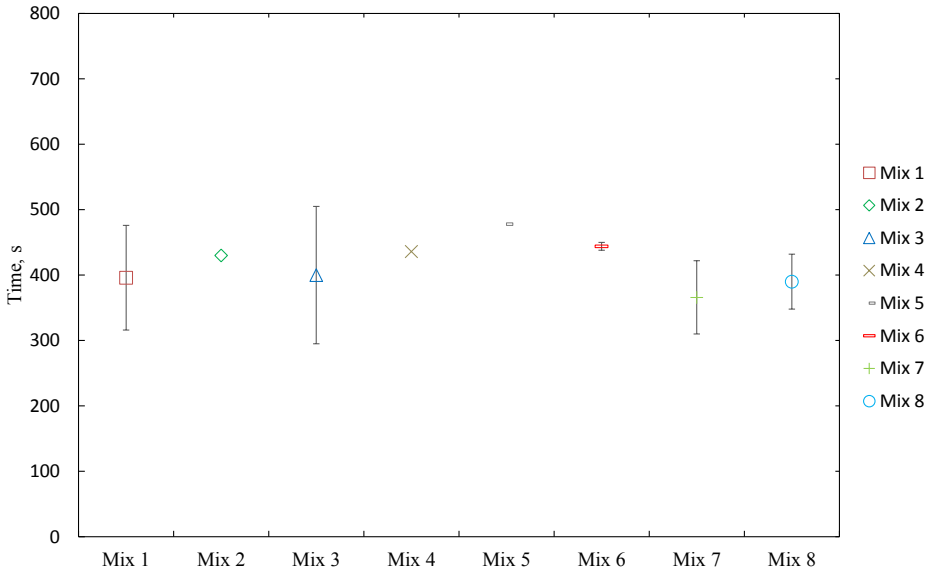

Figure 3.14: Flaming time of all mixes at 1-Day moisture content level

averaged peak HRR, and also the highest individual peak HRR. Mix 2 and Mix 7 (Mostly composed of pine bark) presented high averaged peak HRR too. Mix 2 and Mix 7 increased significantly their peak HRR with the moisture content decrease from Arauco to 1-Day. The ignition delay times of Mix 2 and Mix 7 changes from being the highest in Arauco moisture content to be the lowest at 1-Day moisture content. Mix 8, Mix 2 and Mix 7 have the highest EHC. The ignition delay time reduces in 50 % when the moisture content changes from Arauco to 1-Day. So, the residence time of the fuel in the combustion chamber decrease. There is an increase of 60 % in the average peak heat release rate from Arauco MC to 1-Day MC. This means that there would be a boiler efficiency increase, due the heat release rate increase.

At 2-Day moisture content Mix 3 has the highest average peak HRR and the highest peak HRR of all individual tests. Due to the moisture content decrease, Mix 3 had the highest power generation increment. Mix 2 and Mix 7 have again the lowest ignition delay times. Mix 3 have the highest averaged EHC and the highest individual EHC. Mix 4 and Mix 8 have high averaged EHC too. There is an increase of 80 % in the average peak HRR

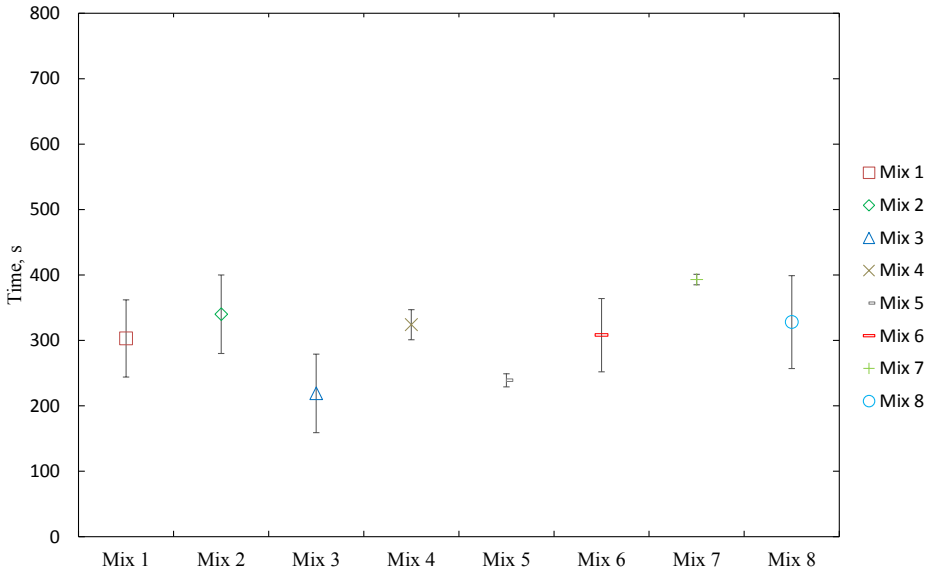

Figure 3.15: Flaming time of all mixes at 2-Day moisture content level

from Arauco MC to 2-Day MC and of 13 % from the average peak HRR from 1-Day to 2-Day.

In summary, Mix 3 seems to be the best mix. Then Mix 2. And if the moisture content decreases to 1-Day or to 2-Day, Mix 8 and Mix 7 become very good mixes too. There would be a high combustion efficiency increase in the boiler due the moisture content decrease from Arauco MC to 1-Day MC. This combustion efficiency increase is explained by the average peak heat release rate increase.

3.7 Performance of the two different methods with biomass

It has been seen in the PMMA results, that there is good agreement between the different methods used by the SCALA to determine the HRR. But PMMA has different composition and properties than biomass. It has been seen that the original depletion factor (Equation 2.10) considers the presence of soot, water vapor and carbon monoxide produced in the reaction, but it has been assumed that there is no carbon monoxide and no soot production,

and water vapor produced in the reaction has been neglected (leading the depletion factor to Equation 2.15). For this reason is necessary to verify the agreement of all methods, in order to be sure that the results are valid. Figure 3.16 shows biomass tests with good agreement between the calorimetric methods. This figure shows the heat release rate obtained with OC and SER method, and also shows the mass loss rates of the samples. It can be seen that that the magnitudes are even closer than the ones of the PMMA tests. The mass loss rate of the top-right graph in Figure 3.16 has a different behavior than the other two calorimetric methods results. Past the 200 seconds the OC and SER HRR increase, while the mass loss rate remains constant. This behavior is explained by an effective heat of combustion increase at that time period. Also, this test reported the highest effective heat of combustion of all tests performed. The effective heat of combustion increase could be explained by a moisture content decrease in the sample.

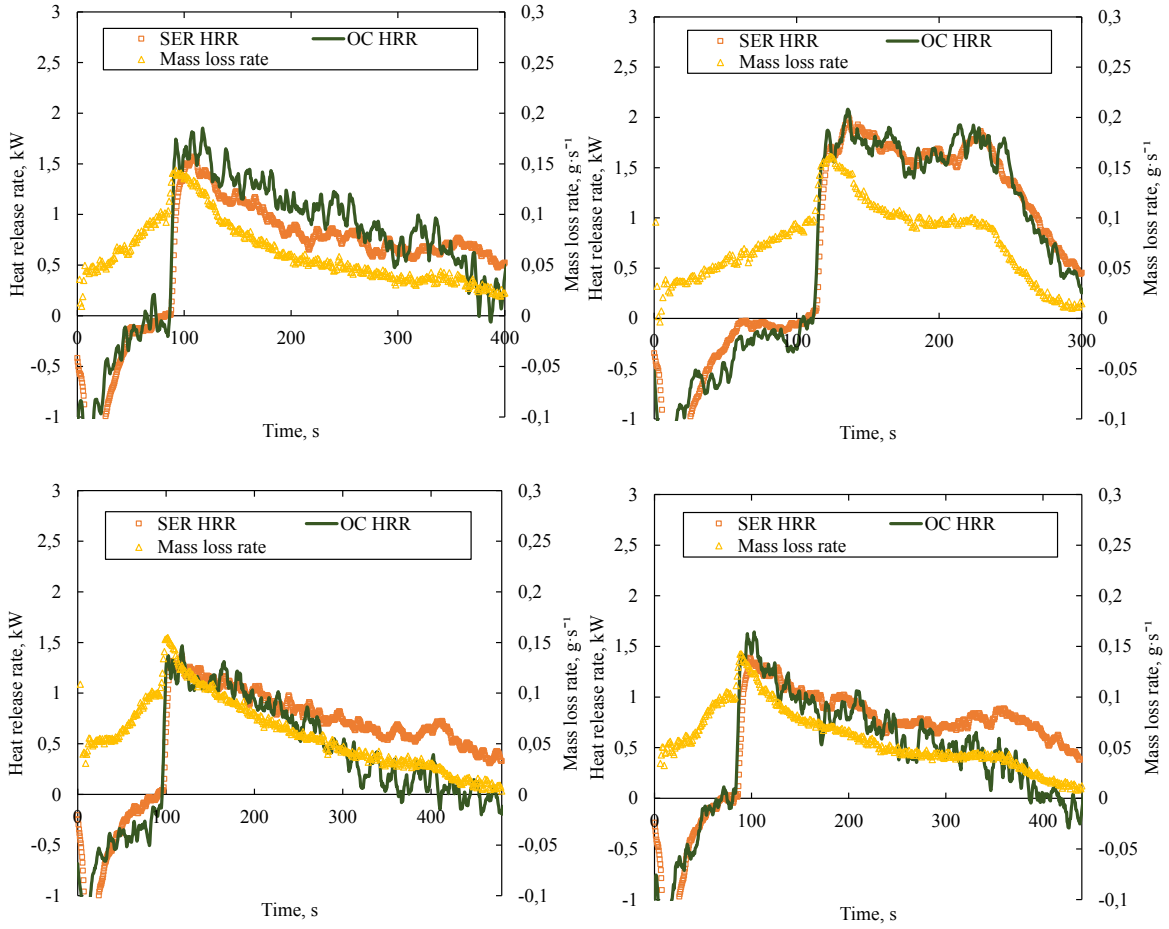

Figure 3.16: Biomass tests at 2-Day MC and $\dot{q}''_{inc}$ = 30 kW·m^{-2}. Top-left: Mix 8. Top-right: Mix 3. Bottom-left: Mix 1. Bottom-right: Mix 8

4 | SCALA performance

This section includes a performance analysis of the calorimeter. Problems occurred during test development will be analyzed. Calculations of the distribution of the incident heat flux are included and also the calculations of the measurement limits of the apparatus are explained.

4.1 Limits in the measurements of heat release rate

The SCALA is capable to measure heat release rates between the range of 0.46 kW and 15.7 kW. The techniques used to calculate this interval are explained in the following sections.

4.1.1 Minimum heat release rate

The minimum heat release rate is determined by the minimum signals that can be measured by the instruments. A Bunsen burner with ethylene was used for this purpose. The ethylene flow was set to 1 L·min^{-1}. This flow constitutes the base line. Then a higher flow was set to the flow meter. The procedure consists in gradually decreasing the ethylene flow and checking if each instrument is measuring the variation between the two different flows. Each flow is maintained for 2 minutes. Then the flow is returned to the base line (1 L·min^{-1}). Table 4.1 shows the variations of the ethylene flow.

Table 4.1: Ethylene flow variations and heat release rate

Time interval, min	0 - 2	2 - 4	4 - 6	6 - 8	8 - 10
Flow, L·min^{-1}	1.0	1.5	1.0	1.25	1.0
HRR, kW	0.94	1.40	0.94	1.17	0.94

The variation of 0.6 kW (From 0.94 kW to 1.40 kW, and from 1.40 kW to 0.94 kW) is detected with the TDLAS technique and also by the thermocouples. The variation of 0.23 kW (From 0.94 kW to 1.17 kW, and from 1.17 kW to 0.94 kW) is not detected with the TDLAS technique and is detected by the thermocouples. Therefore the minimum admissible heat release rate detected by both systems is defined as 0.46 kW.

4.1.2 Maximum heat release rate

There are two variables to consider for determining the maximum HRR suitable to be measured with the SCALA. First, the measurement limits of the instruments. The type K thermocouples allow to measure up to 1200°C, and the exhaust air temperature at the maximum heat irradiance from the heaters does not exceed the 200°C. The maximum temperature difference capable to be measured would be 1000°C. Therefore the maximum heat release rate is not determined by the thermocouple limits. For the oxygen consumption method, the apparatus can measure oxygen concentrations down to 0 ppm. Thus, the maximum HRR is not determined by the oxygen consumption method. The scale has no considerable limitations that could affect the heat release measurements.

The second variable that determines the maximum admissible HRR are the physical characteristics of the apparatus. The variable considered in the following analysis is the flame height. The flame should not impinge on the exhaust duct. If the flame is in contact with the duct walls, its behavior will be altered, and thus will interfere with the measurements. The distance between the surface of the sample (the base of the flame) and the bottom of the exhaust duct is 0.72 m. At the base of the exhaust stack a radiation shield is positioned which would interfere with the flame. There is no detailed study of the minimum distance that should be maintained between the flame and the radiation shield. So, an arbitrary minimum distance between the top of the flame and the radiation shield has been defined, as a percentage of the flame height. The distance between the flame and the radiation shield should be at least the 20% of the flame height. Thus, the flame height should not exceed 0.6 m, resulting in a distance of 12 cm between the top of the flame and the base of the exhaust duct.

There is a relationship between the flame heights and the heat release rates of two different flames Drysdale (2011). This is shown in Equation 4.1. Thus, with the calculated flame height limit (0.6 m) and the heat release rate and height of a reference flame, the maximum heat release rate limit can be calculated. An ethylene flame of a Bunsen burner is used as reference to calculate the maximum heat release rate limit.

$$\frac{L_{ref}}{L_{max}} = \left(\frac{\dot{Q}_{ref}}{\dot{Q}_{max}}\right)^{\frac{2}{5}} \tag{4.1}$$

Where L_{ref} and $\dot{Q}_{ref}$ are the reference flame height and the reference flame heat release rate respectively, and L_{max} and $\dot{Q}_{max}$ are the calculated flame height limit and the maximum heat release rate limit respectively. With the values of L_{ref}, $\dot{Q}_{ref}$ and L_{max}, the term $\dot{Q}_{max}$ is calculated. The calculated value is $\dot{Q}_{max}$ = 15.7 kW.

4.2 Distribution of the incident heat flux on the specimen area

All tests are developed by imposing a constant radiant heat flux over the specimen area. The distribution of the heat flux on the specimen area should be as uniform as possible. The OSU standard mentions that the non-uniformity of the incident heat flux over the specimen area should be less than 5% of the average incident flux (ASTM E906 / E906M-10, 2010). For the Cone Calorimeter the uniformity is typically 2% for horizontal position and tipically 7% for vertical position (Hurley et al., 2015). For the SCALA the non-uniformity of the incident heat flux above the specimen area in the horizontal position is less than 10 %. The methodology to determine the incident heat flux distribution is explained below.

4.2.1 Methodology

A metal plate is positioned on the specimen area. The specimen area is a square of 100×100 mm. The plate has 9 marks that indicate the position where the radiometer should be placed

to measure the incident flux. Figure 4.1 shows the measurement points.

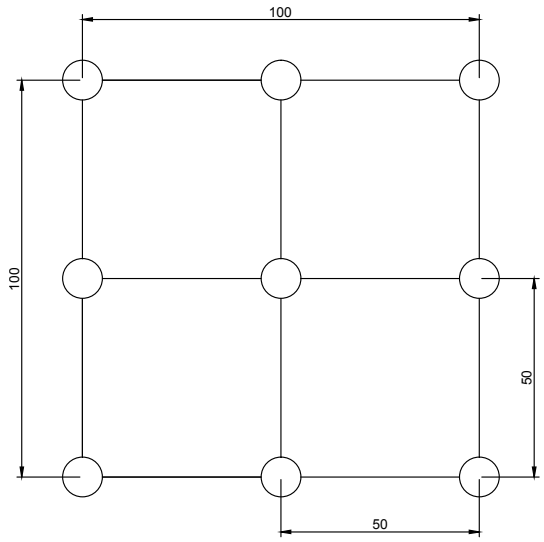

Figure 4.1: Measurement points of the incident heat flux

Equation 4.2 is used to calculate the variation of the heat flux in reference to the average

$$S_i = \left| \frac{\dot{q}''_i - \dot{q}''_{ref}}{\dot{q}''_{ref}} \right| \cdot 100\% \qquad i \in \{1, 2, ..., 9\} \tag{4.2}$$

Where S_i is the variation of heat flux measured in position i in reference to the center incident flux, $\dot{q}''_i$ is the incident heat flux measured in position i and $\dot{q}''_{ref}$ is the incident heat flux measured at the center (position $i = 5$). Table shows the calculated values.

Table 4.2: Variation of the incident heat flux on the specimen area with respect to the center $\dot{q}''_{ref}$

	Left	Center	Right
Back	$S_1 = 6\ \%$	$S_2 = -3\ \%$	$S_3 = 5\ \%$
Center	$S_4 = 9\ \%$	$S_5 = ref$	$S_6 = 9\ \%$
Front	$S_7 = -1\ \%$	$S_8 = -9\ \%$	$S_9 = -3\ \%$

The positions of each value of the table correspond to the position in Figure 4.1, this is the view from above. The heaters are positioned on the left and the right side of the image. Six of the nine values are below the limit established by the OSU standard, and the other three are above it (The differences are is greater than 5 %). The OSU use a diamond-shaped

mask and a bend on the top and bottom of the reflector to achieve the uniformity of the incident heat flux. Thus, using reflectors and metal masks could improve the uniformity of the incident flux on the sample in the the SCALA.

4.3 OC method performance

This section is about problems related to the oxygen consumption method. Two factors are analyzed: unexpected oxygen measurement drifts and overestimated results obtained with the oxygen calibration constant.

4.3.1 Oxygen measurements drift

Some measurements performed with the TDLAS module present variations not explained because of the flame behavior. These unexpected drifts occurred during some biomass tests, during some calibration procedures and also sometimes while no experiment was being carried out. The spurious variations can be perceived by comparing the oxygen measurements with the temperature or the mass loss rate measurements. Figure 4.2 shows spurious oxygen concentration variations to lower or higher magnitudes. Each graph has also the HRR calculated with the SER method and has also the mass loss rate calculation, so the behavior can be compared. At the moment, the source of these misleading measurements is not known. But there is evidence of situations that produce unexpected drifts. During the apparatus heating (In order to reach the steady state before a test) the laser shows big measurement variations, but it tends to stabilize after a while. But also, with no apparent ambient conditions changes, the laser readings experimented unexpected drifts.

In spite of not knowing the nature of the spurious oxygen measurement drifts, a solution is proposed to solve the problem. A beam splitter will be incorporated to the system. The beam splitter splits the laser beam into two signals with different intensity. One signal will measure the oxygen concentration in the exhaust duct. The secondary signal will be directed to a powermeter. Thus, the variations in intensity of the beam that is emitted by the laser will be determined. So, $I_\lambda(0)$ of Equation 2.29 will be determined with the secondary signal.

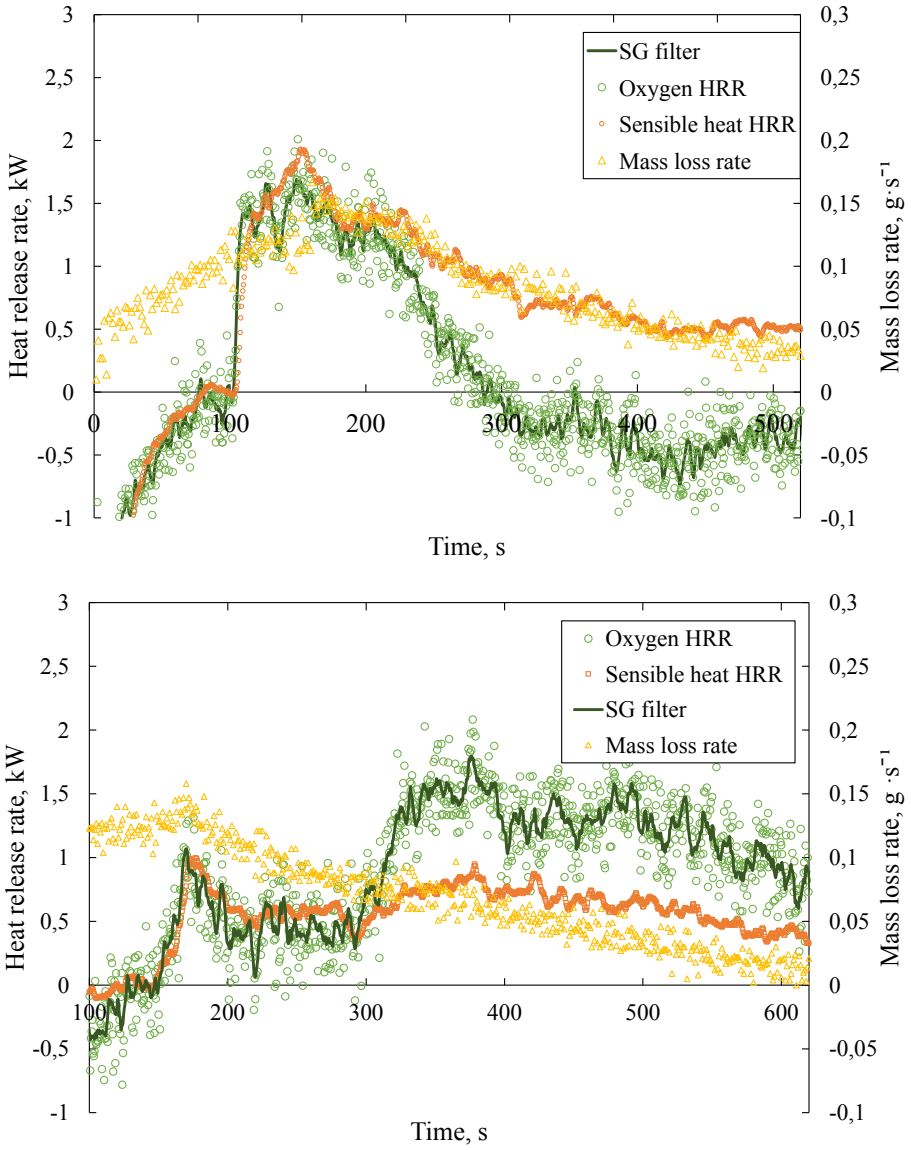

Figure 4.2: Top: Mix 8, 1-Day MC, $\dot{q}''_{inc}$ = 37 kW·m^{-2}, Oxygen measurement drift to lower magnitudes. Bottom: Mix 4, Arauco MC, $\dot{q}''_{inc}$ = 37 kW·m^{-2} Oxygen measurement drift to higher magnitudes

4.3.2 Overestimated results with the oxygen calibration constant

In the chapters above two methods to calculate the heat release rate with the oxygen concentrations measured in the exhaust duct have been presented. The method used in all the experiments performed in this study was the oxygen equation without calibration

constants, described in Section 2.2.2.1. This was because the results obtained with that method have better agreement with the HRR obtained with the other two methods. The results obtained with the equation that uses a calibration constant were higher than the ones calculated with the equation without a calibration constant. In other words, the calibration constant calculated in the calibration procedure with ethylene as fuel was not so representative for the PMMA experiments. Independent of the fuel type, all results calculated with the equation without the calibration constant (Method A) will be lower than the ones calculated with it (considering that ethylene is used for the calibration procedure and the experimental conditions do not change). This because if the constants of the equation used in Method A (Equation 2.17) are multiplied, the resulting constant has a lower magnitude than the calibration constant calculated in Section 2.4.2.2. The HRR calculated with both oxygen consumption methods and the mass loss rate HRR can be seen in Figure 4.3.

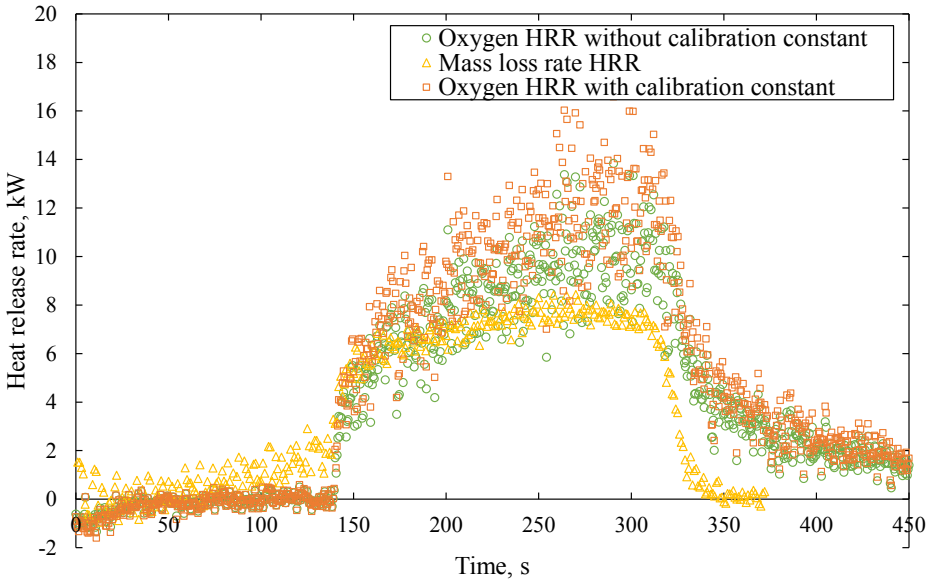

Figure 4.3: Comparison between equations with and without a calibration constant

The difference in the results is attributed to the differences between the calibration fuel and the other fuels tested in this study. The calculation of the calibration constant depends on the conditions imposed by the calibration fuel. The implications of using a calibration

fuel are the following ones. First, to pass from Equation 2.10 to Equation 2.15, it has to be assumed that there is complete combustion, there is no soot production, and that the water vapor produced in the reaction is neglected. This means that if the calibration fuel reacts under incomplete combustion, has soot production, or there is a high amount of water vapor produced, then the calibration constant will be underestimated. On the other side, if the combustion gases and the incoming air do not develop and mix in the duct in the same way for all fuel types and heat release rates, then the calibration constant could be over or under estimated. For example, if the heat release rate of the calibration fuel is low, then the flame is small. Then, there will be more space between the exhaust duct and the flame. The combustion gases will have more space and time to mix with the incoming air. If the calibration constant is calculated in these conditions, and then a test with higher heat release rate is performed, the calibration constant could be overestimated for this test. This is seen in Figure 4.3.

The calibration procedure was conducted with the Bunsen burner at two different heights. Before the definitive position of the sample, the calibration procedures were performed 400 mm below the current position. The calibration constants calculated in those calibration procedures were near the the value of -5 kW·% O_2^{-1}. Now the calibration constants are near the -2.7 kW·% O_2^{-1} (position of the Bunsen burner 400 mm higher than before). If the absolute value of the calibration constant is higher than the correct value, then the results calculated with this calibration constant will be overestimated. This is an evidence that the space between the flame and the exhaust duct probably influences the mixing of the combustion gases and the incoming air. The influence of this space should be studied in the future work. Another possibility is that the outlet gases temperature influenced the oxygen concentration measurements. Due the Bunsen burner position change, higher temperatures were achieved in the gases at the exhaust duct. As seen in Section 2.5.3, temperature variations have an influence on the oxygen concentration measurements.

4.4 SER method performance

This section is about problems related with the SER method. It includes an analysis of the thermal inertia influence at the flame extinction and also the temperature gap at tests with short ignition delay times.

4.4.1 Thermal inertia influence at flame extinction

One of the problems with the SER method is the influence of the thermal inertia of the apparatus on the temperature measurements. As described in Section 2.5.3, the apparatus walls absorbs the heat of the air stream at the beginning of the flaming combustion. Thus, the temperature rise rate of the thermocouple is lower than the heat release rate of the fuel. This can be confirmed by comparing the mass loss rate and the HRR with the SER method (See Figure 2.21 or Figure 2.22). During the extinction of the flame, the temperature decrease rate measured by the thermocouples is lower than the heat release rate of the flame. This is because of the heat transfer from the apparatus walls to the air stream. In other words, the apparatus wall heats the air stream (at the flame extinction), so the temperature recorded will be overestimated. Figure 4.4 shows various HRR curves obtained with the SER method (Performed with biomass). The data is plotted from the flaming ignition to extinction. It can be seen that at the flame extinction of all tests (last values of each test), the HRR is not zero. The red circle in Figure 4.4 indicate the overestimated HRR at flame extinction.

At flame extinction, the HRR is near 0.5 kW. It has to be considered that the HRR last values will be overestimated. It is recommended to calculate the effective heat of combustion at each time interval. With the effective heat of combustion graph it can be seen that its magnitude will gradually start to increase as the HRR starts to be overestimated. This is because the mass loss rate magnitude becomes smaller and the HRR stays at high magnitudes. The EHC calculated with the SER method will tend to infinity at the flame extinction.

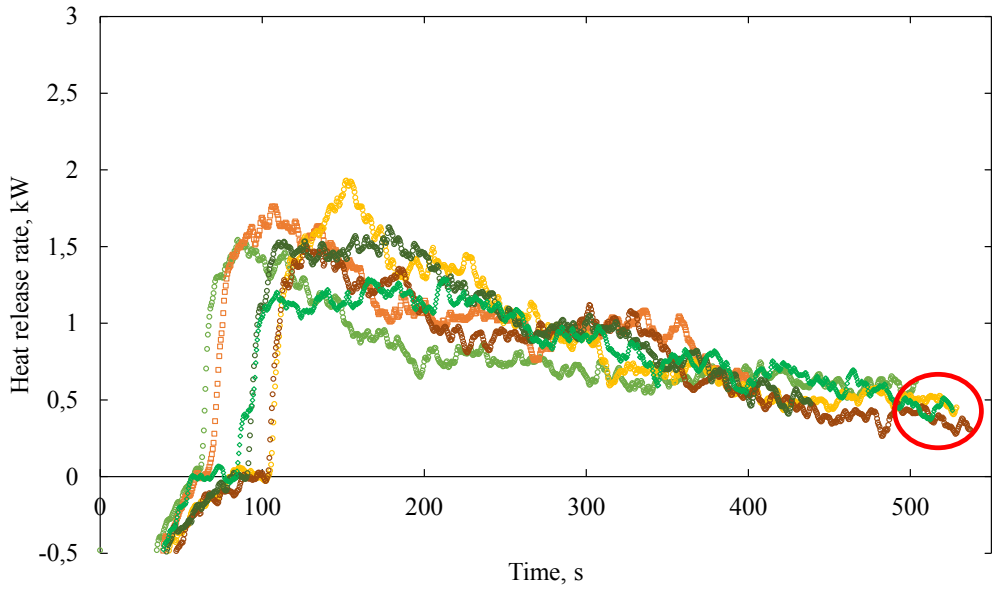

Figure 4.4: Overestimated HRR at flame extinction with the SER method

4.4.2 Temperature lag at tests with short ignition delay time

When performing a test, first the apparatus temperature should reach the steady state. Then the specimen is put into the combustion chamber. As described in the previous chapters, when the window is opened there is a temperature decrease in the apparatus walls. This is observed in the exhaust duct thermocouple. This can be seen also in the graphs presented in this study as the negative HRR before the sample ignition. After a while since the specimen has been inserted into the combustion chamber, the apparatus temperature returns to the steady state point. Then ignition occurs and the temperature rise is used to calculate the HRR of the burning sample. But in some cases (Generally samples with low moisture content level and/or high incident heat fluxes) the sample makes ignition before the apparatus temperature returns to the steady state. Figure 4.5 shows two tests. Both tests are performed with Mix 2 (pine bark). The sample shown at the top has 1-Day moisture content level and the other one at the bottom has a 2-Day moisture content. The top one had an ignition delay time of 63 s and the bottom one had an ignition delay time of 45 s. Ignition has been marked with a red circle in the HRR graph. The bottom test (with the lowest ignition delay time) achieves ignition before the temperature returns to the

steady state levels. A slope change at that point can be seen, because now the exhaust duct thermocouple is measuring the temperature variations due the heat release rate of the flame and also the heat contributed by the radiant heaters. Also some of the heat contributed by the flame is lost through the walls, because the apparatus walls temperature was in transient state. It can be seen that the HRR obtained with the OC method in the top test has better agreement with the HRR obtained with the SER method, than between the same magnitudes in the bottom test. This considering only the first seconds after ignition. These tests were selected because they have similar heat release rates and similar mass loss rates. In summary, ignitions before the apparatus temperature returns to the steady state, affect heat release rate measurements with the SER method in the first seconds after ignition. It gives underestimated values due transient heat transfer through the apparatus walls. This is not significant for the entire test, because the apparatus reached the steady state temperature relatively fast.

The tests in this study have been performed with low incident heat fluxes in order to avoid ignitions before the return to steady state conditions. In some cases this was not achieved, and in spite of that the tests have been considered because ignition occurs near the steady state temperature and this only temperature lag influenced the first seconds after ignition.

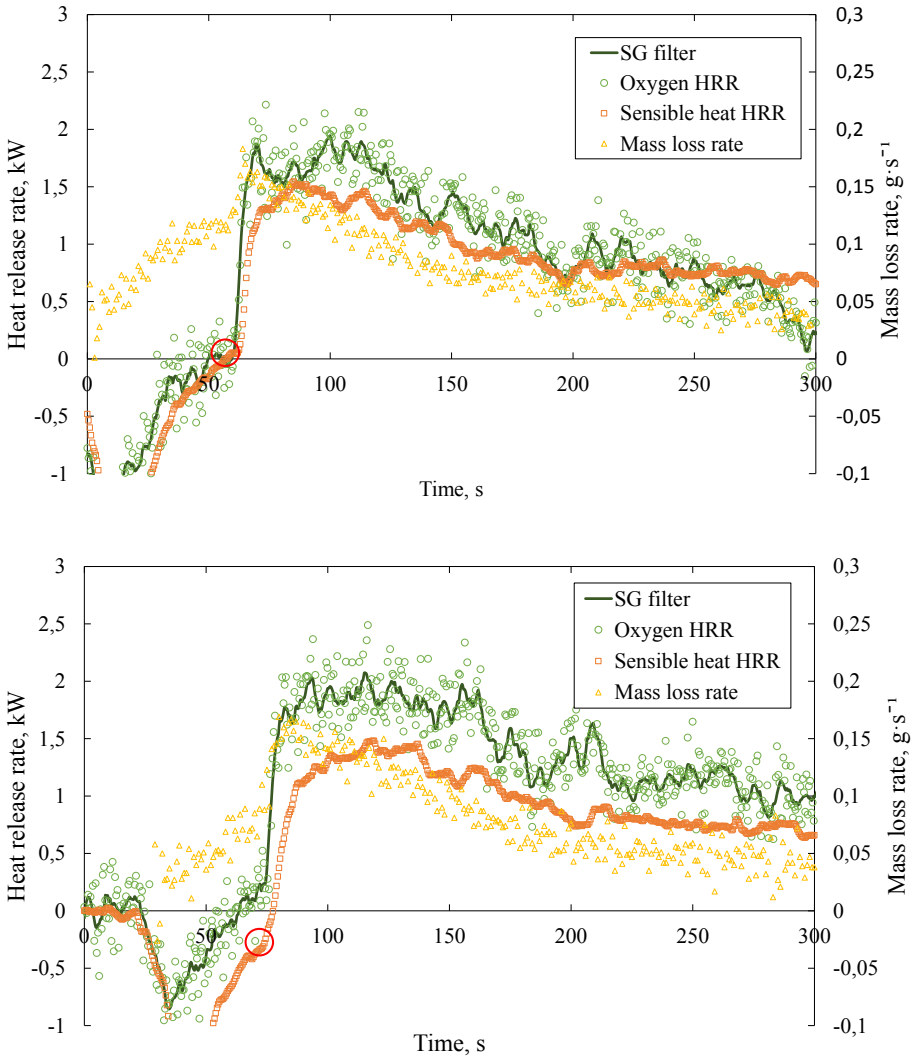

Figure 4.5: Top: Mix 2, 1-Day MC, Ignition delay time = 63 s. Bottom: Mix 2, 2-Day MC, Ignition delay time = 45 s.

5 | Conclusions

Chile is a country with an increasing energy demand. There are incentives to use renewable energy sources for electricity generation. Biomass becomes an interesting energy source to exploit, because of its renewable nature and the conditions in the country that facilitate the biomass growth and use. The study centered in a Celulosa Arauco S.A. power plant. This power plant uses biomass to produce electricity. The biomass mix used in Arauco as feedstock for the boilers is composed of different biomass types with high and varied moisture content. In Arauco they have the options of buy biomass from different suppliers and also they use their own biomass wastes from the cellulose production to supply the boilers. With the biomass used in Arauco, 8 mixes with different biomass types and different moisture contents have been prepared. These biomass mixes have been characterized in order to find an optimal mix, using as parameters the peak heat release rate, the effective heat of combustion, the ignition delay time and the flaming time. Three different moisture content scenarios were studied. One at the original moisture content and two with lower moisture. The incident heat flux on the specimen was varied in order to find the critical heat flux for spontaneous ignition and study the influence of the heat fluxes on the ignition delay time. The critical heat fluxes for spontaneous ignition for sawdust, pine bark and wood chips at the Arauco moisture content are 25 $kW \cdot m^{-2}$, 30 $kW \cdot m^{-2}$ and 25 $kW \cdot m^{-2}$ respectively. The sawdust reported the lowest ignition delay times at all heat fluxes were it achieved ignition, but because of its high moisture content only from 40 $kW \cdot m^{-2}$ onward the number of tests that achieved ignition starts to increase. Below that heat flux only 2 tests achieved ignition, one at 25 $\cdot m^{-2}$ and other one at 30 $\cdot m^{-2}$. At the original moisture content, wood chips result to have the highest average peak heat release rate. It had also the highest ignition rate (percentage of valid ignitions of total tests performed). This means that it make ignition

more times that the other mixes and the ignitions produce more stable flames that the other mixes. It has also the highest EHC in an individual test but not the highest average EHC (Including all tests). It had also the highest flaming time. The EHC at this level was similar to all tests, except by the mix used in Arauco that showed to be low. Pine bark presented the second highest average peak heat release rate and one of the highest EHC. In the following scenario with lower moisture content, the mix with 60 % wood chips 20 % pine bark and 20 % sawdust presented the maximum average peak heat release rate. The mixes composed mostly by pine bark presented high improvements at this scenario. These mixes passed from having the highest ignition delay times to the lowest ignition delay time (due the moisture content decrease). And also presented the highest average peak heat release rate after the mix composed of 60 % wood chips 20 % pine bark and 20 % sawdust. These three mixes had the highest EHC. In the last scenario with the lowest moisture content, the mix composed only of wood chips presented the highest average peak heat release rate, and also has the highest HRR improvements from the previous scenario to this one. It has also the highest average and individual EHC. The lowest ignition delay time were reported by the same mixes that in the previous scenario; the two mixes composed mostly by pine bark. Wood chips is the best biomass and then the pine bark. Mixes with composition 60 % wood chips 20 % pine bark and 20 % sawdust and 20 % wood chips 60 % pine bark and 20 % sawdust becomes really good mixes at lower moisture content levels. Arauco mix seamed not to excel because of the high moisture content of the sawdust. The sawdust presented the highest moisture content. With lower moisture content sawdust improve its performance. The combustion efficiency of all biomass mixes were calculated. Pine bark presented in the three scenarios high efficiency. The highest efficiency was presented by Mix 4 (60 % sawdust, 30 % pine bark and 10 % wood chips) in the scenarios with the lowest moisture content. It is highlighted that pine bark presented one of the highest efficiency in the middle moisture content level, compared with all moisture content scenarios. This means that with low changes in the moisture content, pine bark present high improvements. The highest variations of ignition delay time and average peak HRR were found from Arauco MC to 1-Day MC. The peak HRR increase in 60 % and the ignition delay time decrease in 50 % due the moisture content variation. So, it is recommended to decrease the moisture content

to 1-Day in order to achieve the highest efficiency increase. A financial study should be carried out in order to know the feasibility of decreasing the moisture content of the biomass.

All tests were performed with the Sensible Heat Calorimetry Apparatus (SCALA). This calorimeter was designed, constructed and experimentally validated. The SCALA uses three methods to determine the heat release rate of burning specimens: the sensible enthalpy rise method (SER), the oxygen consumption method (OC) and the mass loss rate method (MLR). The SER method is based on type K thermocouples that measure the enthalpy rise of a constant air flow. The OC method is based on a TDLAS instrument to measure the oxygen concentrations of a constant air flow. The MLR method is based on a precision balance measurements. The SER method uses a calibration constant that assumes that the heat losses through the walls are fuel independent. The OC method assumes that there is complete combustion in the reaction, water vapor produced in the combustion reaction is neglected and that there is no soot production. The total relative uncertainty of the oxygen consumption HRR calculations vary between 10 % and 85 %, where 10% correspond to 16 kW and 85 % correspond to 0.5 kW. The total relative uncertainty of the sensible enthalpy rise HRR calculations vary between 4 % and 23 %, where 4% correspond to 16 kW and 23 % correspond to 0.5 kW. The calorimeter was experimentally validated using PMMA. It was first validated comparing the results of the three methods, where good agreement was achieved. OC method results were higher the other results. Then the results were validated by comparing them on other results in the literature. They were compared with results obtained with the Fire Calorimetry Apparatus (FPA). There was good agreement. The SER method results had better agreement with the nominal values (determined with the mass loss rate method) than the SER method results obtained with the FPA. The OC method results were higher than the rest, but inside an acceptable range. The air losses should be eliminated in order to improve the OC method results.

5.1 Future Work

This section is separated in two parts. One is aimed in improving the calorimeter performance and the other one to extend the biomass characterization study.

5.1.1 Biomass characterization

The representative mix of Arauco used in this study was not complete and was performed using the mix compositions of year 2012. The complete Arauco mix should be tested with the updated mix compositions. Testing was negatively influenced by using spontaneous ignition. This, because of the high moisture content of the samples. Piloted ignition should be used in tests where the samples are at Arauco moisture content, in order to have less variability in the ignition delay times and achieve more valid tests. One considerable problem of this study was the low number of valid tests performed at the Arauco moisture content. With piloted ignition, the mass loss before ignition will be minimized. Another future work is to apply the biomass characterization with the SCALA to other power plants that use biomass as feedstock for their boilers. Also, an ultimate analysis should be carried out to the biomass samples in order to know the chemical compositions and thus calculate their net heat of combustion.

5.1.2 Calorimeter

The following list contains design improvements and modifications that should be implemented in the SCALA in order to improve its performance.

- Install the pilot system to develop piloted ignition tests.
- Include a compressor, which will supply a constant cooling air flow between the windows of the calorimeter. Currently there is an available compressor but the tests have shown that the air flow was not enough to decrease the temperatures of the entire calorimeter walls. The main reason for not using it was that the temperature at the top duct increases with the air flow (The heat absorbed of the calorimeter walls

increased the air flow temperature and then the air flow heated the top duct). This problem will be solved if the air flow is increased. Then a flow regulator should be installed in order to control the flow supplied by the compressor.

- Solve the problem of air losses through the walls. The small openings of the calorimeter should be sealed with high temperature resistance materials, especially the joints of the windows. The air losses problem should be solved before installing a compressor, in order to avoid air flows mixing between the inlet air and the compressor air.

- Correct the measurements performed by the oxygen analyzer by temperature.

- Perform tests with different fuels with known properties in order to study the validity of the calibration constant. Different liquid fuels could be use for this purpose. The SER method results should be compared with the MLR method results.

- Perform tests with different fuels tested by other authors with different calorimeters, in order to validate the methods used by the SCALA using different materials.

- Study the influence of the space between the flame and the exhaust duct on the oxygen concentration measurements. Vary the Bunsen burner position in order to find changes in the calibration constant magnitude.

- Change the rod that holds the sample holder to a ceramic rod in order to decrease the heat conduction between the sample holder and the scale. A great part of the heat that enters into the insulation box where the scale is located, enters because of conduction of the metal rod.

- Improve the air difussion system at bottom of the plenum. The current air diffusor do not route the air flow to all directions, and is responsible of great pressure drops.

- Include a beam splitter system to the laser of the TDLAS instrument. With this system the oxygen measurement unexpected drifts will be solved.

- Change the flowmeter to another one with more capacity. With higher ethylene flows, calibrations with higher heat release rates could be performed. Thus, the validity of the calibration constant in different higher flows could be analyzed.
- Include plugs to the radiant heaters that can be connected to the voltage regulators. This way, it will be easier to change the resistance elements of the radiant heaters (The structure could be easily removed from the apparatus)
- Perform tests with different soot amounts in order to know its influence on the oxygen measurements.
- Include more sample holders with different porosity.

Bibliography

Abbasi, T. and Abbasi, S. (2010). Biomass Energy and the Environmental Impacts Associated with its Production and Utilization. *Renewable and Sustainable Energy Reviews*, 14(3):919–937. 1

Agency, T. U. S. E. P. (2009). Regulation of Fuels and Fuel Additives: Changes to Renewable Fuel Standard Program. *Federal Register*, 74:24904–25039. 1

ASTM D4442-07 (2007). Standard Test Methods for Direct Moisture Content Measurement of Wood and Wood-base Materials. Standard, ASTM International, West Conshohocken, PA. 3.3.1

ASTM E1354-11b (2011). Standard Test Method for Heat and Visible Smoke Release Rate for Materials and Products Using an Oxygen Consumption Calorimeter. Standard, ASTM International, West Conshohocken, PA. (document), 1, 1.2, 1.2.2.1, 1.2, 1.2.3, 2.2.3, 3.5.3

ASTM E2058-03 (2003). Standard Test Methods for Measurement of Material Flammability Using a Fire Propagation Apparatus (FPA). Standard, ASTM International, West Conshohocken, PA. (document), 1.2, 1.2.1.2, 1.2.2, 2.4

ASTM E906 / E906M-10 (2010). Standard Test Method for Heat and Visible Smoke Release Rates for Materials and Products Using a Thermopile Method. Standard, ASTM International, West Conshohocken, PA. (document), 1.2, 1.2.2.2, 1.2.3, 1.3, 2.2.2.2, 2.4.1.2, 4.2

Babrauskas, V. (1984). Development of the Cone Calorimeter—A Bench-scale Heat Release Rate Apparatus Based on Oxygen Consumption. *Fire and Materials*, 8(2):81–95. 1.2.2

Babrauskas, V. (1986). Comparative Rates of Heat Release from Five Different Types of Test Apparatuses. *Journal of Fire Sciences*, 4(2):148–159. 1.2.1, 1.2.1.1, 1.2.4

Babrauskas, V. (1990). *Heat Release in Fires*. Taylor & Francis. 3.5.3

Babrauskas, V. (1992). From Bunsen Burner to Heat Release Rate Calorimeter. *Heat Release in Fires*, pages 7–29. 1.2, 1.2.2

Babrauskas, V. (2006). Effective heat of combustion for flaming combustion of conifers. *Canadian Journal of Forest Research*, 36(3):659–663. 1.1.1

Babrauskas, V. (2016). The Cone Calorimeter. In *SFPE Handbook of Fire Protection Engineering*, pages 952–980. Springer New York, New York, NY. (document), 2.4

Bertran, J. and Morales, E. (2008). Potencial de Generación de energía por Residuos del Manejo Forestal en Chile. *Santiago, Chile. Comisión Nacional de Energía (CNE)/Deutsche Gesellschaft für Technische Zusammenarbeit (GTZ) GmbH*. 1

Biteau, H. (2010). *Thermal and Chemical Behaviour of an Energetic Material and a HeatRelease Rate Issue*. PhD thesis, The University of Edinburgh. 1.2.2, 2.6.1, A

Biteau, H., Steinhaus, T., Simeoni, A., Schemel, C., Marlair, G., Bal, N., and Torero, J. L. (2008). Calculation Methods for the Heat Release Rate of Materials of Unknown Composition. *International Association for Fire Safety Science*, 9. 1.2.1.2, 1.2.1.2, 2.5, 2.5.4, 2.6.3

Brohez, S. (2005). Uncertainty Analysis of Heat Release Rate Measurement from Oxygen Consumption Calorimetry. *Fire and Materials*, 29(6):383–394. 2.6.3, 2.6.3, 2.6.3

CarboChile (2015a). *Ceraboard 100 Datasheet Code 5-5-03 S*. Morgan Thermal Ceramics Inc. 2.3.1.2

CarboChile (2015b). *KAOWOOL HP 1260 Datasheet*. Morgan Thermal Ceramics Inc. 2.3.1.2

Chow, W. and Han, S. (2011). Heat Release Rate Calculation in Oxygen Consumption Calorimetry. *Applied Thermal Engineering*, 31(2):304–310. 1.2.1.2

Comisión Nacional de Energía (2015). Anuario Estadístico de Energía 2005-2015. 1

Comisión Nacional de Energía (2016). Capacidad Instalada de Generación. 3.3

Demirbas, A. (2004). Combustion Characteristics of Different Biomass Fuels. *Progress in Energy and Combustion Science*, 30(2):219 – 230. (document), 1.1

Demirbas, A. (2005). Potential Applications of Renewable Energy Sources, Biomass Combustion Problems in Boiler Power Systems and CombustionRelated Environmental Issues. *Progress in Energy and Combustion Science*, 31(2):171 – 192. 1.1.1

Drysdale, D. (2011). *An Introduction to Fire Dynamics*. John Wiley & Sons. 4.1.2

Drysdale, D. D. (2016). Thermochemistry. In *SFPE Handbook of Fire Protection Engineering*, pages 138–150. Springer New York, New York, NY. 1, 1.1.1

Dyken, S. V., Bakken, B. H., and Skjelbred, H. I. (2010). Linear Mixed-integer Models for Biomass Supply Chains with Transport, Storage and Processing. *Energy*, 35(3):1338 – 1350. 3.5.3

Evans, D. and Breden, L. (1978). Time Delay Correction for Heat Release Rate Data. *Fire Technology*, 14(2):85–96. 1.2.1.1

Filipczak, R., Crowley, S., and Lyon, R. (2005). Heat Release Rate Measurements of Thin Samples in the OSU Apparatus and the Cone Calorimeter. *Fire Safety Journal*, 40:628–645. 1.2.1.1, 2.2.2.2, 2.2.2.2, 2.4.2.2

García, R., Pizarro, C., Lavín, A. G., and Bueno, J. L. (2014). Spanish Biofuels Heating Value Estimation. Part i: Ultimate Analysis Data. *Fuel*, 117:1130–1138. 3.5.3

Huggett, C. (1980). Estimation of Rate of Heat Release by Means of Oxygen Consumption Measurements. *Fire and Materials*, 4(2):61–65. 1.2.1.2

Hurley, M. J., Gottuk, D. T., Hall Jr, J. R., Harada, K., Kuligowski, E. D., Puchovsky, M., Watts Jr, J. M., Wieczorek, C. J., et al. (2015). *SFPE Handbook of Fire Protection Engineering*. Springer. 4.2

International Energy Agency (2015). *Key World Energy Statistics*. International Energy Agency. 1

Janssens, M. (2007). Uncertainty of Fire Test Results. In *Eleventh International Interflam 2007 Conference, London, UK*. 2.6.4

Janssens, M. (2016). Calorimetry. In *SFPE Handbook of Fire Protection Engineering*, pages 905–951. Springer New York, New York, NY. 1, 1.1.1

Janssens, M. L. (1995). Methods and Equations of Fire Calorimetry. *American Forest & Paper Association*, page 12. 1.2.1, 1.2.1.1, 1.2.1.1, 1.2.1.2

John R. Howell, M. Pinar Mengüç, R. S. (2016). *Thermal Radiation Heat Transfer*. CRC press, 6th edition. 2.3.2.3

KANTHAL (2012). *Kanthal Globar SD Silicon Carbide heating elements*. D.2

Khan, M., Tewarson, A., and Chaos, M. (2016). Combustion Characteristics of Materials and Generation of Fire Products. In Hurley, M., editor, *SFPE Handbook of Fire Protection Engineering*, pages 1143 – 1232. Springer. 1.2.2

Koppejan, J. and Van Loo, S. (2012). *The Handbook of Biomass Combustion and Co-firing*. Routledge. 1.1.1

Lyon, R. E. and Abramowitz, A. (1995). Effect of Instrument Response Time on Heat Release Rate Measurements. *Fire and materials*, 19(1):11–17. 1.2.1.1

Ministerio de Energía de Chile (2015a). Antecedentes Sobre la Matriz Energética en Chile y sus Desafíos para el Futuro. 1

Ministerio de Energía de Chile (2015b). Energía 2050. 1

Parker, W. J. (1984). Calculations of the Heat Release Rate by Oxygen Consumption for Various Applications. *Journal of Fire Sciences*, 2(5):380–395. 1.2.1.2, 2.2.2.1, 2.2.2.1, B

PKL Technology Inc. (2015). *SPECTRA-1 Duct Monitor User Manual*. (document), 2.3.2.3, 2.15

RADWAG (2011). *Balances Series PS/X User Manual*. (document), 2.3.2.1, 2.13

Rivera, J. d. D., Davies, G. M., and Jahn, W. (2012). Flammability and the Heat of Combustion of Natural Fuels: A Review. *Combustion Science and Technology*, 184(2):224–242. 3.5.3

Savitzky, A. and Golay, M. J. (1964). Smoothing and Differentiation of Data by Simplified Least Squares Procedures. *Analytical Chemistry*, 36(8):1627–1639. 2.5.3

Smith, E. (1972). Heat Release Rate of Building Materials. In *Ignition, Heat Release, and Noncombustibility of Materials*. ASTM International. 1.2.2

Smith, E. E. (1996). Heat Release Rate Calorimetry. *Fire Technology*, 32(4):333–347. 1.2.2.2, A

Taylor, J. (1997). *An Introduction to Error Analysis: The Study of Uncertainties in Physical Measurements*. University Science Books, 2nd edition. 2.6

Tewarson, A. (1994). Flammability Parameters of Materials: Ignition, Combustion, and Fire Propagation. *Journal of Fire Sciences*, 12(4):329–356. 1.1.1

Tewarson, A. (1995). Calorimetry and Fire Environment. In *Fire Calorimetry*, page 45. DTIC Document. 1.1.1

Tewarson, A. (2002). Generation of Heat and Chemical Coumpounds in Fires. In *SFPE Handbook of Fire Protection Engineering*, chapter 4, pages 3–82–3–161. The National Fire Protection Association Press. 1.2.1.1, 2.6.1

The Engineering ToolBox (2016). *Fuel Gases and Heating Values*. 2.4.1.2

Thompson, N. and Cousins, E. (1959). The FM Construction Materials Calorimeter. *NFPA Q*, 52:186–192. 1.2.2

Thornton, W. (1917). XV. The Relation of Oxygen to the Heat of Combustion of Organic Compounds. *The London, Edinburgh, and Dublin Philosophical Magazine and Journal of Science*, 33(194):196–203. 1.2.1.2

Walters, R. N., Hackett, S. M., and Lyon, R. E. (2000). Heats of Combustion of High Temperature Polymers. *Fire and Materials*, 24(5):245–252. 2.5.1, 2.5.4

A | Heat release rate considering the heat losses through the wall

Smith proposes a methodology to determine the heat release rate considering the heat losses through the wall (Smith, 1996). The energy balance of a burning sample in the calorimeter is described below:

$$\dot{H}_i + \dot{H}_R = \dot{H}_e + \dot{H}_l + \frac{dH_w}{dt} \tag{A.1}$$

Where $\dot{H}_i$ is the heat produced by the radiant panels, $\dot{H}_R$ is the heat released by the burning sample, $\dot{H}_e$ is the heat carried by the air, $\dot{H}_l$ are the heat losses to the surroundings and $\frac{dH_w}{dt} = m_{OSU} c_{p,w} \frac{dT_w}{dt}$ is the heat absorbed by the calorimeter walls, assuming there are no temperature gradients in the walls. When the calorimeter is launched without the sample and it reaches steady state, then:

$$\dot{H}_R = 0 \qquad \frac{dH_w}{dt} = 0$$

Equation A.1 is now reduced to:

$$\dot{H}_i = \dot{H}_e + \dot{H}_l$$

Where $\dot{H}_i$ is known, and $\dot{H}_e$ is calculated. Thus the heat losses to the surroundings can

be determined. If $\frac{\dot{H}_e}{\dot{H}_i} << 1$, then the $\dot{H}_l$ must be calculated and added to the heat release rate analysis. The error can be also reduced by adding more air flow through the calorimeter.

In steady state $\dot{H}_i$ is the total heat released and measured by the calorimeter. Thus $\dot{H}_i = \dot{H}_{ss}$, where the subscript "ss" means steady state. This is important for determining the heat release rate of any sample, having as reference the heat released by the radiant panels. This is represented by $\dot{Q}_{R,OSU} = \dot{H}_R - \dot{H}_{ss}$. Using steady state as reference:

$$\dot{Q}_{R,OSU} = \dot{Q}_{e,OSU} + \dot{Q}_{l,OSU} + m_{OSU} c_{p,w} \frac{dT_w}{dt}$$

Now if the burning sample is replaced with a burner or a radiant heater with a constant and known power, in steady state, the heat losses can be calculated as:

$$\dot{Q}_{l,OSU} = \dot{Q}_{R,OSU} - \dot{Q}_{e,OSU}$$

Where $\dot{Q}_{R,OSU}$ is defined and $\dot{Q}_{e,OSU}$ is calculated. And it also is known that:

$$\dot{Q}_{l,OSU} = K_{l,OSU}(T_{wss} - T_{wssi})$$

Where $K_{R,OSU}$ is the heat transfer coefficient, T_{wss} is the wall temperature with the burner inside at a constant power, and T_{wssi} is the wall temperature at the initial steady state (only the radiant panels working).

As $\dot{Q}_{l,OSU}$ is known, and T_{wss} and T_{wssi} are determined by the thermocouples, $K_{l,OSU}$ can be calculated. If the power of the burner is modified in different ranges several times, $K_{l,OSU}$ can be modelled in function of T_{wss}.

Then, in the cool-down if $\dot{Q}_{R,OSU}$ is set to 0 at any time t, the coefficient $mc_{p,w}$ can be

calculated with Equation A.2

$$mc_{p,w} = \frac{\dot{H}_e + \dot{H}_l}{\frac{dT_w}{dt}} \tag{A.2}$$

The slope of wall temperature $\frac{dT_w}{dt}$ is calculated with the graph of wall temperature in function of time.

Finally the heat release rate is determined by:

$$\dot{Q}_{R,OSU} = \dot{m}_a c_p (T_e - T_{ss}) + K_{l,OSU}(T_w - T_{wss}) + m_{OSU} c_{p,w} \frac{dT_w}{dt}$$

Where T_o is the temperature of the outlet gases, T_{oss} the temperature of the outlet gases in the initial steady state, $\dot{m}_a$ is the mass flow of air, c_p is the specific heat of air, T_w is the wall temperature, T_{wss} is the wall temperature at the initial steady state, $m_{OSU} c_{p,w}$ is the mass multiplied with the specific heat of the materials of the calorimeter, but it is calculated experimentally. Biteau calculates an uncertainty of 18% using this method Biteau (2010).

B | Oxygen consumption with carbon monoxide production method

Parker (1984) proposed a method to calculate the heat release rate during a combustion reaction, by measuring the concentration of oxygen and carbon monoxide in the exhaust gases. This is expressed in equation B.1:

$$\dot{Q} = \left(\phi - \left(\frac{E'' - E'}{E'}\right)\left(\frac{1-\phi}{2}\right)\frac{X^A_{CO}}{X^A_{O_2}}\right) E' X^0_{O_2} \dot{V}_T \tag{B.1}$$

Where X^A_{CO} and $X^A_{O_2}$ are the concentration in carbon monoxide and oxygen the analyzers respectively, $X^0_{O_2}$ is the initial concentration of oxygen, $\dot{V}_T$ is the volume flow rate of air into the system, ϕ is the oxygen depletion factor, and E' is defined as:

$$E' \equiv E\rho_0 \frac{M_{O2}}{M_{AIR}} \tag{B.2}$$

Where M_{O2} and M_{AIR} are the molar masses ($g \cdot mol^{-1}$) of oxygen and air respectively and ρ_0 is the density of air. E'' is the heat release per volume of O_2 consumed in the burning of CO. The values of E' and E'' are 17.2 and 23.1 $MJ \cdot m^{-3}$ respectively.

The oxygen depletion factor is defined as:

$$\phi = \frac{X_{O_2}^{A^0} - \frac{X_{O_2}^A}{1 - X_{CO}^A}}{X_{O_2}^{A^0}\left(1 - \frac{X_{O_2}^A}{1 - X_{CO}^A}\right)}$$

Where $X_{O_2}^{A^0}$ is the oxygen concentration measured with the analyzer before the tests. It considers that the water vapor is trapped out. The relationship between $X_{O_2}^0$ and $X_{O_2}^{A^0}$ is described next:

$$X_{O_2}^0 = X_{O_2}^{A^0}\left(1 - X_{H_2O}^0\right) \tag{B.3}$$

$X_{O_2}^0$ considers the water vapor present in the air. But, if $X_{H_2O}^0$ is assumed to be zero, then $X_{O_2}^0 = X_{O_2}^{A^0}$, and ϕ is:

$$\phi = \frac{X_{O_2}^0 - \frac{X_{O_2}^A}{1 - X_{CO}^A}}{X_{O_2}^0\left(1 - \frac{X_{O_2}^A}{1 - X_{CO}^A}\right)}$$

C | Biomass experiments

Table C.1: Peak HRR (kW) of all biomass mixes at different moisture contents

Moisture content	Mix 1	Mix 2	Mix 3	Mix 4	Mix 5	Mix 6	Mix 7	Mix 8
Arauco	0.86	1	1.10	0.83	0.90	0.65	0.49	0.87
1-Day	1.29	1.58	1.15	1.11	1.23	1, 3	1.52	1.69
2-Day	1.58	1.39	2.00	1.52	1.46	1.24	1.62	1.51

Table C.2: Minimum and maximum heat release rates of the biomass mixes at different moisture content

MC level		Mix 1	Mix 2	Mix 3	Mix 4	Mix 5	Mix 6	Mix 7	Mix 8
Arauco	min	0.71	0.72	0.86	0.65	0.66	0.63	0.49	0.79
	max	0.93	1.29	1.46	1	1.17	0.67		0.91
1-Day	min	1.04	1.57	1.07	1.11	1.23	1.24	1.3	1.51
	max	1.53		1.22			1.37	1.76	1.93
2-Day	min	1.36	1.28	1.66	1.39	1.24	1.01	1.57	1.44
	max	1.92	1.49	2.32	1.64	1.68	1.58	1.66	1.58

Table C.3: Time to ignition of all mixes at different moisture content

Moisture content	Mix 1	Mix 2	Mix 3	Mix 4
Arauco	105 ± 30	210 ± 31	171 ± 43	127 ± 54
1-Day	89 ± 18	63	110 ± 77	92
2-Day	96 ± 20	45 ± 0	94 ± 20	78 ± 8
Moisture content	**Mix 5**	**Mix 6**	**Mix 7**	**Mix 8**
Arauco	140 ± 53	181 ± 54	291	190 ± 130
1-Day	117	94 ± 55	73 ± 47	101 ± 8
2-Day	128 ± 34	116 ± 21	41 ± 4	99 ± 15

Table C.4: Flaming time of all mixes at different moisture content

Moisture content	Mix 1	Mix 2	Mix 3	Mix 4
Arauco	320 ± 166	292 ± 237	484 ± 26	282 ± 241
1-Day	396 ± 80	430	400 ± 105	436
2-Day	303 ± 59	340 ± 60	219 ± 60	324 ± 23
Moisture content	Mix 5	Mix 6	Mix 7	Mix 8
Arauco	427 ± 264	287 ± 230	406	443 ± 165
1-Day	478	444 ± 6	366 ± 56	390 ± 42
2-Day	239 ± 10	308 ± 56	393 ± 8	328 ± 71

C.1 Final mass of the burnt samples

Table C.5: Final mass of burnt samples

Moisture content	Mix 1	Mix 2	Mix 3	Mix 4	Mix 5	Mix 6	Mix 7	Mix 8
Arauco	7.2	2.6	2.3	8	2.1	8.4	4.5	1.7
1-Day	0.8	5.4	1.7	3.3	3	2.1	2.8	2
2-Day	0.7	3	2.1	2.4	1.9	1.7	3.6	1.8

C.2 All tests at each moisture content level with SER method

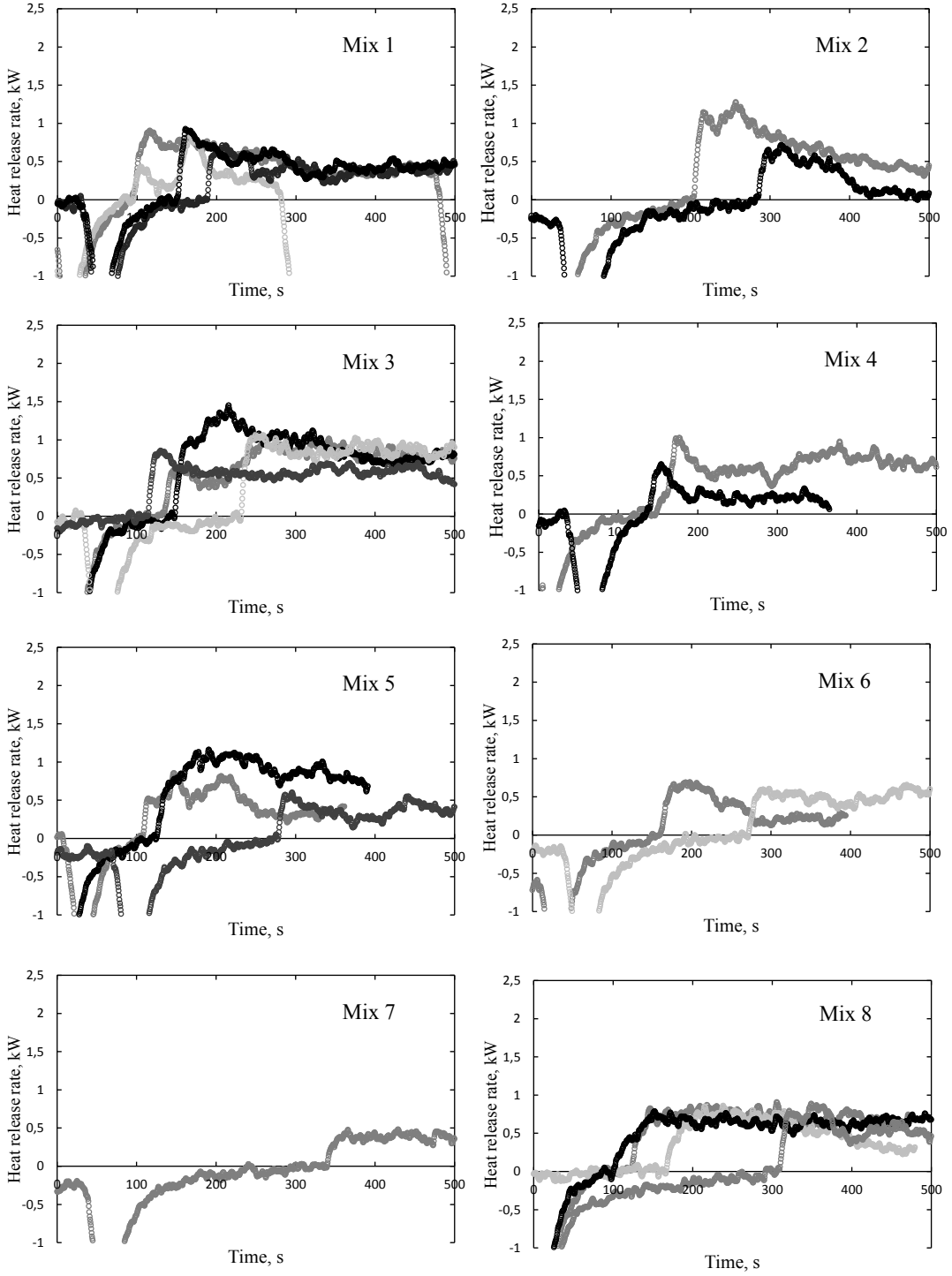

Figure C.1: HRR with SER method at arauco moisture content level

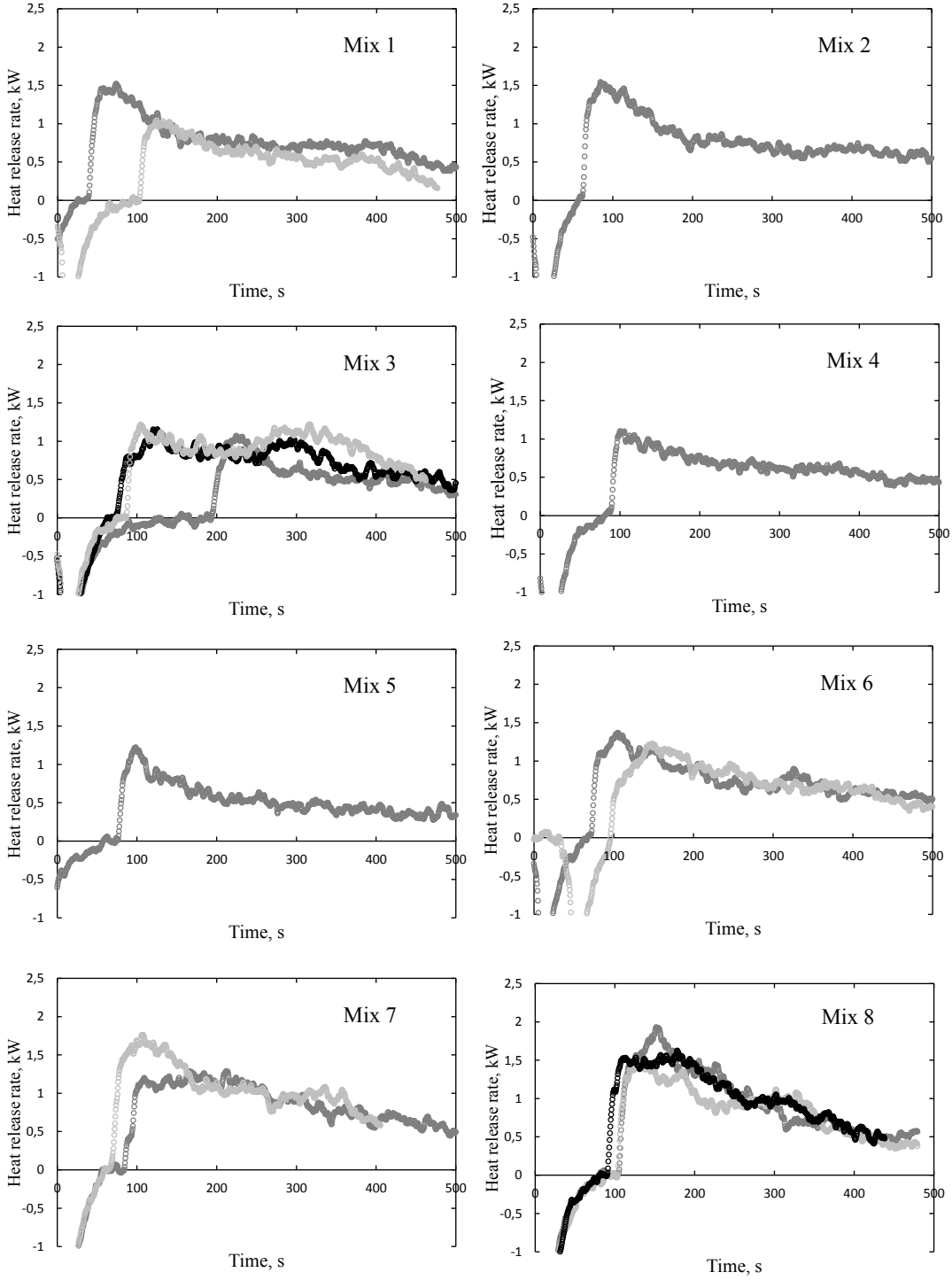

Figure C.2: HRR with SER method at 1-Day moisture content level

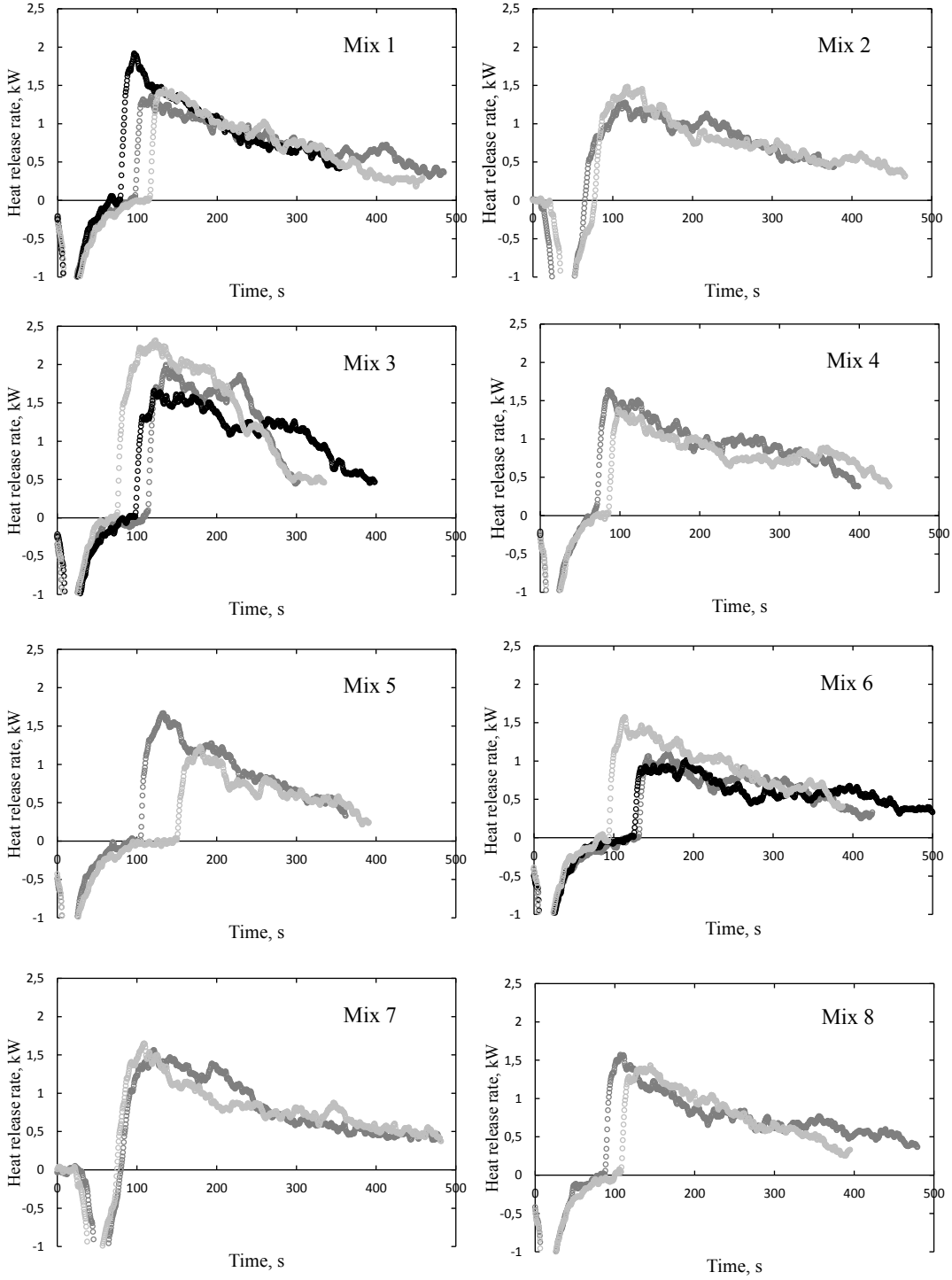

Figure C.3: HRR with SER method at 2-Day moisture content level

D | Radiant heaters

D.1 Drawings of the radiant heaters

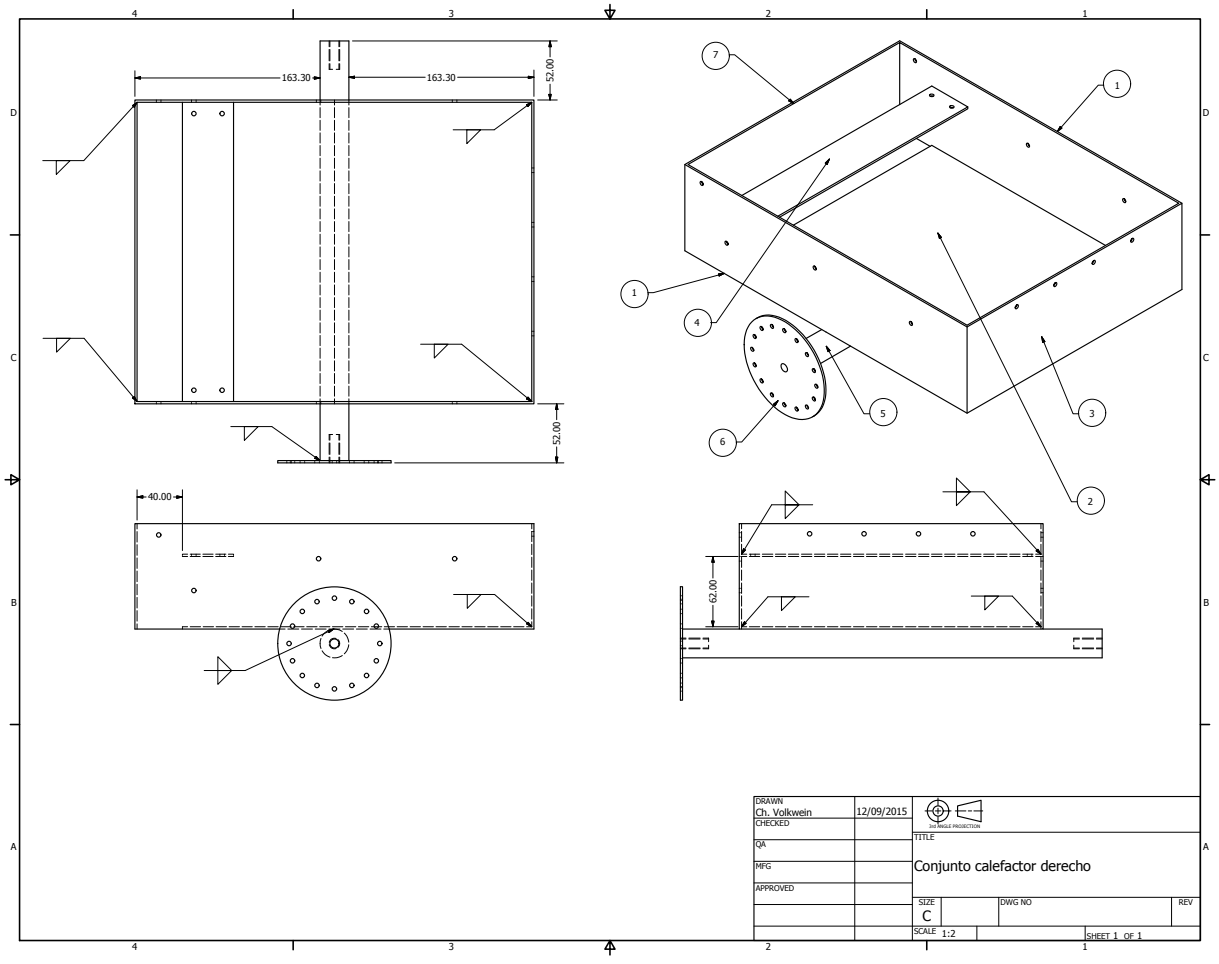

Figure D.1: Right heater

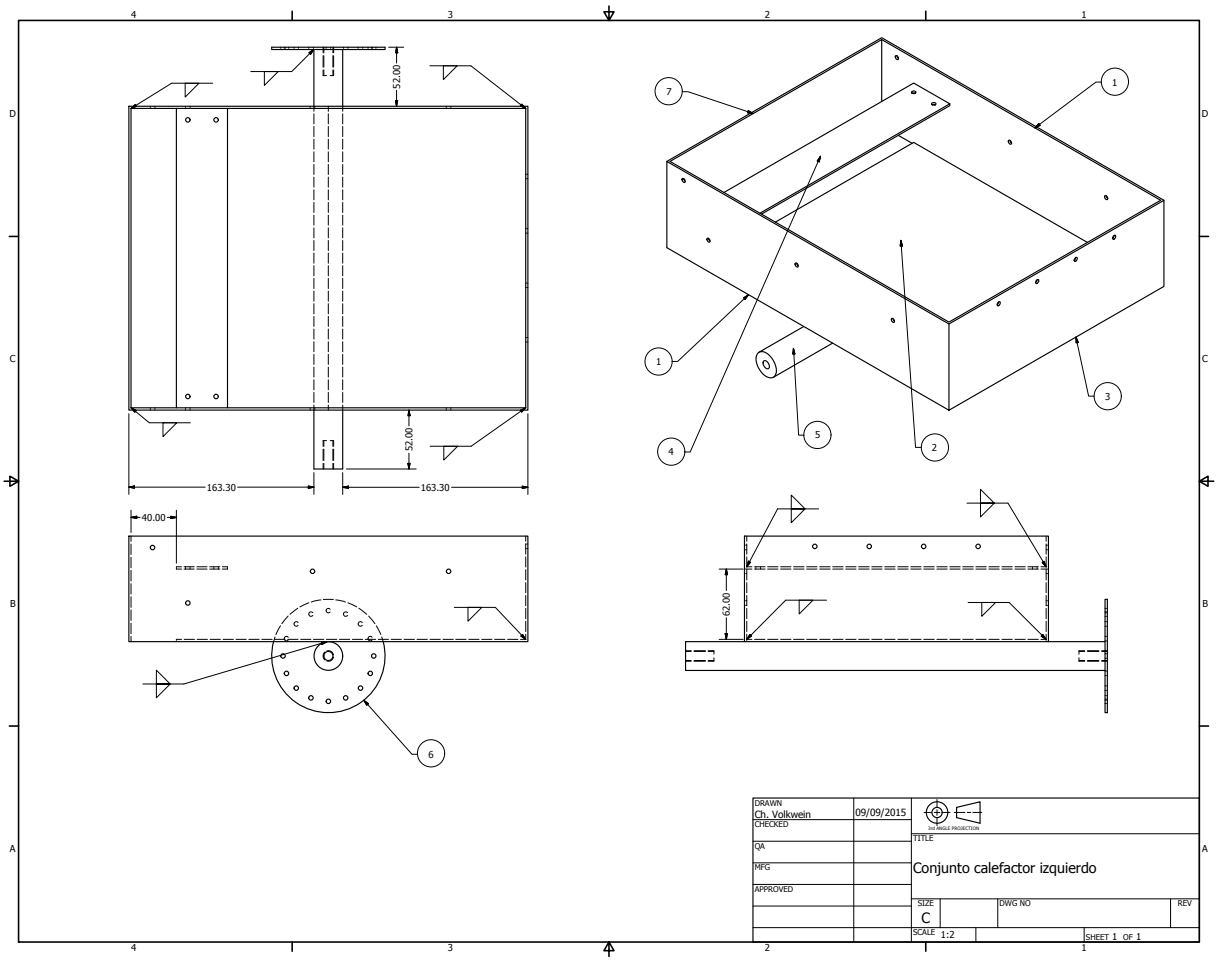

Figure D.2: Left heater

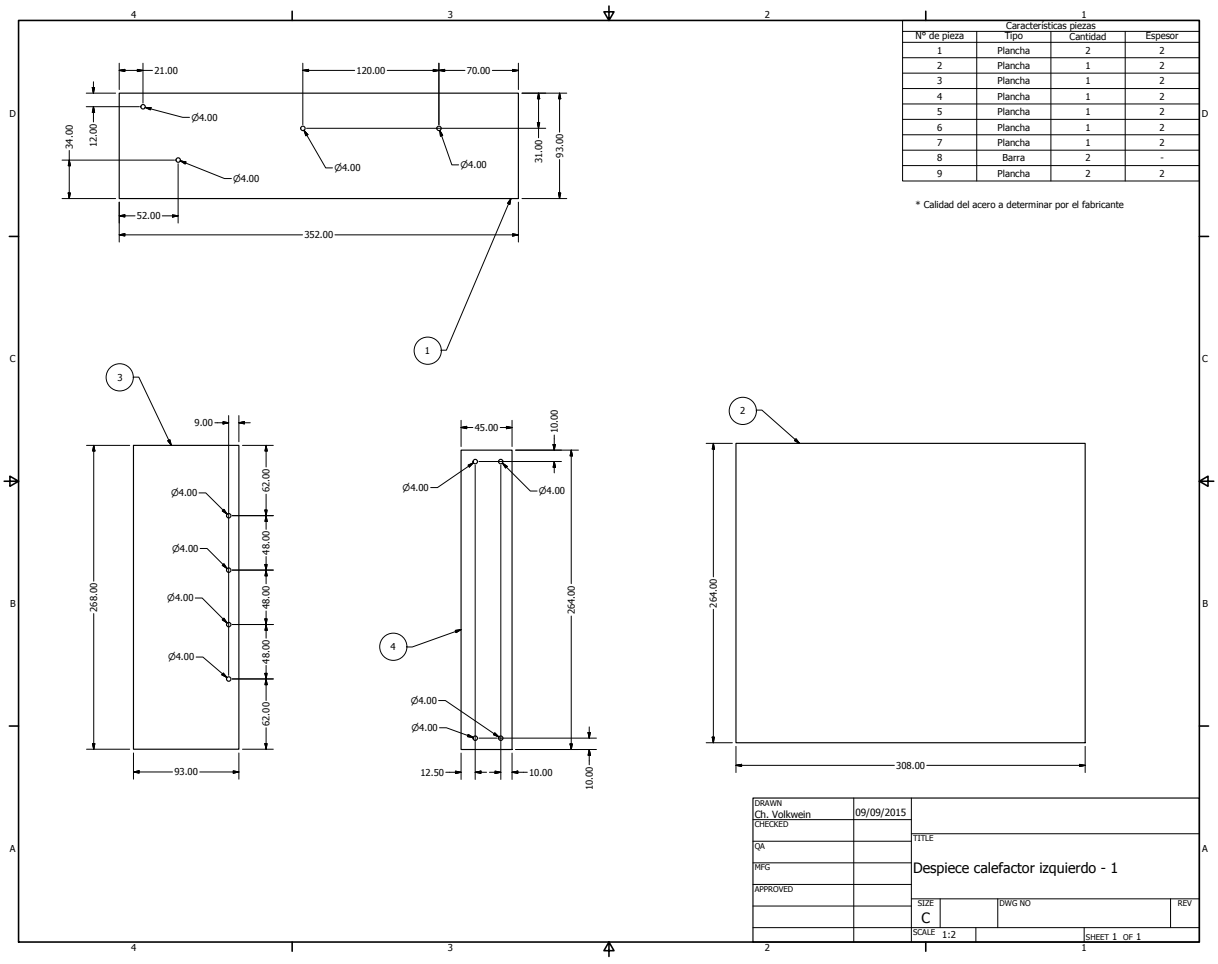

Figure D.3: Pieces of left heater 1

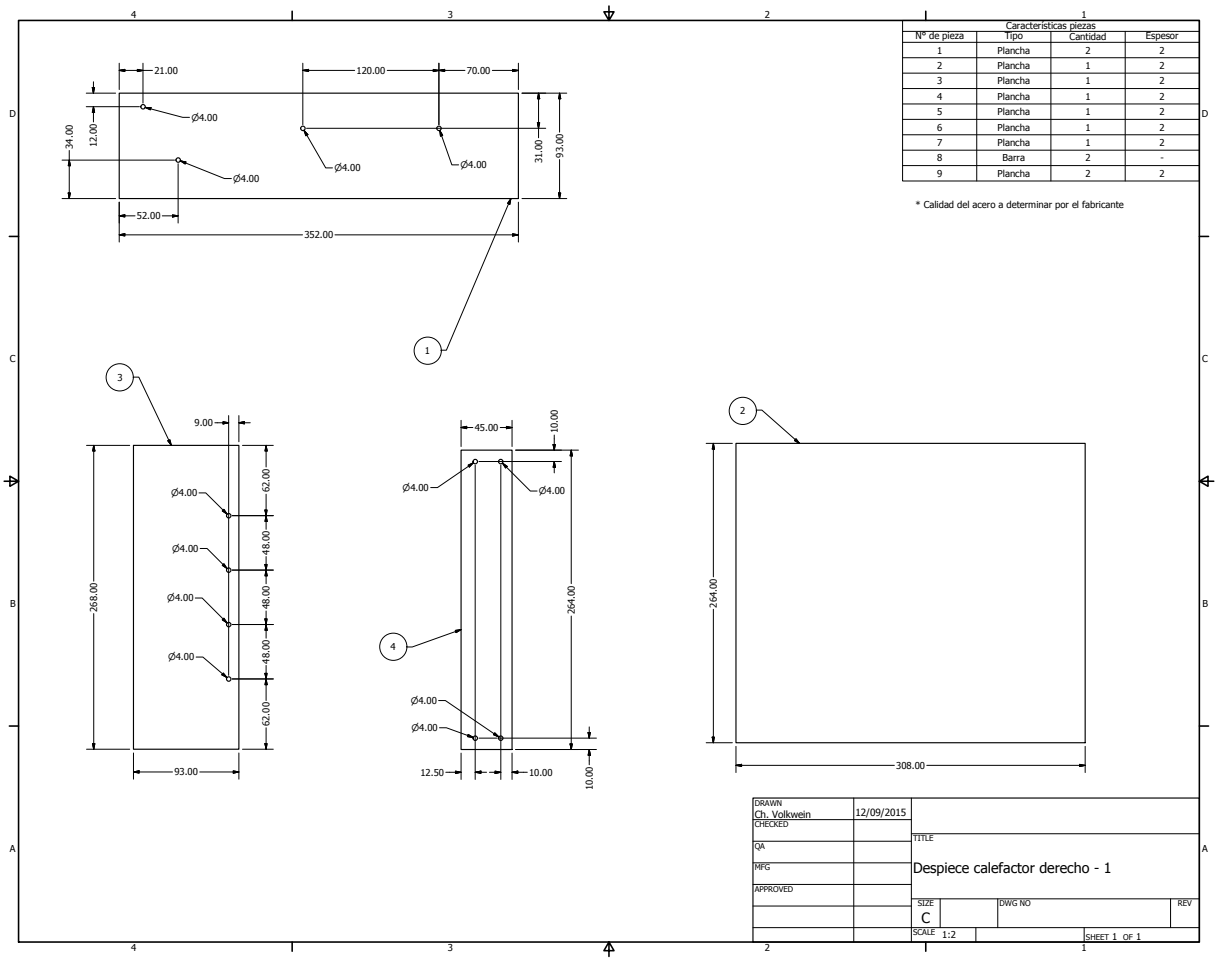

Figure D.4: Pieces of right heater 1

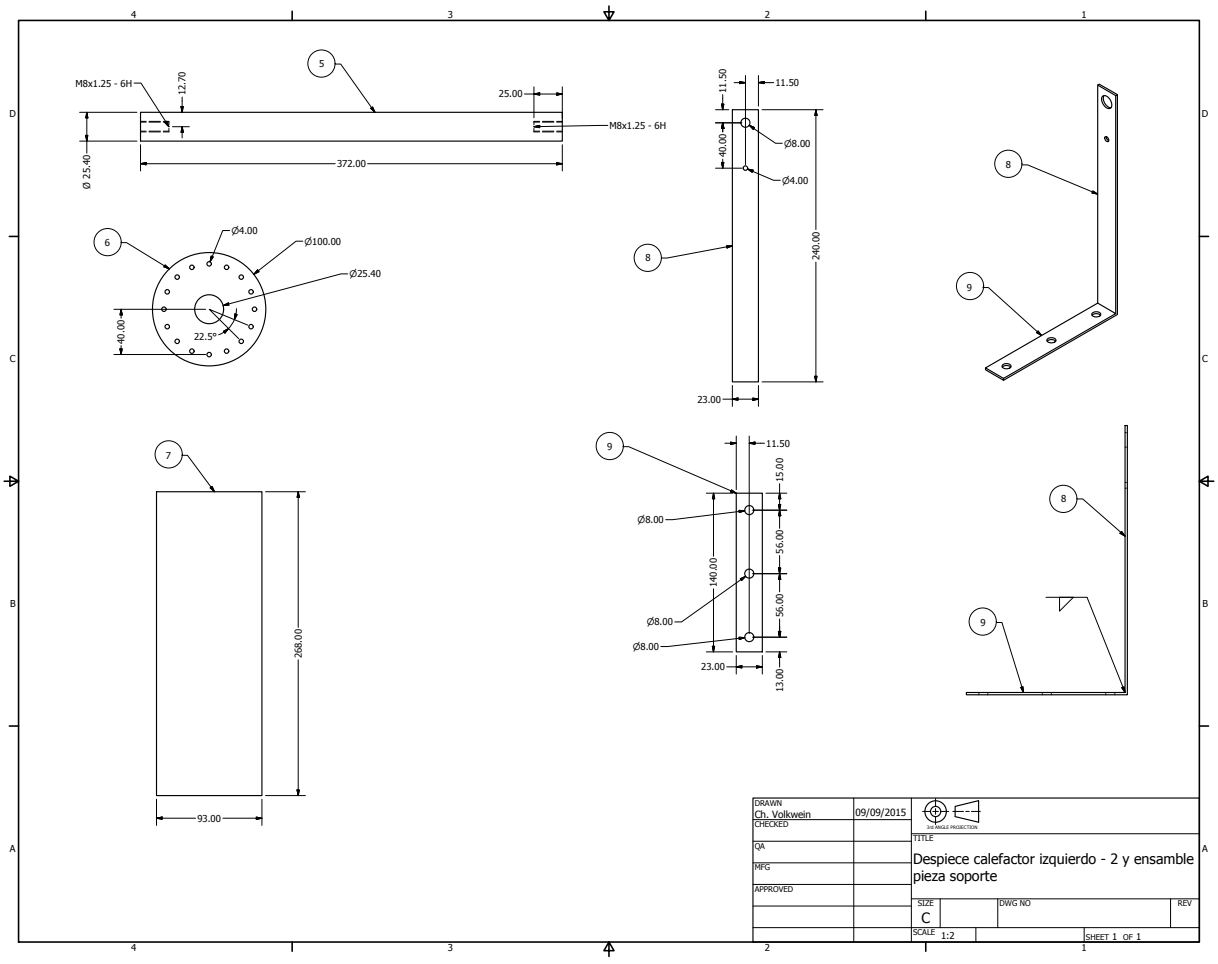

Figure D.5: Pieces of left heater 2

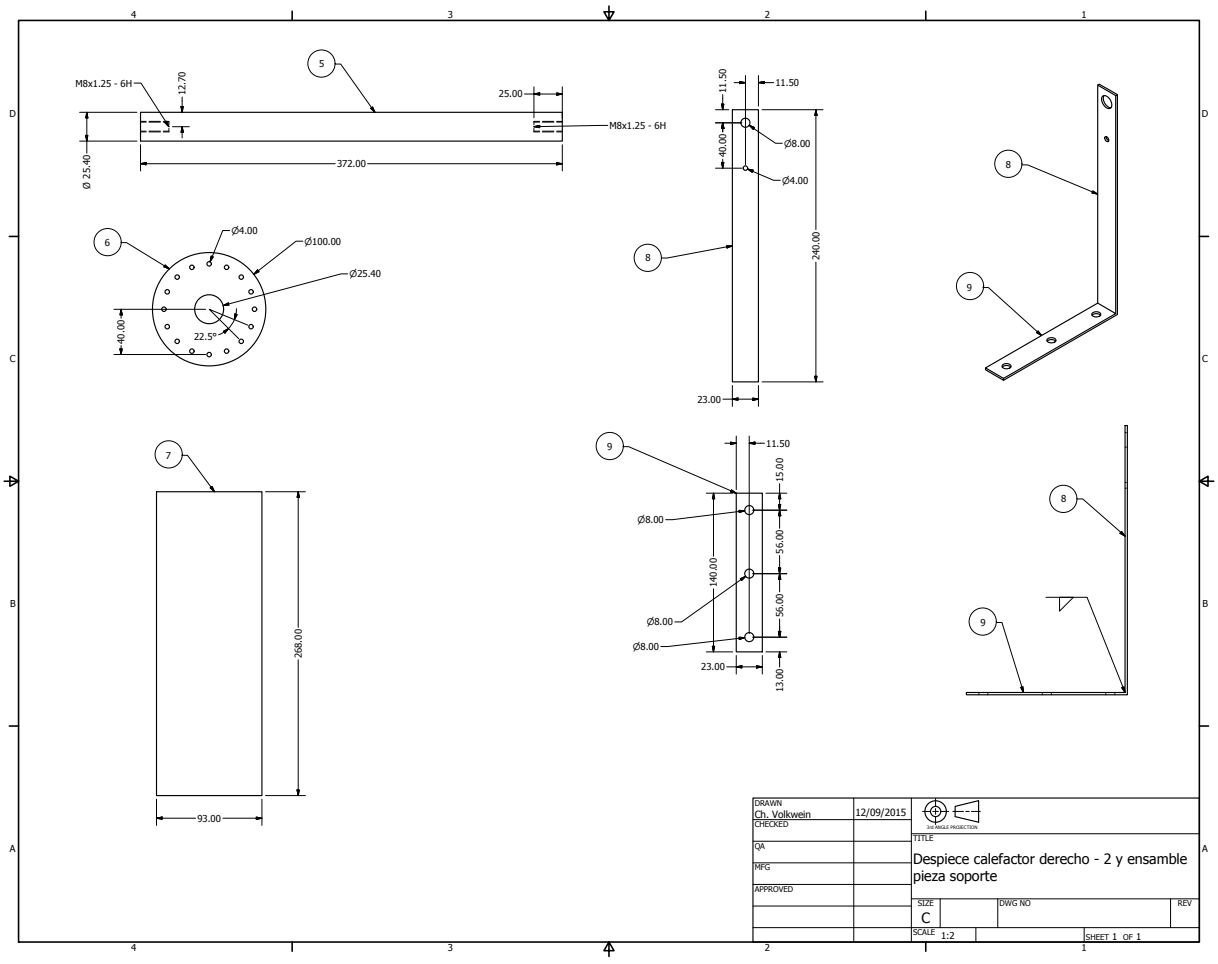

Figure D.6: Pieces of right heater 2

D.2 Calculation of the dimensions and the resistances magnitude of the SiC elements

In order to have an adequate heat flux supply, the dimensions and resistances magnitude of the SiC elements were calculated first. Four electric outlets of 25 A each one were considered for the calculation. Based on Python model results, it was determined that two surfaces of dimensions 200×200 mm at 1000°C were necessary to achieve the required heat flux. So, the SiC elements hot zone length was established to 20 cm. Kanthal recommends to not exceed the load of 15 $W \cdot cm^{-2}$ in the heating elements, and that the space between the

heating elements should not be less than 2 diameters of the element (KANTHAL, 2012). In order to have more area at 1000°C, the minimum diameter was selected: 12 mm (this way more SiC elements could be put on the area). The minimum area between each element was set to 1 diameter(in agreement with the manufacturer). 4 SiC elements were required to fill the 200×200 mm area, and for the two surfaces a total 8 SiC elements were required. The voltage in the laboratory is 220 V. But it was set to 190 for the calculation, in case that it was necessary to increase the voltage to increase the heat flux (using the voltage regulators). Then the current was set to a value lower and near 25 A. Finally, the connection type was defined in order to maximize the load with the 15 $W \cdot cm^{-2}$ as the top limit. Each two SiC elements was defined to be in serial connection. Then, by setting the current to 23.17, the value of the resistance and the load are obtained: 4.1 ohms and 14.6 $W \cdot cm^{-2}$ respectively. Table D.1 shows all the constants and variables calculated. The calculations are made of 1 resistance. So if the power is multiplied by 8, then the total maximum power is 17.6 kW. Currently the heaters are working with a maximum load of 8 $W \cdot cm^{-2}$ (providing an incident flux on the specimen area of 50 $W \cdot m^{-2}$). This was set as an arbitrary limit to avoid premature wear of the SiC elements.

Table D.1: Parameters used to calculate the resistance magnitude of one SiC element

Diameter	Length	Voltage	Current	Resistance	Power	Load
0.012 m	0.2 m	190 V	23.2 A	4.1 Ω	2.2 kW	14.6 $W \cdot cm^{-2}$

D.3 Construction of the heaters

The radiant heaters assembly procedure is the same for both radiant heaters. The main elements that compose the heaters are shown in Figure 2.8. The assembly of the main parts of radiant heaters is specified in Figure D.7, and the electrical connections are shown in Figure D.8. The ceramic fiber blankets and boards are cut with a saw. Three ceramic fiber blanket pieces are cut with the same dimensions and put one over each other below the metal slab. The aim of these pieces is to insulate the electrical connections. Two ceramic fiber board pieces are located on the base of the structure. One board piece is put between both the boards and the blankets. Board pieces are located at the sides of the structure to

avoid heat losses in those directions. Eight channels are made in one board to hold the SiC elements position. The channels are made by sanding the material with a screw.

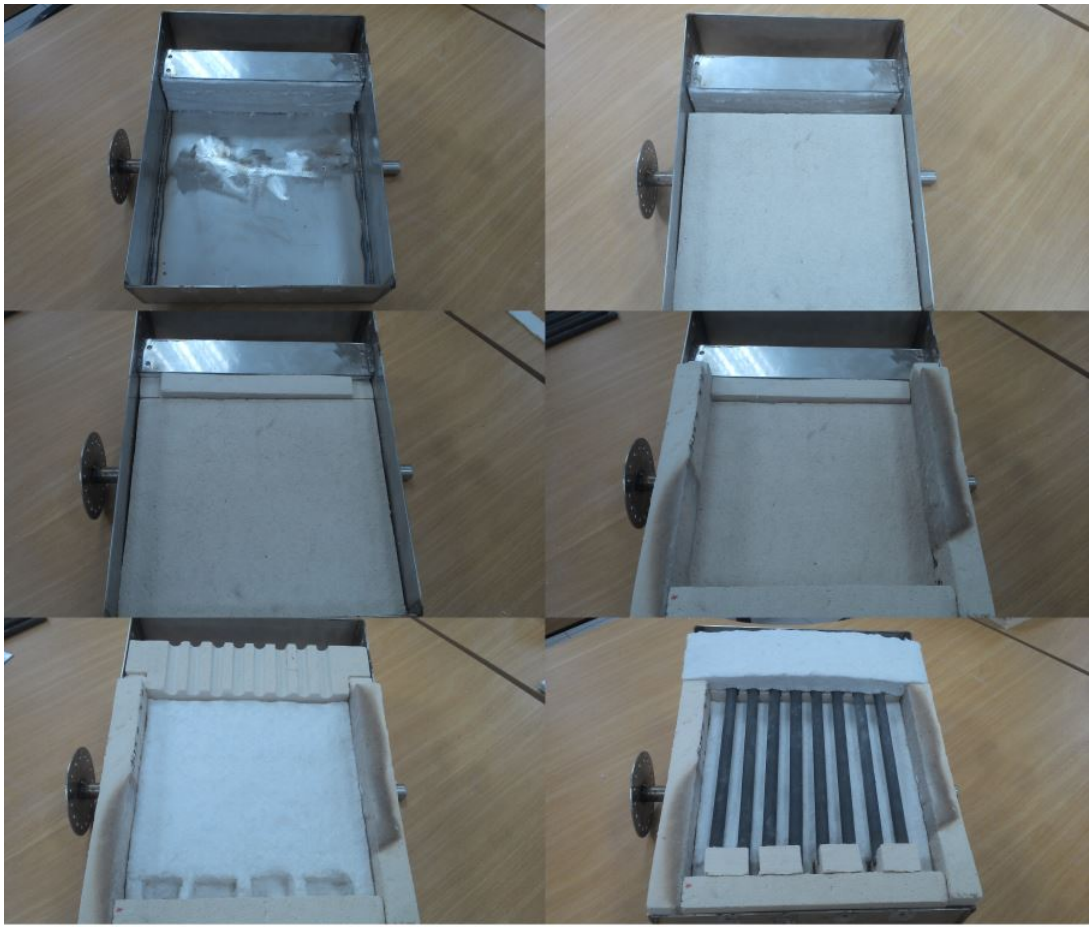

Figure D.7: Radiant heaters assembly - Part 1

A blanket piece is put on the base, and 4 board pieces with channels are put to hold the end of the SiC elements (Actually a long board piece with a duct is used instead of the 4 little pieces, but both designs are suitable). Finally the SiC elements are placed on their positions and a blanket piece is put above the start of the elements. A metal slab is located above the blanket and is fixed with four bolts. The bolts are not tightly fixed. There should not be much pressure over the SiC elements. All boards are fixed with screws.

The electrical connection is made with connecting braids and G-Type clamps fabricated by the same manufacturer as the SiC elements. These types of connectors can stand high

temperatures and do not oxidize through time. Each serial connection is plugged to earth for safety purposes. Before the assembly of the heaters, the big insulation boards and blanket (Used over the base of the structure) are perforated to permit the pass of a thermocouple. Four stain L-shaped profiles are located above the board that holds the end of the SiC elements. They are fixed with screws.

Figure D.8: Radiant heaters assembly - Part 2

E | Visual Basic code

```
Module2 - 1

Sub ordenardatos()
' Order the data of the precision balance
' Modified: 30/05/2016
' Author: Christopher Volkwein
' The first data should be set on row number 7

Dim i As Integer
Dim j As Integer
Dim k As Integer

i = 7 ' Assuming that the data start here
j = 7
i = 7

    Columns("A:A").Select
    Application.CutCopyMode = False
    Selection.TextToColumns Destination:=Range("A1"), DataType:=xlDelimited, _
        TextQualifier:=xlDoubleQuote, ConsecutiveDelimiter:=True, Tab:=True, _
        Semicolon:=False, Comma:=True, Space:=True, Other:=False, FieldInfo:=_
        Array(Array(1, 1), Array(2, 1), Array(3, 1)), DecimalSeparator:=".", _
        ThousandsSeparator:=",", TrailingMinusNumbers:=True


Do While Sheet1.Cells(i, 7) <> 0 Or Sheet1.Cells(i + 1, 7) <> 0 Or Sheet1.Cells(i + 2, 7) <>
0 _
    Or Sheet1.Cells(i + 3, 7) <> 0 Or Sheet1.Cells(i + 4, 7) <> 0 Or Sheet1.Cells(i + 5, 7) <
> 0 _
    Or Sheet1.Cells(i + 6, 7) <> 0 Or Sheet1.Cells(i + 7, 7) <> 0 Or Sheet1.Cells(i + 8, 7) <
> 0 _
    Or Sheet1.Cells(i + 9, 7) <> 0 Or Sheet1.Cells(i + 10, 7) <> 0 Or Sheet1.Cells(i + 11, 7)
 <> 0
    If Sheet1.Cells(i, 7) <> 0 Then
        Sheet1.Cells(j, 9) = Sheet1.Cells(i, 5)
        Sheet1.Cells(j, 10) = Sheet1.Cells(i, 6)
        Sheet1.Cells(j, 11) = Sheet1.Cells(i, 7)
        If IsNumeric(Sheet1.Cells(i + 2, 3)) And Sheet1.Cells(i + 2, 3) <> 0 Then
            Sheet1.Cells(j, 12) = Sheet1.Cells(i + 2, 3)
        Else
            If IsNumeric(Sheet1.Cells(i + 2, 2)) And Sheet1.Cells(i + 2, 2) <> 0 Then
                Sheet1.Cells(j, 12) = Sheet1.Cells(i + 2, 2)
            Else

                If IsNumeric(Sheet1.Cells(i + 2, 1)) Then
                    Sheet1.Cells(j, 12) = Sheet1.Cells(i + 2, 1) / 1000
                Else
                    Sheet1.Cells(j, 12) = Sheet1.Cells(i + 2, 4)
                End If
            End If
        End If
        j = j + 1
    End If
    i = i + 1
Loop
End Sub
```

Figure E.1: Visual Basic code to process the data of the precision balance